MICROCAPILLARY MEMBRANES FOR PURIFICATION OF BIOMOLECULES

IPSHITA MANDAL

TRINITY HALL

February 2016

This dissertation is submitted for the degree of

Doctor of Philosophy

Abstract

Opportunities exist for alternative chromatography separation media which possess high binding capacity and throughput, avoid column packing, are economically feasible for single-use disposability and work with standard chromatography systems. Two types of microcapillary membranes, hollow fibre membranes (HFM) and microporous walled microcapillary film (MMCF) membranes have been previously studied for a diverse range of filtration applications. The MMCF membranes unique geometry has not yet been studied for separation of biomolecules. The aim of this thesis is to develop microcapillary membranes for proof-of-concept biomolecule separations through various chromatography module constructions, surface chemistries and matrix composition modifications.

The microcapillary membranes used in this work have been produced through a non-solvent induced phase separation process using ethylene vinyl alcohol copolymer. The matrices are constructed into two types of modules, straight columns and helical columns, and the flow behaviour and dynamic binding capacity of each is studied.

The matrix surface is modified using sulfonic acid groups for cation-exchange chromatography and quaternary amines for anion-exchange chromatography. The straight MMCF module operates on standard AKTA^{TM} chromatography systems at pressures of up to 1.5 MPa and linear velocities of up to 54,000 cm h^{-1}. A sharp column breakthrough is observed with a dynamic binding capacity at 10% breakthrough of 13.8 mg lysozyme/ml adsorbent volume. Frontal analysis bio-separation studies of lysozyme and BSA show a purification of 98.8% of lysozyme in the eluted sample. The anion functionalised straight MMCF module has a dynamic binding capacity of 10% breakthrough of 1.26 mg ovalbumin/ ml adsorbent volume, isolating BSA from lysozyme to the limit of detection of the gel assay used.

The concept of activated carbon (AC) in membranes for removal of impurities is applied to the HFM matrix geometry by modifying the NIPS process to form AC-HFM mixed-matrix membranes. AC-HFMs with AC compositions of 0.7%, 3.2%, 6.3%, 11.8% and 21.1% by mass are extruded. Generally, as the AC composition of the HFM increases, the average pore size across the capillary membrane decreases, and the overall amount of adsorption of test molecules methylene blue and humic acid increases.

This thesis contributes to the study of microcapillary membranes as a chromatography medium which is high capacity, high throughput, and pressure tolerant whilst avoiding column packing. This thesis sets the research area for advanced bioprocessing studies by optimising the porosity and permeability of the microcapillary membranes, studying affinity chromatography, and advanced large biomolecule studies using mixed-matrix microcapillary membrane studies.

Preface

The work presented in this thesis was carried out in the Department of Chemical Engineering and Biotechnology, University of Cambridge between October 2011 and July 2015. This dissertation is the result of my own work and includes nothing which is the outcome of work done in collaboration except as declared below and specified in the text. I further state that no substantial part of my dissertation has already been submitted, or, is being concurrently submitted for any such degree, diploma or other qualification at the University of Cambridge or any other University of similar institution except as declared below and specified in the text.

Parts of Chapters 2 and 3 were published in:

Mandal, I., Townsend, M. J., Darton, N. J., Bonyadi, S., & Slater, N. K. H. (2014). A microporous walled micro-capillary film module for cation-exchange protein chromatography. Journal of Membrane Science, 466, 123–129. doi:10.1016/j.memsci.2014.04.049

Lazar, R.A., Mandal, I., Slater N.K.H. (2015). Effect of bore fluid composition on microstructure and performance of a microporous hollow fibre membrane as a cation-exchange substrate. Journal of Chromatography A, 1394, 148–153. doi:10.1016/j.chroma.2015.03.037

Chapter 5 was work done during supervision of IIB students Michael Carson, Jackson Lippold and MPhil ACE student Yongjun Kwon.

There are 60 figures and tables in this thesis. The word count for this thesis is 35,389 words. It does not exceed the prescribed word limit for the relevant Degree Committee.

Acknowledgements

“Miracles do happen”- I would like to thank my supervisor Prof Nigel Slater for opening up the opportunity of working with him and allowing me to grow as an independent scientist. I would also like to thank my funding bodies, the Engineering and Physical Sciences Research Council (EPSRC) and Prince of Wales Cambridge Commonwealth Trust. Funding credits also go to Trinity Hall Travel Grants, Department of Chemical Engineering and Biotechnology’s Shell Fund and Cambridge Philosophical Society for supporting travel funding to international conferences.

There are many people in the department who have had a direct contribution to this PhD research. Dr Nick Darton for introducing and engaging me into the project. Dr Sina Bonyadi for handing me over his rig and sharing his passion for membrane extrusions. Matthew Townsend and Dr David McNally for introducing me to various lab techniques. Dr Bart Hallmark for his advice in MCF extrusion and fluid dynamic studies. Prof Alan Turnacliffe for allowing me to use his lab facilities from time to time.
I would also like to thank technicians Maggie Wallduck, Dr Simon Butler and Zlatko Saracevic for their help in setting up experiments. Dr Neil Williamson and Dr Matthew Watson for their help with molecular biology experiments. Dr Jeremy Skepper for taking scanning electron micrograph images. Gary Chapman from the workshop and Ian Patterson from the stores for helping me construct various modules. Amanda Taylor for her administrative support and chirpy enthusiasm. John Gannon and Kevin Swann from electronics. Jim Thompson and Jon Cowper from IT.

Special thanks go to Dr Stephen Gerrard and Radu Lazar for being the most awesome and fun loving office colleagues. Sergio Argandona, Krishnaa Mahbubani, Christian Guyader and Duncan Sharp for their company in the lab. Jonathan Scarlett, Wolfgang Schmied, Arielle Bonneville-Roussy and Wared Seger for their continual friendship and support through hard times.

My family for their continual support- Bankim Mandal, Sharmila Mandal and Arpita Mandal. Most of all I would like to thank my partner, Simon Johnson, for his constant support and belief till the very last page.

Dedicated to Lt. Ranajit Kumar Mandal,

Who would have been proud that I took up the challenge of

Engineering research at Cambridge

Table of Contents

Abbreviations

α	Langmuir adsorption constant
A	absorbance
	cross sectional area
A_s	asymmetry factor
AC	activated carbon
BET	Brunauer-Emmett-Teller
BSA	bovine serum albumin
BSP	British standard pipe
C	concentration
CF	correction factor
CIP	clean-in-place
CLSM	confocal laser scanning microscopy
cm	centi meter
CM	carboxymethyl
CSPP	Cambridge solution processing platform
De	Dean number
DEAE	diethylaminoethyl
DMSO	dimethyl sulfoxide
d_p	average pore diameter
DNA	deoxyribonucleic acid
DBC	dynamic binding capacity
EBC	equilibrium binding capacity
$\varepsilon_{protein}$	protein molar extinction coefficient
et al.	et alia
EVOH	ethylene vinyl alcohol

F	feed
FEP	perfluoropolymer
FPLC	fast performance liquid chromatography
g	gram
	unit for centrifugation
GE	General Electric
h	hour
	reduced plate height
HCP	host cell protein
HETP	height equivalent of a theoretical plate
HF	hollow fibre
HFM	hollow fibre membrane
HPLC	high pressure liquid chromatography
l	length
inj	injection
k	permeability
K_d	equilibrium disassociation constant
kDa	kilo Dalton
L	litre
	length
m	mass
M	molar
mA	milli absorbance
max	maximum
mg	milli gram
min	minute
ml	milli litre

mm	milli metre
mM	milli molar
MMCF	microporous walled microcapillary film
MMM	mixed-matrix membrane
MPa	mega Pascal
mS	milli Siemens
MW	molecular weight
N	theoretical plates
ng	nano gram
NHS	N-hydroxysuccinimide
NIPS	non-solvent induced phase separation
NMCF	non-porous microcapillary film
nm	nano meter
NMP	N-methyle-2-pyrrolidone
OD	optical density
P	pressure
Pa	Pascal
PAGE	polyacrylamide gel electrophoresis
PBS	phosphate buffered saline
PDMS	polydimethylsiloxane
PES	polyethersulfone
PhRMA	pharmaceutical research and manufacturer association
PVA	poly(vinylalcohol)
PVP	polyvinylpyrrolidone
Δp	change in pressure
pI	isoelectric point

q	amount of protein adsorbed
Q	linear velocity
	quaternary amine
	volume per time
Re	Reynolds number
R^2	coefficient of determination of a liner regression
rpm	rate per minute
RTD	residence time distribution
s	second
SDS	sodium dodecyl sulfate
SEM	scanning electron microscope
SP	sepharose
Tris	tris(hydroxymethyl)aminomethane
U	units
USA	United States of America
UV	ultraviolet
UK	United Kingdom
V	volume
	Volt
wt.	weight
°C	degree Celsius
µ	viscosity
µl	micro litre
µM	micro molar

List of Tables and Figures

CHAPTER 1 INTRODUCTION

1.1 Motivation

Biomolecules constitute 900 of 3000 total drug candidates currently under development and in clinical testing (Ho, 2013), placing a big demand on biomanufacturing processes. A significant bottleneck in the process lies in downstream processing which can account for up to 80% of total production costs (D'Souza et al., 2013; Freitag, 2014). Purification of biomolecules in downstream processing is different to that of small molecule drugs, due to their biologically active structure and larger molecular size. Unfortunately conventional chromatography units are still scaled up from purifications developed in laboratories, hence are largely empirical (G. Carta & Jungbauer, 2010). Conventional technologies can have limitations in packaging requirements, sterilising the matrix in between use, how high flow velocities they can tolerate and flow dependent binding capacity of the medium.

The motivation behind this review is firstly to understand the key issues in biomolecules purification through the study of most commonly used chromatography media in the industry. A diverse range of media were studied in terms of their base matrix support chemistry, overall material properties and bead or membrane geometries. Understanding the medium nature also helps deduce the advantages and limitations the various chromatography media possess.

Microcapillary membranes have existed since the 1950's in their earliest form as hollow fibre membranes (HFM). They have since been developed into multiple capillary formats of both non-porous and porous nature. Their use in biomolecules separations has been fairly limited due to their earlier low surface area due to non-porosity. The aim of this thesis is to characterise and develop microcapillary membranes for model

biomolecule separations and study their suitability as an alternative chromatography medium.

1.2 Literature review

This review highlights the current growing state of the biopharmaceutical industry and upcoming biomolecules. It introduces the broader bio-manufacturing process and discusses the downstream bio-processing bottleneck. Current separation technologies are summarised and criticised for their performance parameters with their limitations and future development opportunities. Previous research on microcapillary membranes is summarised with key research developments and advantages highlighted. This is put in context of how microporous walled microcapillary membranes could meet current biomolecules separation challenges.

1.2.1 Biomolecules and the growing demand on biomanufacturing

Biopharmaceuticals have established their dominance in sales for the pharmaceutical industry. Most pharmaceutical companies now showcase biomolecule drugs in their ten best-selling drugs. According to the Pharmaceutical Research and Manufacturer Association (PhRMA) 2012 report, biomolecules constitute 900 of 3000 total drug candidates currently under development and in clinical testing (Ho, 2013). Demand on biomanufacturing is growing both with new drug candidates and increasing volume of existing drugs as biosimilars (Hagel, Jagschies, & Sofer, 2008).

The main biomolecules are recombinant proteins (e.g. enzymes and antibodies), vaccines, blood products (e.g. cellular components and plasma) and plasma derived proteins (Ho, 2013; Subramanian, 2007). Monoclonal antibodies are rapidly dominating, with sales already at 48% of all biological sales in 2010 (Guiochon & Beaver, 2011; Ho, 2013). The volume demand is increasing with the patent expiry of

many innovator drugs leading to biosimilars production. Biosimilars are “me-too” versions of innovative biopharmaceuticals which are off patent, conceptually equivalent to generics in the pharmaceutical industry. To grow biomanufacturing there is a need to increase product quantity in terms of capacity and throughput. Whilst current technologies are being optimised and new technologies being developed, product quality and process validation must remain robust for regulatory authorities (Hagel, Jagschies, & Sofer, 2008).

Production scale up occurs in upstream processing. Developed cell lines usually stored in cell line banks are scaled up in a stepwise fashion in batch reactors to volumes of 10,000 L or larger (Kelley, 2009). With increasing demand, the strategy so far has focused on decreasing production costs in upstream processing by increasing product titers (Bhut, Christensen, & Husson, 2010). This has been achieved by increasing bioreactor production capacity, optimised expression levels of biological product, and higher cell densities (Kelley, 2009). Previous studies on biomolecules product yields, estimate concentrations at the end of upstream processing to be at 2 - 5 g L^{-1} (Guiochon & Beaver, 2011; Kelley, 2009), whilst current yields for monoclonal antibodies are over 10 g L^{-1} (Tao, Ibraheem, Conley, Cecchini, & Ghose, 2014).

1.2.2 Challenges in downstream processing

With high product yields from upstream processing (Wurm, 2004), the manufacturing bottleneck has shifted to downstream processing, with a requirement to develop purification processes capable of dealing with high product concentrations. Downstream process can account for up to 80% of the total product costs (D‘Souza et al., 2013; Freitag, 2014).

The goal of downstream processing is to recover the maximum amount of target product from upstream cell culture, at commercially viable costs and processing times. Post precipitation and cell extraction, the three important purification steps in downstream processing are primary capture, purification and polishing. The capture step depletes the product solution of majority of impurities while bringing the target product in to a defined buffer solution. Cell viability is normally low post-extraction, hence the speed of the capture processing time is critical (Subramanian, 2007). Subsequent purification and polishing steps are necessary to remove residual host cell proteins, DNA or adventitious agents such as viruses for acceptable regulatory requirements of the final product (Hagel et al., 2008).

Conventional industrial chromatography units are scaled up from purifications developed in laboratories, hence they are largely empirical (G. Carta & Jungbauer, 2010). This limits the batch sizes that can be used, linear velocities and capacities of conventional columns. Chromatography is a relatively slow process that requires expensive separation media and large volumes of buffers (D'Souza et al., 2013). There is considerable economic pressure to optimise and develop new technologies that have high throughput characteristics whilst maintaining capacity.

1.2.3 Purification of biomolecules

A biomolecule is made by a living organism and includes large molecules such as proteins and nucleic acids and small molecules such as primary and secondary metabolites. Chromatography for the purification of small molecules such as amino acids, lipids and sugars is fairly simple but in the initial days there were key limitations in large molecules purification. The large size of the protein, its penetration of adsorbent material, instability of the protein molecule dependent on the choice of solvents, and the distribution of binding sites across protein domains were key

challenges for larger biomolecule separations (Peterson & Sober, 1956). Early chromatography studies focus on proteins that can be purified in large quantities, for example from blood, egg white and toxins. Protein purification techniques in those days were developed by Edwin Joseph Cohn who led a project during World War II for isolating the serum albumin fraction in blood plasma. Serum albumin is useful for maintaining the osmotic pressure of the blood vessel, which helped in keeping soldiers alive (Tan & Yiap, 2009). Chromatography is introduced for the purification of biologicals in the 1970s (Hagel et al., 2008).

1.2.4 Ion-exchange chromatography

Perhaps the first example of ion-exchange purification can be attributed to Moses, who purified acrid water with the aid of a special type of wood (*Ex*:15:25) (Hagel et al., 2008). In the field of chromatography, ion-exchange has been used for several decades for the separation of small inorganic ions. Ion-exchange chromatography for larger biomolecules came to be used when hydrophilic materials of large pore sizes were introduced in the late 1950s.

Biological macromolecules such as proteins, deoxyribonucleic acid and viruses can carry a net positive or negative charge depending on their surface chemistry and the pH of the environment they are in (Hagel et al., 2008). The net charge of a biomolecule is used in ion-exchange chromatography to specifically bind to a resin matrix surface, while uncharged or differently charged impurities are washed out. The charged biomolecules bind to the charged group functionalised resin matrix surface due to electrostatic forces. The targeted biomolecule is eluted from the resin matrix by changing the buffer ion concentration, usually by changing the concentration of sodium chloride. The elution phase is analysed using a UV or electrical conductivity detector.

The protein biomolecule consists of polymer chains of amino acids, which can be charged depending on the pH of the environment (Ghosh, 2002). Isoelectric point (pI) is the pH value at which a protein has no net charge. In a buffer with a pH below the pI value, it will be positively charged as a cation. In a buffer with a pH above the protein's pI, the protein will be negatively charged as an anion.

Lysozyme is a model protein often used to characterise novel chromatography matrices. It is an enzyme which damages bacterial cell walls by catalysing hydrolysis of certain molecules within the cell wall such as peptidoglycans (Strang, 1984). It is robust, well-characterised, easily and cheaply assayed, commercially available at a low price, and above all plentiful in a cheap source of hen eggs. It has a high pI of 11.0 and a low M_r 14,600. The pI allows for easy isolation of the lysozyme by ion-exchange chromatography in a single-step, and the M_r allows for a clear-cut qualitative analysis by SDS-polyacrylamide electrophoresis. Bovine serum albumin (BSA) is a serum albumin derived from cows. It is used as a model protein for ion exchange chromatography for the same practical feasibility attributes as lysozyme. BSA has a pI 4.7 and a M_r of 66,500.

If charged groups on an ion-exchanger are titratable, the ion-exchanger is said to be 'weak' (Hagel et al., 2008). If the charge is independent of pH over the range commonly used, the exchanger is said to be 'strong'. Thus, the ion-exchanger being classed as weak or strong has nothing to do with the strength of the interaction.

1.2.5 Commonly used chromatography media

In the following section a critical analysis of currently used resin materials and matrices for chromatography media are evaluated.

1.2.5.1 Matrix supports

Chromatography for the purification of biomolecules are generally carried out in aqueous phase, hence hydrophilic biopolymers are usually used as solid resin supports (Hammond, 1995). In the early days of chromatography, resins were made from polymers such as dextran, polyacrylamide and agarose. While these materials are effective at laboratory scale, they lack the strength to withstand flow velocities required for industrial scale chromatography (Lenhoff, 2011). Desirable features of a solid matrix support are (Giorgio Carta & Jungbauer, 2010):

- High mechanical strength
- Insolubility- absence of toxic leachable
- Hydrophilic character
- Sufficient permeability and a large specific area
- Non-specific adsorption
- Appropriate surface chemistry to attach specific ligands
- Stability in running, elution and storage solutions
- Resistance to microbial and enzymatic attack

Appropriate resins can be developed by cross-linking of different types of natural, inorganic and synthetic materials.

1.2.5.1.1 Natural polysaccharides

Some of the natural polysaccharides that have been used in chromatography matrices are cellulose, dextran, agarose, chitinase and starch. The hydroxyl groups available on surface, even in the interior microstructure, are accessible for chemical modification (Kalia, Kaith, & Kaur, 2011). This is advantageous for increasing the binding capacity of the medium.

First application of natural polysaccharides for biomolecules preparation was reported with cellulose beads by Peterson and Sober in 1956 (Peterson & Sober, 1956). Cellulose is abundant in nature in cell walls of plants (D'Souza et al., 2013). Commercially available celluloses are cross-linked with bifunctional reagents to make them stable against chemical attacks (Hammond, 1995). Cellulose beads have regularly arranged layers which provide acceptable flowthrough in a packed column geometry.

In 1961, dextran based media were also reported for purification of biomolecules (Flodin, 1961). Dextran is a branched chain glucose polysaccharide produced in sugar solutions by various strains of *Leuconostoc mesenteroides* (Hammond, 1995). The key advantage of a dextran matrix is its good linear veliocity due to its rigidity, however it has higher non-specific adsorption. Their use is also limited by their lower porosity (Hammond, 1995).

Another alternative is agarose, a linear polysaccharide present in agar. Its structure contains relatively large voids which allows large biomolecules to diffuse in (Hammond, 1995). They are useful for even passing through cells through the chromatography medium, as used under the trade name of Sepharose 6MB™. The stability of the agarose gel can be increased through cross-linking. Due to the structural nature of agarose it is usually stored in wet or moist state and also needs to be protected from microbial growth. Despite stability issues, agarose is widely acclaimed as the matrix of choice for large biomolecules due to its loose structure, hydrophilic polysaccharide nature and very limited binding of biochemical substances due to a lack of natural charged groups (Lowe, 1979).

In Chapter 3 a comparison has been drawn between the novel microcapillary membranes and Sepharose XL beads which have a matrix structure of 6% agarose with bound dextran.

1.2.5.1.2 Inorganic supports

Inorganic supports can be classified into metals, metal oxides, ceramics and glasses (Weetall & Lee, 1989). Typical examples are silica, controlled pore glass, charcoal, iron and nickel oxides. The exposed hydroxyl groups in these are accessible to biomolecules especially at high pH values (Giorgio Carta & Jungbauer, 2010). Their key advantages are their mechanical strength and large pores that allows for fast flowthrough. They also have a smaller likelihood of being non-specifically attached by microorganisms and enzymes (Hammond, 1995).

However, their limited chemical and physical stability affects the use of a wider range of effluents and buffers for chromatography. They are also not competitive matrix supports for high capacity biomolecules chromatography and hence not widely used in the industry for this application.

1.2.5.1.3 Synthetic copolymers

Synthetic copolymers are cross-linked macroporous polymers in beaded or spherical form with a defined size and porosity. Their inherent mechanical stability gives them good flow characteristics even under high pressures. They are biologically inert hence have a lower likelihood of being attacked by microorganisms and enzymes. Synthetic copolymers can be operated with pressures of up to 7 bar and usually tolerate a wide pH range (Hammond, 1995). Some synthetic polymers have resistance to extreme chemical conditions such as pH, oxidizing environment or autoclaving. Common to all synthetic copolymers is their relative hydrophobicity. Very hydrophobic materials

require coating with hydrophilic materials in order to prevent fouling and low protein recovery (Giorgio Carta & Jungbauer, 2010). Three commonly used synthetic copolymers are polyacrylamide, acrylate and vinyl gels.

Polyacrylamide gels are produced with a range of pore sizes. Commercial polyacrylamide beads are purchased in dry state and are swollen in aqueous solutions for periods of 4 – 48 hours depending on their porosity. Non-specific adsorption to the matrix backbone is restricted to very acidic, very basic and aromatic compounds. Ionic groups on the matrix are almost non-existent and ion-exchange is limited to ionic strengths below 0.02 M. Advantages of these gels are most evident in purification of carbohydrates or carbohydrate-binding macromolecules. (Hammond, 1995)

Acrylate gels are characterised by a high degree of hydrophilicity due to the presence of primary alcohol groups and also of a secondary amide function. They can be used under pressures of up to 2 - 3 bar. They are non-biodegradable, and stable at low (-20 °C) and high (121 °C) temperatures. Denaturing agents have no effect on the gel because its structure involves no hydrogen bonds. It is stable in acidic pH but less stable at high pH (Hammond, 1995).

Vinyl gels have a pressure stability of up to 7 bar. They may be used between pH 1 to 14. The high chemical stability has led to applications at high temperature and therefore they can also be autoclaved. Fractogel TSK™ is particularly suitable for large scale industrial application (Hammond, 1995).

1.2.5.1.4 Summary

Key parameters summarising solid matrix supports are in **Table 1.1**.

Table 1.1 Comparison of solid matrix supports (Giorgio Carta & Jungbauer, 2010; Hammond, 1995).

	Natural polysaccharides (e.g. cellulose, dextran, agarose)	Inorganic materials (e.g. hydroxyapatite, silica, TiO_2)	Synthetic copolymers (e.g. polyacrylamide, acrylate, vinyl)
Solid density	Low (90-96% H_2O)	High (50-80% H_2O)	High (50-80% H_2O)
Mechanical strength	Limited	Good	Good
Porous nature	Smaller pores (gels)	Large pore sizes	Large pore sizes
Functionalization	Easy	Relatively difficult	Relatively difficult
Clean-in-Place	Resistant	Resistant	Resistant
Non-specific binding	Low	Moderate to high	Moderate to high

1.2.5.2 Matrix geometry

Along with the matrix support's material nature, the geometry of the matrix also impacts chromatographic parameters. Most matrix geometries can be placed in a continuum between bead and membrane geometry. Bulk biomolecules are transferred from aqueous phase to the matrix surface by two dominant mass transfer mechanisms, diffusion and convection, as highlighted in **Figure 1.1**. In the bead geometry the dominant mass transfer mechanism is diffusion and in membrane geometry the dominant mechanism is convection.

Diffusion is a thermal movement that is driven by concentration differences and is inversely proportional to the size of the component (D'Souza et al., 2013). Diffusion speed depends on the size and shape of the molecules as well as on the viscosity of the surrounding fluid (Freitag, 2014). Temperature increase leads to faster diffusion

but is normally not an option in chromatography due to the thermo-sensitivity of most proteins. Therefore, diffusion is a process that always takes time and can be accelerated only to a certain extent.

Convective mass transfer is induced by an external force where the mass transfer rate is controlled by external volumetric flow rate, for e.g. by a pump, and is practically independent of molecular size. In conventional chromatography for large biomolecules, mass transfer can be diffusion dependent and consequently their separation resolution and dynamic binding capacity decreases as linear velocity increases (D'Souza et al., 2013).

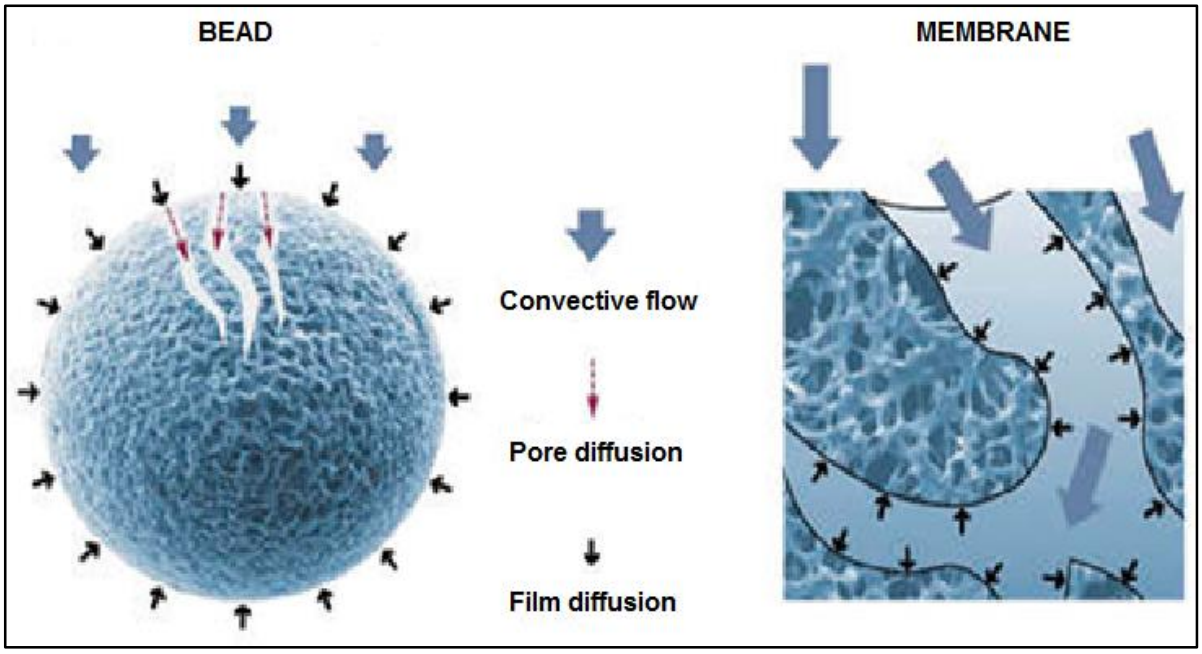

Figure 1.1 Mass transfer mechanism in bead and membrane matrices. In the bead geometry mass transfer predominantly takes place by intra and inter particle diffusion from aqueous phase to smaller pore sizes, dependent on residence time (indicate by small black and red arrows). In membrane geometry mass transfer predominantly takes place by convection where mass transfers from high concentration in aqueous phase to low concentration on the matrix surface. Convection is a faster mass transfer mechanism than diffusion. Adapted from (Fraud et al., 2009; Freitag, 2014; Ghosh, 2002).

Five key chromatography technologies currently used are critically discussed below. Packed, expanded and moving bed columns have a bead based geometry; monoliths and membrane adsorbers are membrane based.

1.2.5.2.1 Packed bed column

Packed bed columns are most widely used in industry, as they are well established in chromatographic theory and their scalability established from laboratory scale (Hagel et al., 2008). They are made from packing conventional beads of specific surface chemistry and dimension into a column format. Packing is conducted in a controlled manner so as not to introduce impurities or air in the column. Problems in the packing process can also lead to cracks in the bed through which channelling takes place, leading to “short circuiting” of sample flow (Ghosh, 2002). The height of a packed bed column is a major limitation due to high back pressure, even at 20 cm bed height (Yu, McLean, Hall, & Ghosh, 2008) . Back pressure limits the linear velocities that can be used for separation across the column. Therefore for scaling up purifications, column diameter is increased to widths of up to 1.2 m (Ghosh, 2002). The surface area of macroporous beads can range between 25 — 800 m^2 g^{-1} with average pore diameters between 20 Å — 500 Å (Fritz & Gjerde, 2009). The number of theoretical plates (N) and residence times are dependent on different separation media, volumes and liquid velocity. A RTP Capto S 20 at a linear velocity of 30 cm h^{-1} has theoretical plates/m packed bed of 5432 N m^{-1} (GE Lifesciences). A MabSelect HiScreen column at 10% breakthrough by frontal analysis at a nominal linear velocity of 100 cm h^{-1} in a column of bed height of 10cm, has a residence time of 6 min (GE Lifesciences). The predominant mass transfer mechanism in a packed bed chromatography resin is diffusion which is relatively slow, leading to long processing times (Hagel et al., 2008). Mass transfer can be increased if the bead size is decreased to increase intra-particle

diffusion, however this further increases pressure drop across the column (Lenhoff, 2011). While extracting bound protein, diffusion-out at elution requires high recovery buffer volume.

Although packed bed columns have limitations especially in pressure drop, packing validation, high processing time and low linear velocities, they are still the most popular in industry. This is because of their high binding capacities and good retention profiles leading to high resolution of components.

1.2.5.2.2 Expanded bed column

The expanded bed resin is suspended by pumped crude feed flow, allowing the resin to expand by upward flow of mobile phase. Target protein is adsorbed on the resin particles, while whole cells and cell debris, amongst other impurities, wash through. This method combines capture of target protein, removal of particulates and initial purification. Expanded bed columns can recover protein from non-clarified feed source. Resin distribution is controlled by varying resin density and size. A Streamline 25 Expanded Bed system (GE Healthcare) has a surface area of 450 m^2 g^{-1}, average pore diameter of 9 nm and number of theoretical plates of 19 N (Li & Chase, 2009). An initial settled bed height of 42 cm had a mean residence time of liquid in the expanded bed of around 28 min (Li & Chase, 2009). Due to the reduction in processing steps, expanded beds can have overall yields over 90% (Hjorth, 1999). Compared to packed beds, they have a shorter processing time and there is less release of host cell protein (HCP) due to reduced shear stress. However, since the biomass interacts directly with resin particles, there can be biomass aggregation that fouls the column. Similar to packed beds, high liquid volumes are required for extracting bound protein (Chase, 1994; Hagel et al., 2008).

Expanded beds are not economically practical for large scale production as the cost of resin and equipment required is more expensive than packed bed technology (Hagel et al., 2008). The resins must be frequently changed due to fouling, and buffer consumption is quite high. Hence both in terms of capacity and costs associated, it is not practical for commercial use.

1.2.5.2.3 Monolith column

Monoliths are chromatography media that are cast as a single block and inserted into a chromatography housing. They are characterized by a highly inter-connected network of channels, sometimes compared to a sponge. Monoliths have a much higher porosity than packed bed columns as they are made up of continuous bed structures. This bed structure is built *in situ* than being produced by the random packaging of beads. A recently developed cross-linked monolith has a surface area of 430 m^2 g^{-1} and a column efficiency of 51000 plates/m (Lv, Lin, & Svec, 2012). A polyethylene glycol diacrylate monolith has a mean through-pore size distribution between 3.52 to 1.50 µm (Aggarwal, Tolley, & Lee, 2012). Their structure leads to short diffusion distances and multiple paths for sample dispersion. Residence time depends on pore size and effects the amount of adsorption. A pore size of about 9 µm requires a residence time of about 1.5 min to overcome mass transfer limitations for BSA (Svec, Tennikova, & Deyl, 2003). This fast mass transfer allows for reduction in process times and increase in recovery rates. The binding capacities of monolith columns vary depending on target protein size. Small biomolecule separations can lead to high back pressure (Gagnon, 2008). When using large biomolecules convective mass transfer and relatively low pressure drops are advantages.

The cost of the monolith technology for scale up and downstream processing of molecules restrict their use to certain applications of large biomolecules (Cramer &

Holstein, 2011; Ghosh, 2002; Jungbauer, 2010; Trilisky, Koku, Czymmek, & Lenhoff, 2009). Their high linear velocity and reduced pressure drop makes them useful for analytical applications where high binding capacity is not needed (Cramer & Holstein, 2011).

1.2.5.2.4 Membrane adsorbers

The development of membrane adsorbers with a range of pore sizes and a chemically modified surface took place in the mid-1980s. Membrane geometry and mass transfer mechanism is described in **Figure 1.1,** dominated by convection. Membrane geometry allows for processing at high linear velocities at low pressures, independent of binding capacity. This reduces processing times and makes it easier for parallel scale up for industrial use. However, membranes do not have as high a binding capacity as packed bed columns due to their lower surface area per unit bed volume (Bhut et al., 2010; Cramer & Holstein, 2011; Klein, 2000). A typical Sartobind membrane adsorber has a surface area of 36.4 cm^2 ml^{-1} membrane volume, an average pore diameter of 3-5 µm, and height equivalent theoretical plates ranging between 0.49 — 0.67. The typical residence time for membrane adsorbers is only a few seconds (Al-Rubeai, 2011). A majority of active binding sites are located inside the macropores/micropores of the resins, resulting in long intra-particle diffusional path-lengths in addition to film diffusion. Also these tiny pores can potentially result in the exclusion of large biomolecules (Orr, Zhong, Moo-Young, & Chou, 2013). Non-uniform membrane porosity can lead to variable flow resistance within the membrane frame and improper convective flow, resulting in early saturation of binding sites in large pores, incomplete utilization of binding sites in small or dead-end pores, and ultimately decrease in dynamic binding capacity of the membrane (Orr et al., 2013).

Membranes are simple to manufacture and hence the cost of stationary phase is reduced (Orr et al., 2013). They are particularly of interest for processing large volumes of dilute stream, polishing processes in antibody and therapeutic protein purifications as well as of large biomolecules such as virus and plasmid DNA (Orr et al., 2013). Their disposable nature, low buffer consumption, and reduced equipment costs, significantly reduce downstream bioprocessing costs (Orr et al., 2013). With their lower binding capacity compared to bead geometries, membrane adsorbers are better applied in bioprocess polishing steps (Hagel et al., 2008). Membrane adsorbers are being developed further for capture steps and have to overcome similar limitations to that of monoliths (Bhut et al., 2010).

1.2.5.2.6 Summary

Conventional chromatography methods such as packed bed columns have mass transfer limitations due to the nature of their bead geometry and material characteristics, resulting in low purification efficiency. Several other innovative matrix geometries such as monolithic columns and membrane adsorbers have been developed for improving chromatography performance. Monoliths can be related as a stack of membrane adsorbers and share a common limitation of low binding capacities due to a reduced surface area.

Table 1.2 summarises and compares the five technologies above for key parameters for preparative chromatography.

Table 1.2 Summary of key parameters that evaluate four key preparative chromatography technologies.

Key parameters	Packed bed column GE SP Sepharose XL®	Expanded bed column Streamline SP® (Hjorth, 1999)	Monolith column Monolithic cryogel (Chen et al., 2008)	Membrane adsorber Pall Mustang S modified Supor®
Packing requirement (Hagel et al., 2008)	Yes	No	No	No
Linear velocity Volumetric flow rate	300-500 cm h^{-1} 2-10 ml min^{-1}	300-500 cm h^{-1} Not available	Not available 1-4 ml min^{-1}	Not available 1-4 ml min^{-1}
Pressure drop	0.15 MPa	0.10 MPa	4.0 MPa	0.55 MPa
Primary mass transfer mechanism (Darton, Reis, Mackley, & Slater, 2011)	Diffusion	Diffusion	Convection	Convection
Dynamic Binding Capacity	160 mg ml^{-1} lysozyme/ adsorbent volume	70 mg ml^{-1} lysozyme/adsorbent volume	4.51×10^{-3} µmol ml^{-1} lysozyme/adsorbent volume	47 mg ml^{-1} lysozyme/ membrane volume
Geometry Scale up	Poor	Good	Good (modular)	Good (modular)
Disposable (Hagel et al., 2008; Sandle & Saghee, 2011)	No	Yes	No	Yes

Novel matrix geometries have been developed in recent years that combine certain properties from these traditional chromatographic technologies, an example of which are nanofibers.

Nanofiber adsorbents are a non-woven fibre matrix produced by electrospinning (Dods, Hardick, Stevens, & Bracewell, 2015; Hardick, Dods, Stevens, & Bracewell, 2015). The morphology appears open with large black spaces between the straight fibre strands. Reported surface areas of nanofibers made of poly(ethylene oxide) and nylon 6 have ranged between 10 — 20 m^2 g^{-1}. The nanofiber diameter can be modified by electrospinning conditions, but for the chromatography studies have an average diameter of 0.5 µm. Nanofibers for chromatography need to be packaged into a cartridge and filter holder format. This module setup itself if scalable by changing the dimensions of the holder or changing the number of compression layers of nanofibers. They can be operated at a range of linear flow velocities between 2000 — 12,000 cm h^{-1}, with the lowest residence time as 0.3 s. The highest pressure drop that these nanofiber cartridges can tolerate is 0.05 MPa. The dynamic binding capacity of the Nano-DEAE is 5.0 mg ml^{-1} BSA/ adsorbent volume and an equilibrium binding capacity of 10.7 mg ml^{-1} BSA/ adsorbent volume. Electrospun nanofiber adsorbents offer the flowrate and mass transfer advantages of membranes for adsorption applications with a comparable surface area and porosity. They are well suited to be setup into continuous chromatography systems due to their tolerance to a high range of linear flow velocities. The low cost production process and biodegradability of cellulose is well suited for single-use disposability.

There is a current trend for the use of single use technologies in bioprocessing. These are sterile, usually made of pharmaceutical grade plastic, and disposable. This replaces traditional bioprocessing equipment and eliminates the steps of recycling,

cleaning and sterilisation such as in the case of clean-in-place (CIP) procedures. Cleaning takes up 20-30% of the chromatography cycle expenditure and accounts for 60-80% total buffer used. Investment in single use and disposable preparative chromatography matrices reduces processing time and manufacturing costs. In terms of regulatory validation, it implements systems that are more reliable, flexible and improve sterility assurance (Brems et al. , 2013; Cramer & Holstein, 2011; Hagel et al., 2008; Sandle & Saghee, 2011).

1.2.6 Microcapillary membranes

1.2.6.1 Ethylene vinyl alcohol as a matrix support

Ethylene vinyl alcohol (EVOH) is a synthetic hydrophilic copolymer with exposed hydroxyl groups. It is widely used in the food packaging industry (Lopez-Rubio et al., 2005) since it is recyclable as post-consumer plastic waste (Marsh & Bugusu, 2007; Mayer et al., 1996). There is a growing interest in this polymer in the fields of biomedical science and water treatment because of its biocompatibility and hydrophilicity (Bonyadi & Mackley, 2012).

Separation applications of EVOH have limited reports in literature. EVOH is a candidate for matrix support since it displays mechanical strength, high thermal stability, chemical and biological resistance and is easy to sterilise (Avramescu, Gironès, Borneman, & Wessling, 2003). Its hydrophilic vinyl alcohol unit and hydrophobic ethylene unit in the molecular structure makes it difficult to be contaminated during protein separations (Zhang, Zhang, Li, & Li, 2009). Hydroxyl groups also provide a suitable chemical platform to chemically attach other functional groups, which would be useful for biomolecules separations.

1.2.6.2 Non-porous microcapillary film

Non-porous microcapillary film (NMCF) were first developed in 2005 by Hallmark et al. (Hallmark et al., 2005). The novelty lies in the hybrid geometry between flat sheet and single capillary fibres. NMCFs have embedded hollow capillaries initially extruded with polyethylene. NMCFs can be extruded in a multiple capillary geometry during the melt extrusion process depending on the chosen dye geometry. Over the years NMCFs have been developed and studied for various applications including organic synthesis (Hornung, Mackley, Baxendale, & Ley, 2007), heat exchange (Hallmark, Hornung, Broady, Price-Kuehne, & Mackley, 2008) and solar heat collector (Dorfling et al., 2010).

In terms of purification applications, NMCFs have been tested for protein purification using cation-exchange chemistry (Darton et al., 2011) and anion-exchange chemistry (Darton et al., 2012). These studies found mass transfer resistance in the NMCF to be low due to convection being the dominant mechanism. Low pressure drops formed across the NMCF length even at high linear velocity ranges of 19,800-99,720 cm h^{-1}. However, the dynamic binding capacity of lysozyme at < 120 µg ml^{-1} was too low for use in preparative chromatography. Whilst having high throughput, low pressures and no packaging requirements as advantages to the NMCF chromatography application, the protein adsorption capacity was fairly low compared to other chromatography materials currently being used in the industry.

1.2.6.3 Hollow fibre membrane

Single hollow fibre thermoplastics are a well-developed technology. Hollow fibres have been developed into hollow fibre membranes (HFMs) using a non-solvent induced phase separation (NIPS) process. HFMs have existed since the 1950s and have been developed for various applications in reverse osmosis, filtration, gas separation with a

range of different polymers (Feng, Khulbe, Matsuura, & Ismail, 2013; Peng et al., 2012). The main advantage of the HFM geometry is the larger effective membrane area per unit volume. It also offers better mechanical support leading to ease of handling comparative to non-porous hollow fibres. Kuraray, a Japanese company has patented and commercialised the fabrication of EVOH hollow fibres mainly for a kidney dialysis application (Yamashita, Tanaka, Tanii, Kubotsu, & Kawai, 1982). HFM have an internal bore size of 1 mm and an outer wall structure that is highly interconnected, bi-continuous and macrovoid free. The outermost region is the densest with pore sizes 0.1 - 0.5 µm, the middle region at 1 µm pores, while the innermost region has the largest pores in the range of 10 - 20 µm (Bonyadi & Mackley, 2012).

1.2.6.4 Microporous walled microcapillary film membranes

Microporous walled microcapillary film (MMCF) membranes are a combination of microcapillary film and membrane geometry. Bonyadi et al. developed a NIPS system to extrude HFM and MMCF (Bonyadi & Mackley, 2012). MMCF has a similar porous microstructure to HFM. The outermost region is the most dense with pore sizes 0.1 - 0.5 µm in diameter, the middle region has pores of 2 - 3 µm pores, while the innermost region goes down to smaller pores in the range of 0.3 - 0.5 µm (Bonyadi & Mackley, 2012). This unique combination of capillary geometry walled with micropores reduces the mass transfer limitations that conventional packed media face of diffusion dependent flow. It is likely the porous nature of the microporous membrane walls and the high throughput capillary geometry gives this novel chromatography medium combined properties of bead and membrane geometries. MMCFs provide easier process handling and efficient module fabrication for scale up. These unique advantages could be potentially advantageous for other applications in biomolecules chromatography and wastewater treatment (Bonyadi & Mackley, 2012).

1.2.7 Quantitative binding capacity analyses

The equilibrium binding capacity (EBC) represents the total theoretical amount of protein that can be bound per unit volume of the medium. It can be measured by modelling bound biomolecule capacity at various biomolecule concentrations, a model such as Langmuir if often used to describe a binding model. It can also be measured by a static method allowing a chromatography matrix to reach binding equilibrium at a defined biomolecule concentration.

However, in downstream bioprocessing under flow conditions a significant proportion of the theoretical capacity is not accessed. The dynamic binding capacity (DBC), the capacity of the medium during flow conditions, is regarded as of a greater practical value to the end user (Darton et al., 2011). For the purposes of this thesis, DBC is taken to be the apparent capacity at 10% column breakthrough, which is typically used in the industry (*Capto™ S, Capto Q, and Capto DEAE*, 2006).

1.2.7.1 Frontal and dynamic binding capacity analysis

Frontal analysis is executed by continuously adding a defined standard protein solution through the module. The component with the least affinity for the stationary phase passes along the module while the component with a greater affinity gets adsorbed to the stationary phase. Eventually this component passes along the module column, when the capacity limit of the stationary phase is exceeded. The frontal chromatogram (also known as breakthrough curve) gives an indication of when the module is completely saturated. When this happens, the concentration of target protein going in, equals the concentration of target protein coming out. It gives a measure of when to stop the loading depending on how much bed remains unused, and how much of the product is lost. Excessive loading gives rise to loss of some

product, whereas insufficient loading leaves the column under-utilized (Bailey, 1986). In an ideal column breakthrough there is a sharp almost perpendicular breakthrough of instantaneous full column capacity adsorption. In reality breakthrough curves look more like **Figure 1.2**.

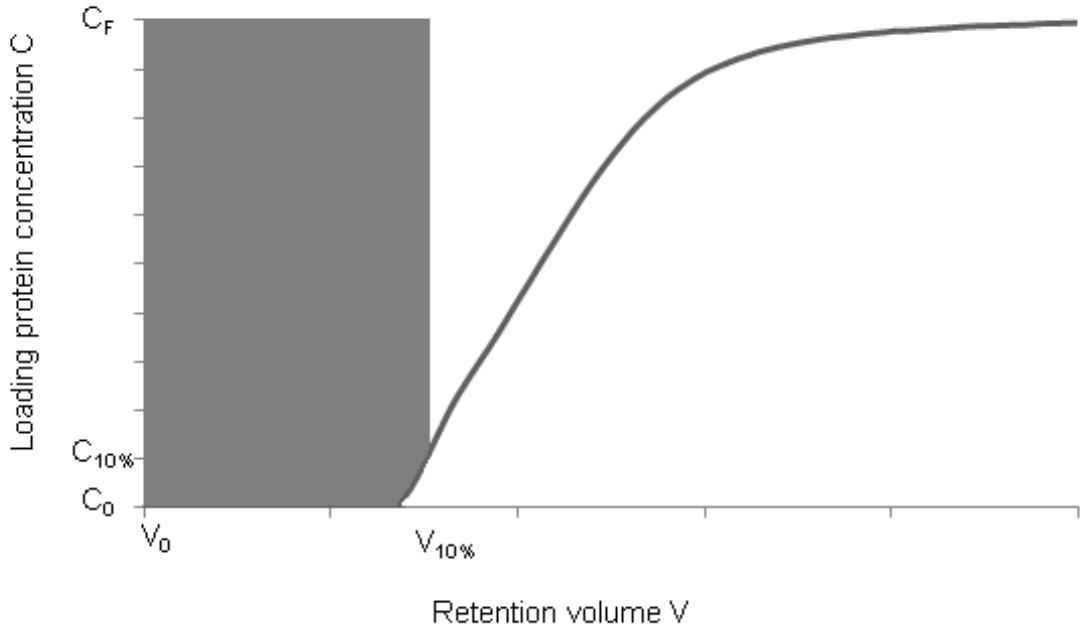

Figure 1.2 Model frontal chromatogram showing the variables required to calculate dynamic binding capacity at 10% breakthrough.

Frontal chromatograms are normally used to measure the dynamic binding capacity of a medium. The column is loaded with a protein solution at a specific concentration and linear velocity. The loading is stopped at a specific percentage breakthrough and the protein is eluted to get the dynamic capacity.

DBC at 10% breakthrough was calculated using **Equation 3.3** (Kosior, Antošová, Faber, Villain, & Polakovič, 2013):

$$DBC_{10\%} = \int_{V_0}^{V_{10\%}} (C_F - C_0)\, dV$$

(**Equation 3.3**)

C_F and C_0 are protein concentrations in the feed and at a specific retention volume V. V_0 is the dead volume and $V_{10\%}$ is the volume of the loaded protein solution at 10% breakthrough $C_{10\%}$. V_0 is the microporous membrane volume and systemic dead volume that is not involved directly in adsorption. This was calculated using a non-modified microcapillary membrane module to measure model protein breakthrough.

Table 1.3 Model calculation of $DBC_{10\%}$ of a straight MMCF module at linear velocity of 10,800 cm h^{-1}

$C_{10\%}$ (mAU)	**Protein area unbound mAU.ml)**	**Protein area bound (mAU.ml)**	**Protein mass bound (mg)**	**DBC 10% (mg/ml)**
245.614	127.719	9220.2294	18.442	13.8

1.2.7.2 Saturation binding capacity analysis

To calculate the saturation binding capacity, the adsorbent surface is loaded with protein till it was near 100% breakthrough and the saturation height in optical density units is recorded. After washing out any non-specifically bound protein, the module is eluted under high salt conditions and the area under the elution peak was integrated. The mass of lysozyme bound was calculated by **Equation 3.4** as per parameters in **Figure 1.3**:

$$Mass\ bound\ (mg) = \frac{C_{inj}\ \left(\frac{mg}{ml}\right) \times Elution\ Area\ (mA.U.ml)}{100\ \%\ saturation\ height\ (mA.U.)}$$

(Equation 3.4)

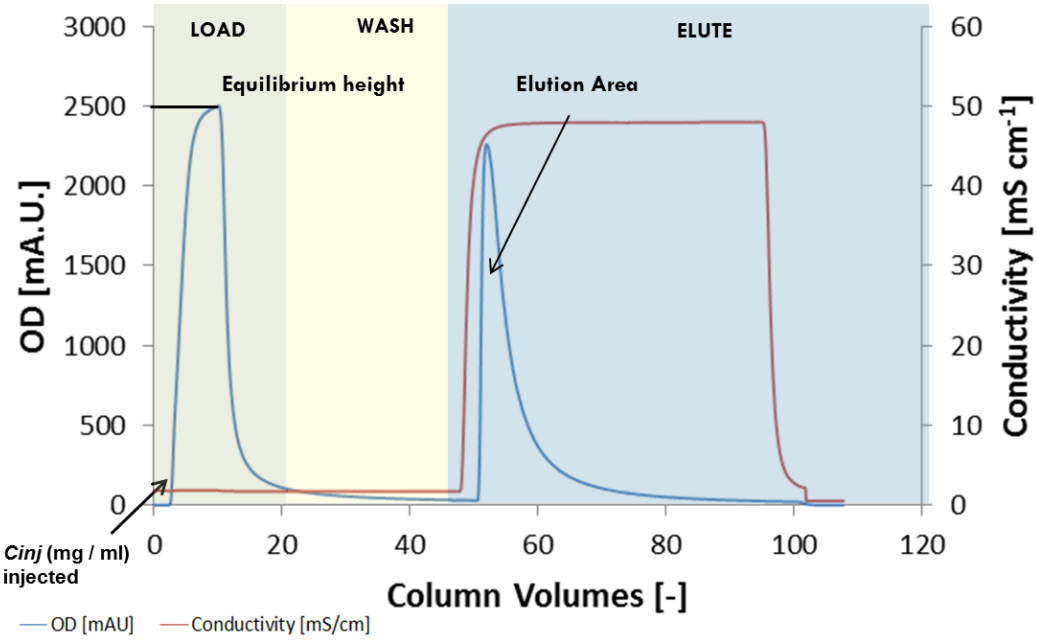

Figure 1.3 Model for calculating mass bound to an adsorbent surface. The equilibrium height is an average over three runs. The blue line denotes the OD mA.U. trace; the red line is conductivity in mS cm^{-1}.

1.2.7.3 Ligand binding density and equilibrium binding capacity analysis

Typically protein binding kinetics is represented using a single or multi-component form of the Langmuir isotherm though other adsorption isotherms accounting for system non-idealities have been applied as well, including multi-site isotherm, random sequential adsorption isotherm, spreading isotherm, and steric mass action isotherm (Orr et al., 2013). When the protein solution is in contact with the adsorbent an equilibrium is achieved between the protein in solution and protein bound to the adsorbent. Any concave adsorbent isotherm is favourable as it means strong adsorption occurs even in dilute solution. Convex adsorbent isotherm on the other hand is said to be unfavourable. As for surface area analysis, for surface ligand analysis the BET equation is not applicable as multiple layers do not form.

Linear isotherms are described by **Equation 3.5**:

$$q = K_d C$$

(Equation 3.5)

Where *q* is the amount of protein adsorbed per amount of adsorbent. *C* is the protein solution concentration and K_d is the equilibrium disassociation constant.

Langmuir isotherm is described by **Equation 3.6**:

$$\theta = \frac{(\alpha C_{inj})}{(1 + \alpha C_{inj})}$$

(Equation 3.6)

Where θ is the fractional coverage of the surface, α is the Langmuir adsorption constant and C_{inj} is the lysozyme concentration used at injection.

The Langmuir equation is based on three assumptions: (i) no protein is adsorbed on the adsorbent surface free from a ligand (ii) one ligand site can only be occupied by one protein molecule (iii) individual ligand sites are independent from each other, i.e. bound molecules do not affect adjacent sites. If the mass bound at different protein concentrations at a particular linear velocity fits the Langmuir isotherm, it can be assumed that the medium fulfils the assumptions stated above.

Equation 3.7 below relates the amount of protein at a certain loading concentration (*q*) to the maximum binding capacity of the medium (q_{max}) (Darton et al., 2011).

$$q = \theta q_{max}$$

(Equation 3.7)

Substituting in **Equation 3.6**, **Equation 3.7** can be rewritten as:

$$q = q_{max} \frac{(\alpha C_{inj})}{(1 + \alpha C_{inj})}$$

(Equation 3.8)

q_{max} represents the binding capacity of the medium at equilibrium i.e. EBC.

1.3 Conclusion

Demands on biomanufacturing have been growing both with new drug candidates and in terms of increasing volume of existing drugs, especially as the biosimilars market is growing. With increasing demand, the production strategy has focused on decreasing costs in upstream processing by increasing product titers. Upstream processing has reached high product yields and the production bottleneck has shifted to downstream processing which needs purification processes capable of dealing with high product concentrations. Early chromatography studies focus on large biomolecules that can be purified in large quantities. The large size of the protein and its penetration of adsorbent material, instability of the protein, and the distribution of binding sites across protein domains are key limitations for large biomolecule separations.

Conventional chromatography methods such as packed bed columns have poor mass transfer and physical characteristics, resulting in low purification efficiency. Conventional purification systems are fairly empirical from bench scale. This limits the batch sizes that can be used, linear velocities and capacities of conventional columns. Several other innovative matrix geometries such as monolithic columns and membrane adsorbers are being developed for improving chromatography performance however they share a common limitation of low binding capacities due to a lower surface area. There is a need for having both high binding capacity and throughput in any novel chromatography medium.

NMCFs have been studied for protein chromatography and whilst having high throughput, low pressures and no packaging requirements, the binding capacity was considerably lower than current chromatography media. MMCFs with their novel

geometry could have a higher binding capacity whilst maintaining high throughput features.

1.4 Aims, Objectives and Thesis Structure

In this thesis the aim to investigate relevant properties of microcapillary membranes, and conduct modifications either through chemical changes in the surface polymer chemistry or by incorporating an inorganic particle, and test for biomolecules separations.

This aim will be reached through the following objectives:

- Investigating the physical nature of microporous capillary membranes and designing a separation module and testing its flow characteristics.
- Studying macromolecular biomolecule purifications via ion-exchange chromatography techniques of cation and anion-exchange chromatography.
- Altering the chemical composition of microporous microcapillary membranes through incorporating inorganic particles and studying if and how they adsorb organic impurities.

In this thesis we firstly investigate the physical nature of microporous capillary membranes in Chapter 2 where we conduct studies on porosity, surface area, module construction, flow studies and residence time distribution. In Chapters 3 and 4, based on the understanding and module development of microporous microcapillary membranes, the surface polymer chemistry is modified and studies for cation and anion exchange chromatography are conducted. In Chapter 5, an inorganic particle activated carbon is incorporated into the polymer structure and physically studies on

the novel membrane structure, and separations using a model dye and humic acid are conducted.

CHAPTER 2 MICROCAPILLARY MEMBRANES MANUFACTURE, CHARACTERISATION AND MODULE ASSEMBLY

2.1 Overview

The aim of this chapter is to describe the production process of microcapillary membranes, and to characterise their porosity and surface area. An additional objective is also to develop these membranes into separation modules, subsequently characterise their flow behaviour and residence time distribution.

Fluid flow study on hollow fibre membrane (HFM) was done in collaboration with Yongjun Kwon, an MPhil candidate I was supervising. The residence time distribution of HFM straight module was done in collaboration with Radu Lazar, a PhD candidate also in Prof Nigel Slater's research group.

2.2 Background

2.2.1 Non-solvent induced phase separation process

Non-solvent induced phase separation (NIPS), a membrane production process, was first developed in the early 1960's by Loeb and Sourirajan (Loeb & Sourirajan, 1964). In this patent, it is used to produce defect-free anisotropic membranes with significantly higher throughput for desalinating brine solutions. The flat-sheet porous membranes are formed from a polymer solution containing a polymer, a good solvent and maybe some additives. This polymer solution is coated as a thin film on a porous mechanical support and immersed into a coagulation bath, consisting of a non-solvent. The polymer film solidifies through exchange between the miscible solvent and non-solvent (Guillen, Pan, Li, & Hoek, 2011). Water is the most commonly used non-

solvent in the external coagulation bath in the NIPS process due to cost and environmental impact reasons.

Bonyadi et al. generate microporosity in ethylene vinyl alcohol (EVOH) polymer using a modified NIPS process (Cambridge solution processing platform as shown in **Figure 2.1** in HFM and microporous walled micro-capillary film (MMCF) membranes (Bonyadi & Mackley, 2012). In HFM extrusion, the polymer solution is pressured through the annular section of the die, whilst a bore fluid is co-extruded out of the central nozzle. The bore fluid is usually a non-solvent or a mixture of a non-solvent/solvent (Baker, 2004). The HFM microstructure differs across the wall, with the inner capillary wall influenced by the bore fluid whilst the outer capillary wall is influenced by the non-solvent in the external coagulation bath. Parameters that also affect hollow fibre membrane extrusions are the type of polymer, polymer solution velocity via the gas pressure, additives used and the air-gap distance (Guillen et al., 2011).

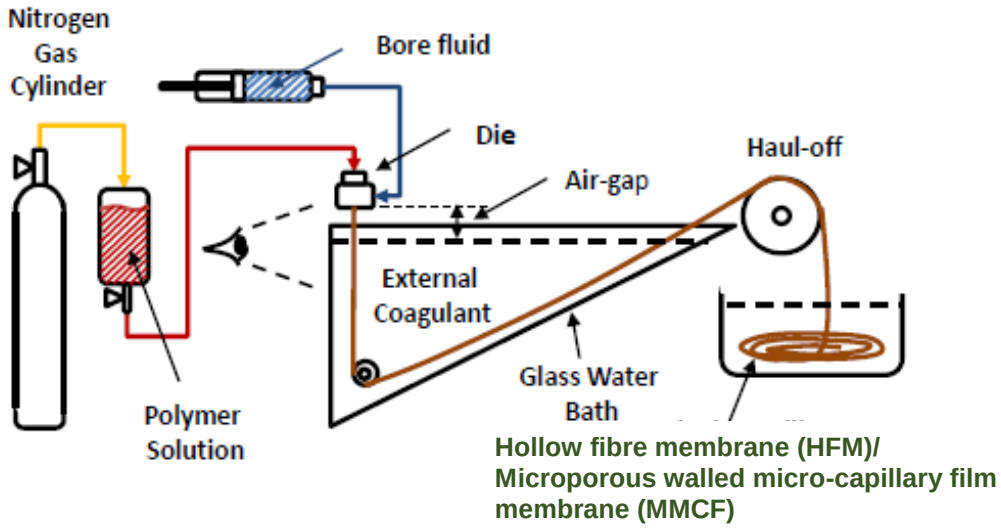

Figure 2.1 Design of the Cambridge solution processing platform (CSPP) (Adapted from Bonyadi et al. 2012).

Bonyadi also studied the macro- and microstructure of the HFM and MMCF membranes after the NIPS process (Bonyadi, 2012). HFM, as shown in **Figure 2.2**,

have an internal bore size of 1 mm and the outer capillary wall is inter-connected and macrovoid free. The inner capillary region has pores between 10 – 20 µm, the middle region has pores approximately of 1 µm size, and the outer capillary region has pores between 0.1 - 0.5 µm. MMCF, as shown in **Figure 2.3,** has inner capillary pores between 0.3 - 0.5 µm, middle region has pores between 2 - 3 µm, and the outer capillary region has pores between 0.1 - 0.5 µm.

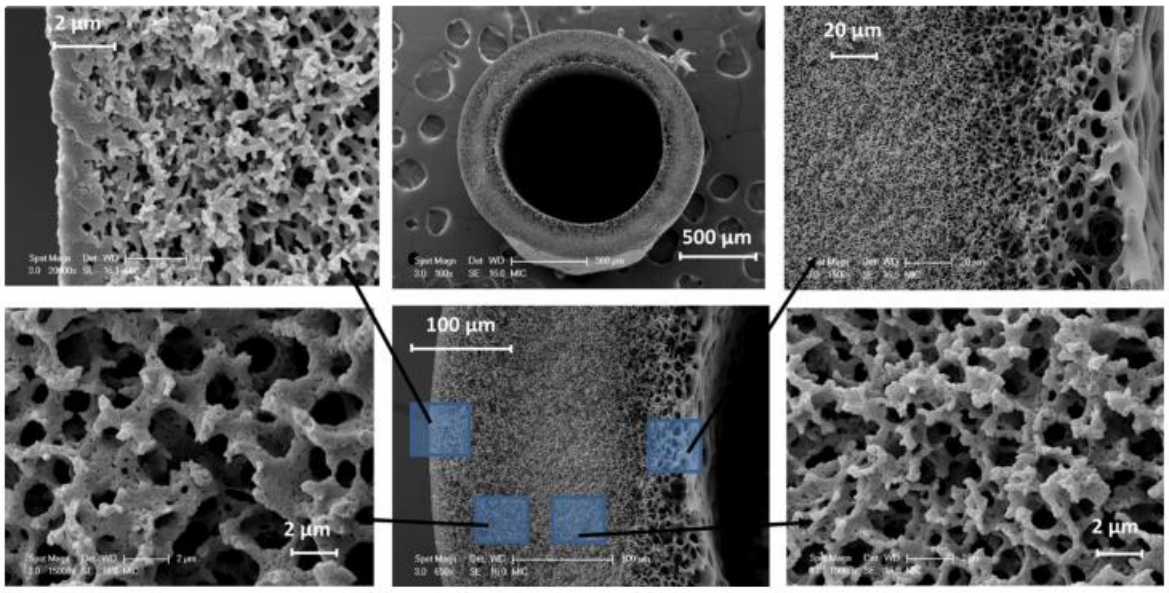

Figure 2.2 Scanning electron microscope images showing HFM cross-sectional microstructure (Photos taken from Bonyadi & Mackley, 2012)**.**

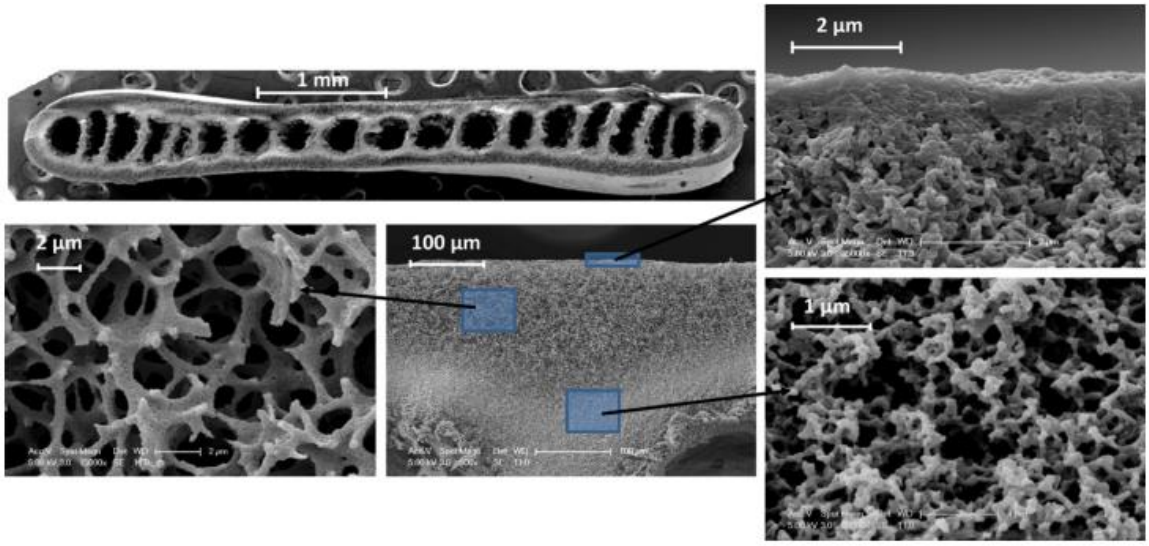

Figure 2.3 Scanning electron microscope images showing MMCF cross-sectional microstructure (Photos taken from Bonyadi & Mackley, 2012)**.**

In this chapter, the microcapillary membranes are reproduced using the NIPS process and studied for their porosity and surface area characteristics using Scanning Electron Micrograph imaging. Their surface area and pore size distribution are studied using mercury intrusion porosimetry.

2.2.2 Fluid flow studies

2.2.2.1 Reynolds number

The nature of fluid flow is important for chromatography to deduce if there is laminar or turbulent flow and how this may affect biomolecule adsorption. The nature of flow affects the interaction between the fluid flow and matrix, and excessive turbulence may cause protein denaturation and in turn affect column performance (Lottes, Arlt, Minceva, & Stenby, 2009).

The Hagen-Poiseuille equation for laminar flow has previously been used for fluid flow studies on the non-porous microcapillary film (NMCF) (Hornung, Hallmark, Hesketh,

& Mackley, 2006). The theoretical pressure drop, Δp, is calculated along column length l_c, diameter d, the fluid viscosity μ, and volumetric flow rate Q_c (**Equation 2.1**):

$$\Delta p = \frac{128 \times l_c \times \mu}{\pi \times d^4} \times Q_c$$

(**Equation 2.1**)

An assumption was made that under continuous flow, the pressure drop across each capillary is identical. Therefore, through each capillary, the flow-rate fraction was proportional to d_c^4. The capillary linear velocity v_c, can be calculated using **Equation 2.2:**

$$v_c = \frac{Q_c}{A_{cs}}$$

(**Equation 2.2**)

Wherein A_{cs} is the cross-sectional area of an elliptical capillary. For each capillary the mean Reynolds number, Re_c, where p is the fluid density is calculated using **Equation 2.3:**

$$Re_c = \frac{v_c \times \rho \times d_c}{\mu}$$

(**Equation 2.3)**

The average of all capillary Reynolds numbers, Re_c, in one microcapillary membrane is termed the mean Reynolds number, Re_m, of the microcapillary membrane.

2.2.2.2 Dean number

Helical module is an assembly wherein the microcapillary membrane is wrapped around a central rod, to add more turbulence to its flow behaviour. Helical modules have been assembled previously with HFMs and shown to increase permeability at the cost of higher pressure drops (Kuakuvi, Moulin, & Charbit, 2000). A similar study

with MMCF membrane to increase turbulence and study its effect on capacity is of interest. Numerical studies of laminar flows in curved pipes has been studied extensively in the literature since the Dean study (Dean, 1928). In a curved central pipe, secondary circulation perpendicular to the main follow occurs, named as the "Dean effect". Dean vortex flow displays similar advantages to Taylor vortex flow but with the additional features of being scalable, not consuming additional energy, and not have sealing difficulties (Woodgate, 2001). Dean vortices have been shown to produce flux enhancement over linear membranes in applications of ultrafiltration of yeast suspensions (Kluge, Rezende, Wood, & Belfort, 1999) and macromolecules (Kuakuvi et al., 2000) (Moulin et al., 1999).

Centrifugal forces are known to cause fluid elements to move towards the outer-wall whilst viscous forces bring the fluid elements back towards the inner-wall. The Dean number is a direct measure of the competing centrifugal and viscous flows that are finally seen as Dean vortices (Doorly & Sherwin, 2009). The Dean number is defined by **Equation 2.4**:

$$De = 4\,Re_D\sqrt{\frac{D}{R_C}}$$

(Equation 2.4)

Where R_C is the radius of curvature, D is the capillary diameter and Re_D is the Reynolds number based on mean velocity and capillary diameter as shown in **Figure 2.4.**

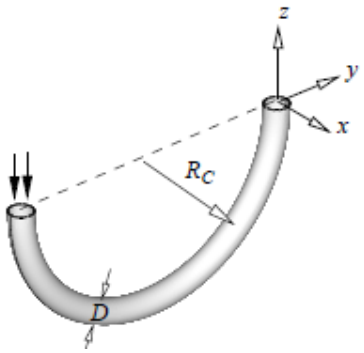

Figure 2.4 Schematic diagram showing a capillary wrapped in a curve, and the key variables R_C radius of curvature, and D the capillary diameter used to calculate the Dean number (Doorly & Sherwin, 2009).

2.2.3 Residence time distribution studies

A residence time distribution study is carried out to quantitatively study the behaviour of a tracer molecule through the pores of a microcapillary membrane. A pulse of a tracer molecule is passed through the column and the retention volume of the peak and the peak broadening is measured as metrics for column efficiency.

Column efficiency is defined by two key parameters:

- Peak broadening determined by an equivalent number of theoretical plates (equilibrium stages)
- Peak symmetry determined by the peak asymmetry factor A_s

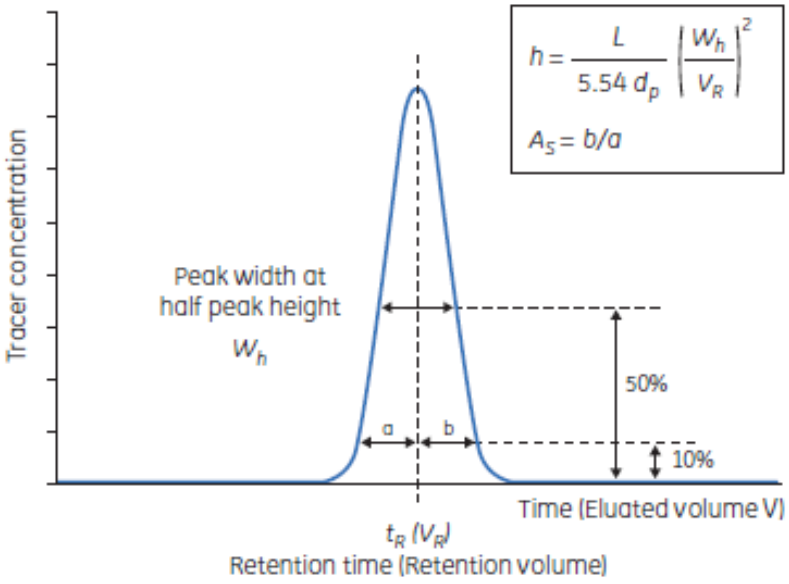

Figure 2.5 Ideal tracer pulse for a residence time distribution study (GE Healthcare, 2010).

The relative peak width is defined as number of theoretical plates (*N*) is calculated as in **Equation 2.5**; height equivalent of a theoretical plate (*HETP*) is calculated as in **Equation 2.6** or reduced plate height (*h*) is calculated as in **Equation 2.7**. The concept of reduced plate height was introduced by Giddings (Giddings, 1964) to standardise behaviour and performance obtained from diverse forms of chromatography. The reduced plate height is the plate height in centimetres divided by the particle diameter in centimetres.

$$N \approx 5.54 \left(\frac{V_R}{W_h}\right)^2$$

(Equation 2.5)

$$HETP = \frac{L}{N}$$

(Equation 2.6)

L is the height of the microcapillary membrane module.

$$h = \frac{HETP}{d_p}$$

(Equation 2.7)

d_p is the average pore diameter. Optimal column efficiency has a reduced plate height of $h \leq 3$.

The asymmetry factor A_S describes the deviation from an ideal Gaussian peak shape and is calculated from the peak width at 10% of peak height:

$$A_s = \frac{b}{a}$$

(Equation 2.8)

An asymmetry factor A_S close to 1 is ideal, but an acceptable range is $0.8 < A_S < 1.8$.

2.3 Materials and Methods

2.3.1 Chemicals

HFM and MMCF matrices were made from EVOH co-polymer (Kuraray, Hattersheim, Germany). N-methyle-2-Pyrrolidone (NMP) was used as a solvent for EVOH. NMP, PVP and glycerol were all purchased from Sigma Aldrich (Dorset, UK). NMP has been commonly used in solution polymer processing due to its strong ability to solubilise polymers, its water miscibility and low environmental impact (Bonyadi & Mackley, 2012). Polyvinylpyrrolidone (PVP) was used as a processing aid and pore forming agent (Wienk et al., 1996). PVP also improves pore interconnectivity and increases hydrophilicity (Guillen et al., 2011), both of these properties are useful for chromatography applications. Glycerol was used as one of the bore fluids, as well as for post-processing storage. Epoxy glue for coating microcapillary membranes was

purchased from Huntsman (Cambridge, UK). The coating polydimethylsiloxane (PDMS) was purchased from Dow Corning (Seneffe, Belgium). Column fittings, adaptors and valves were bought from GE Healthcare (Hatfield, UK). Modelling clay was purchased from Newclay (Devon, United Kingdom). Rhodamine 6G was purchased from Sigma Aldrich (Dorset, UK). The silicone elastomer and catalyst were brought from RS (London, UK). Polyurethane was bought from Onecall Farnell (Leeds, UK).

2.3.2 Production of HFM and MMCF membranes

Micro-capillary membranes were extruded by the NIPS system developed by Bonyadi in the CSPP rig (Bonyadi & Mackley, 2012). The NIPS process and key parameters of the extrusion are briefly described here. Polymer solutions of composition 15/10/75 % EVOH/PVP/NMP were made. The solution was made in a three-neck round bottom flask containing the NMP solvent and the respective compositions of EVOH pellets and PVP powder were stirred in. PVP increased the viscosity of the polymer solution and gave a more even flow through the extrusion dye. The polymer dispersion was heated in a 70°C water bath and agitated for 12 hours to form a homogenous solution. **Table 2.1** describes the specific parameters used for HFM and MMCF membrane extrusions. Further details on the NIPS extrusion as conducted on the CSPP rig is discussed in its standard operating procedure as described in **Appendix 1**.

Table 2.1 Key extrusion parameters for producing HFM and MMCF membranes.

	HFM	**MMCF**
Number of nozzles	1	19
Nozzle size	1.0 mm	0.5 mm
Bore fluid	80/20 % NMP/water	Glycerol
Bore fluid volumetric flow rate	0.5 ml min^{-1}	0.5 ml min^{-1}
Polymer solution mass flow rate	1.5 g min^{-1}	1.4 g min^{-1}
Air gap distance	8 mm	8 mm

The extruded microcapillary membranes were post-treated in water for 2-3 days to complete the phase separation process and to allow for the PVP and NMP release over time. Membranes were then immersed in 50% aqueous glycerol solution for 24 hours and then air dried.

2.3.3 Scanning electron microscopy

Microstructure characterisation to study the microcapillary membrane cross-sections was carried out using a FEI Philips scanning electron microscope (SEM). In order to obtain sharp cross-sections, SEM samples were prepared by fracturing membranes in liquid nitrogen followed by sputter coating with platinum. At least three cross-sections were analysed on Image J for taking pore measurements. 10 different pore sizes were recorded for each cross-section.

2.3.4 Porosimetry studies

Porosimetry is an analytical technique used to determine various quantifiable aspects of a material's porous nature, such as pore diameter and surface area. Mercury

intrusion porosimetry allows one to acquire data on a broad dynamic range from 0.003 µm to 360 µm (Webb, 2001), which is within the known pore sizes of the microcapillary membranes. Measurements were made through analysis from the Micromeritics AutoPore IV 9500 instrument, in duplicate. The Brunauer-Emmett-Teller (BET) theory, which is an extension of the Langmuir theory, was used to measure the surface area.

2.3.5 Construction of chromatography modules

Chromatography modules were designed for usability in commonly used AKTA™ chromatography systems and for them to be comparable in bed height to currently used chromatography columns. The coatings were placed around the microcapillary membranes to stop solvent from leaking from inside of the capillaries and pores to outside of the microcapillary membranes. The coatings, however, had to have the necessary viscosity to prevent them significantly penetrating the outside microcapillary membrane pores. The coatings were also chosen so as to not affect surface modification and purification molecules that were to be used through the module during separations. Various test modules had to be constructed with different lengths of microcapillary membranes and different coatings.

Approximately 250 mm of microcapillary membrane was cut and washed thoroughly with distilled water to remove surface impurities. The microcapillary membrane was placed in an 8 mm circular plastic tube and coated with slow drying epoxy glue. Care was taken to introduce minimal bubbles or air gaps. The ends were trimmed to a 200 mm length and standard AKTA™ column adaptors were fitted (**Figure 2.7)**. A PDMS coating instead of epoxy glue coating column was also constructed for a qualitative flow distribution study. HFM straight modules were constructed to a final length of 10 cm (**Figure 2.6)** as a longer HFM length was too delicate for the above coating method.

A water leak test was conducted using a high pressure liquid chromatography (HPLC) pump (Knauer, St. Neots, Cambridgeshire).

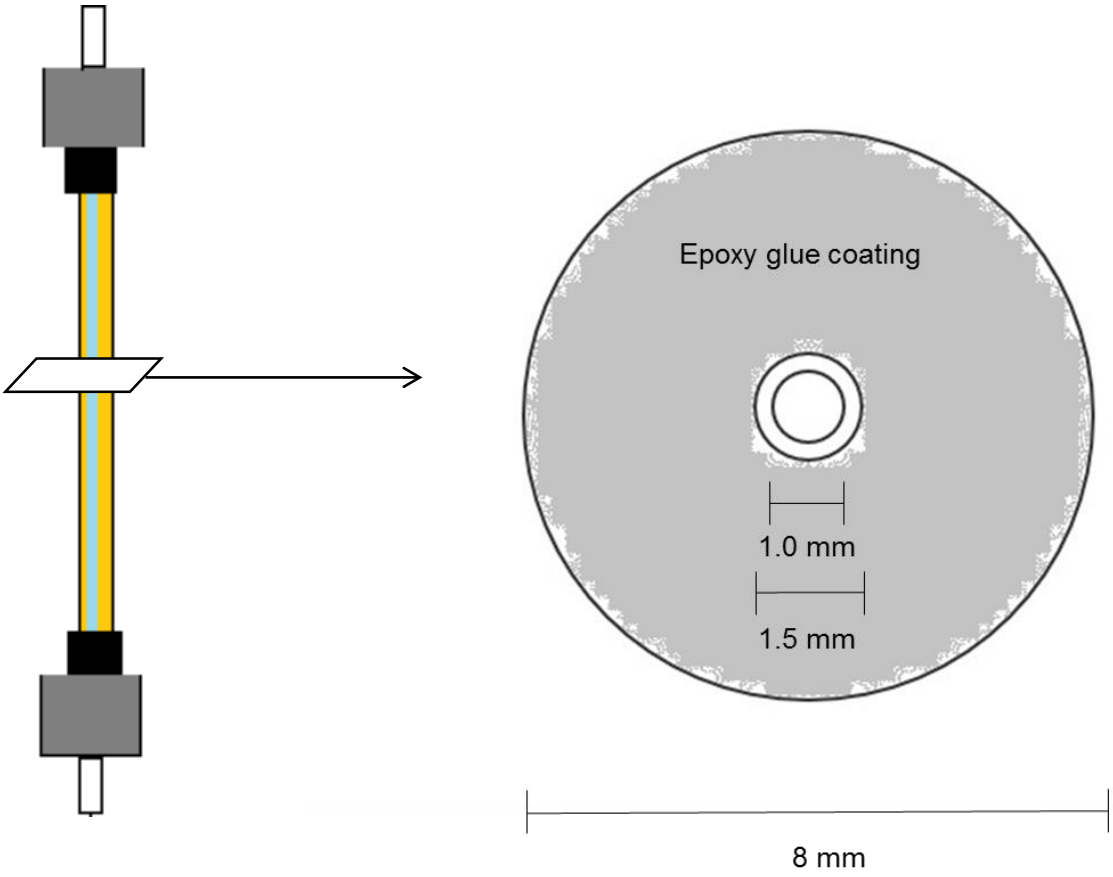

Figure 2.6 Schematic cross-section of a 10 cm HFM straight module coated in epoxy glue coating. The HFM outer diameter is 1.5 mm and inner diameter is 1.0 mm. The HFM membrane is enclosed in an 8mm circular plastic tube.

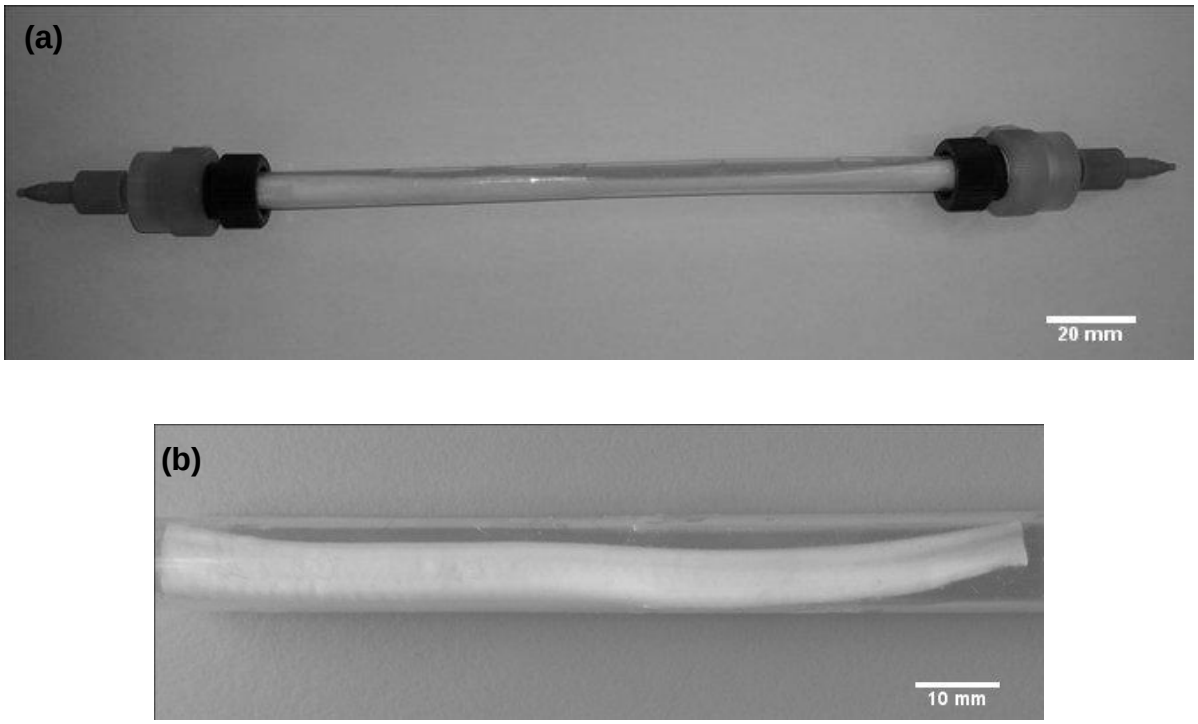

Figure 2.7 Photographs of MMCF membrane in a straight module using (a) epoxy glue coating and (b) PDMS coating.

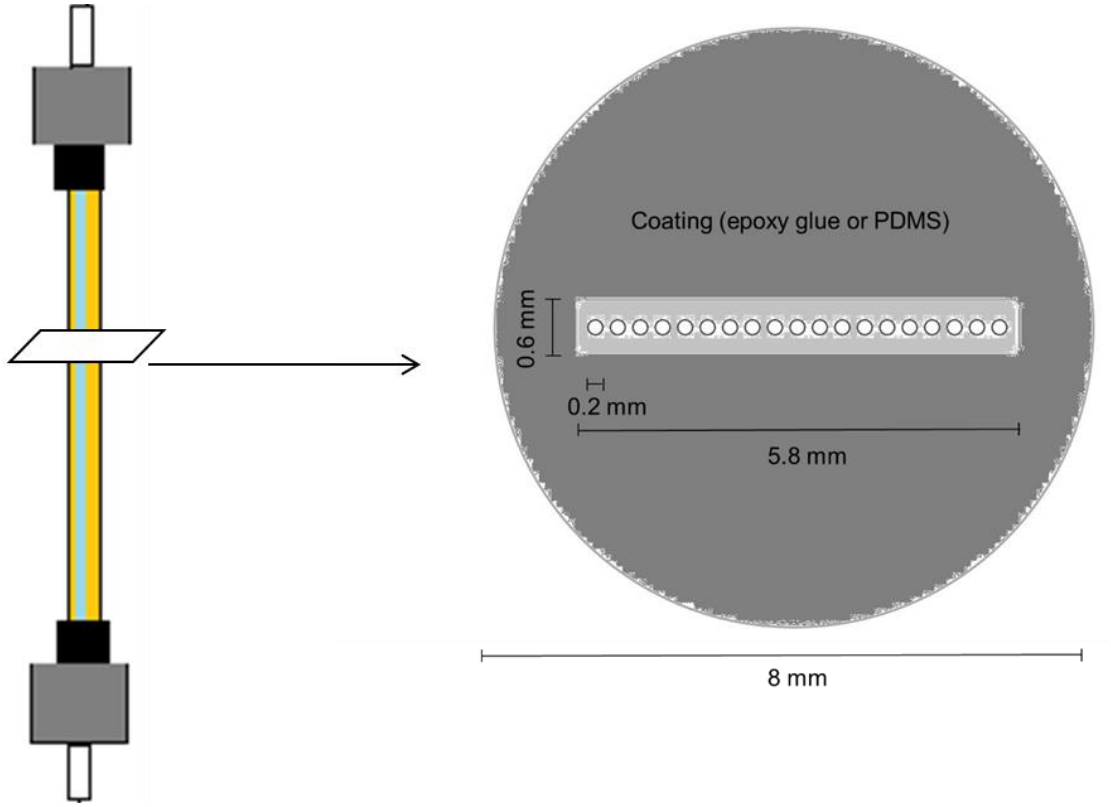

Figure 2.8 Schematic cross-section of a 20 cm MMCF straight module coated in epoxy glue coating or PDMS. The MMCF length is 5.8 mm and breadth is 0.6 mm. The inner capillaries have a diameter of approximately 0.2 mm. The HFM membrane is enclosed in an 8mm circular plastic tube.

A helical module was developed as an alternative module geometry for the MMCF membrane to add further turbulence and decrease flowthrough behaviour. Four different versions of the helical module were assembled before achieving the final successful parameters for mould building and a leak-free module. The helical module was produced through a casting in a mould process. Firstly, the helical module shape was made as shown in **Figure 2.9**. A 19 mm brass rod was connected with standard ¼ inch BSP (British Standard Pipe) fittings on both ends. An 8 mm stainless steel rod was welded on both ends. This was in turn connected to a narrower 6 mm stainless steel rod which would go inside the 19 mm helical module cast to wrap the MMCF membrane. A wooden frame was made for a two-piece silicone mould of dimensions 380 mm by 80 mm by 50 mm. The wooden frame was assembled with screws and G-clamps. Half of the wooden frame was filled with modelling clay. The helical module

shape was pressed half-way into the modelling clay. Registration keys of diameter 9.5 mm were drawn into the clay to help secure and seal the two parts of the mould. A wax based mould release was triple brush coated on the top surface of the modelling clay and helical module shape. Next, the silicon mould was stirred carefully with RTV hardener for vulcanisation whilst avoiding introducing air bubbles. This was poured carefully in the mould frame, again taking care not to introduce air bubbles. After a couple of hours 3 mm hardboard of the mould base dimensions was placed on the back of the silicone mould to give it skeletal strength. The silicone mould was left to set overnight. The mould frame setup was then inverted and the modelling clay was removed carefully. A wax based mould release was triple brush coated on the top surface of the silicone mould and helical module shape. The second half of the silicone mould was set similarly as described above.

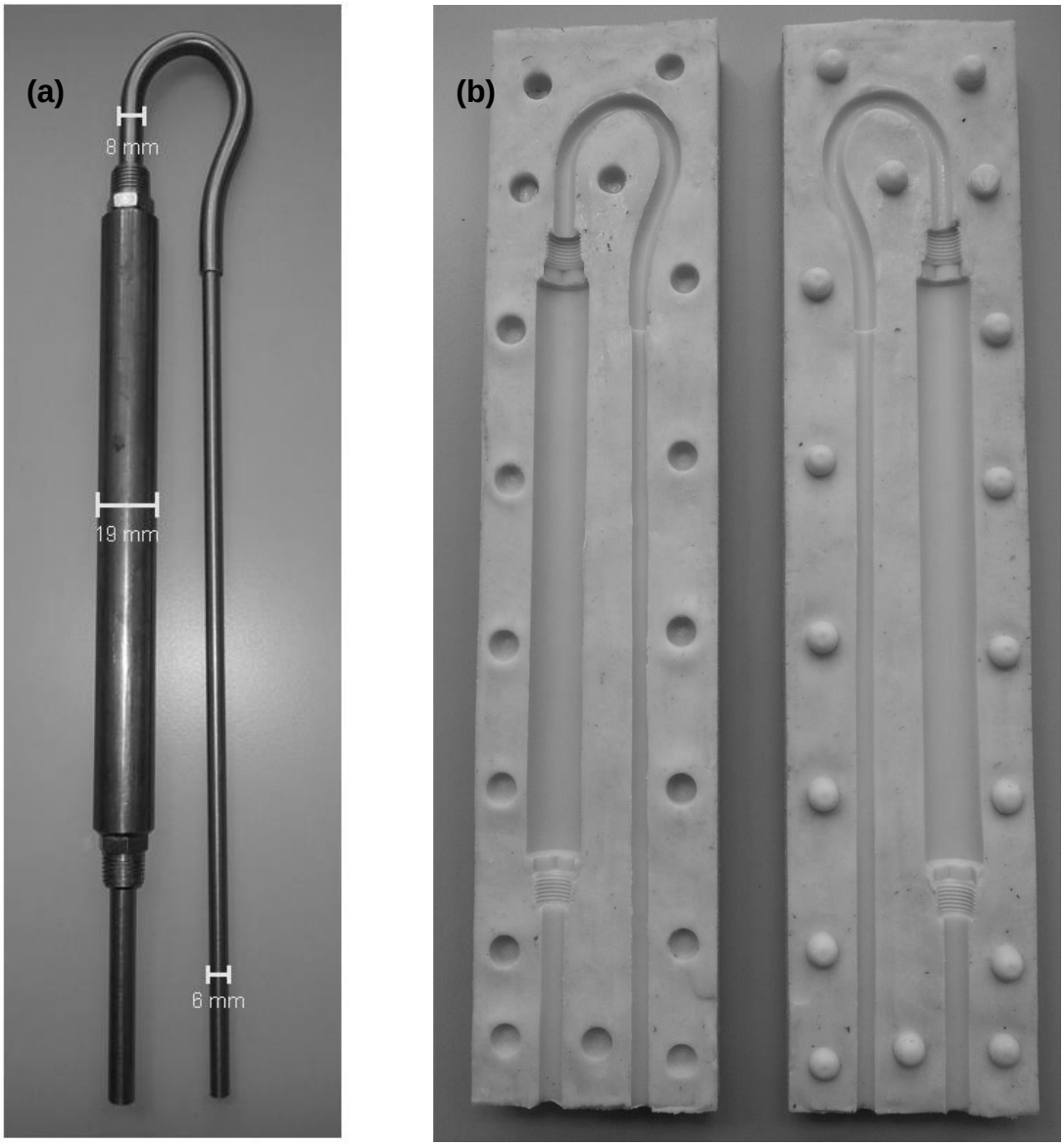

Figure 2.9 Helical module development of (a) model helical module and (b) silicone mould.

Polyurethane (Polytek EasyFlow 60, Kent, UK) was used as a coating for MMCF membrane due to its lower viscosity and ability to be used with the chemicals in ion-exchange chemistry. Silicone mould release was sprayed onto the mould for post-casting release. Polyurethane was mixed and poured into the silicone mould. One of the mould exits was attached to a UV Pump (BOC Edwards, Model MJ12) to remove air bubbles from polyurethane solution. The two-piece mould was closed and held

together with rubber bands. This was allowed to set for couple of hours. Once the first set of solid polyurethane helical module was made, the 6 mm polyurethane rod was used to wrap up 600 mm of MMCF membrane around in a helical fashion. Silicon grease was coated around the MMCF membrane so that polyurethane would not seep into the pores of the MMCF through the outer capillary wall pores. This rod-MMCF membrane setup was placed inside the silicone mould and casted with polyurethane. Standard AKTA column adaptors were attached to the ¼ inch BSP as shown in **Figure 2.10**.

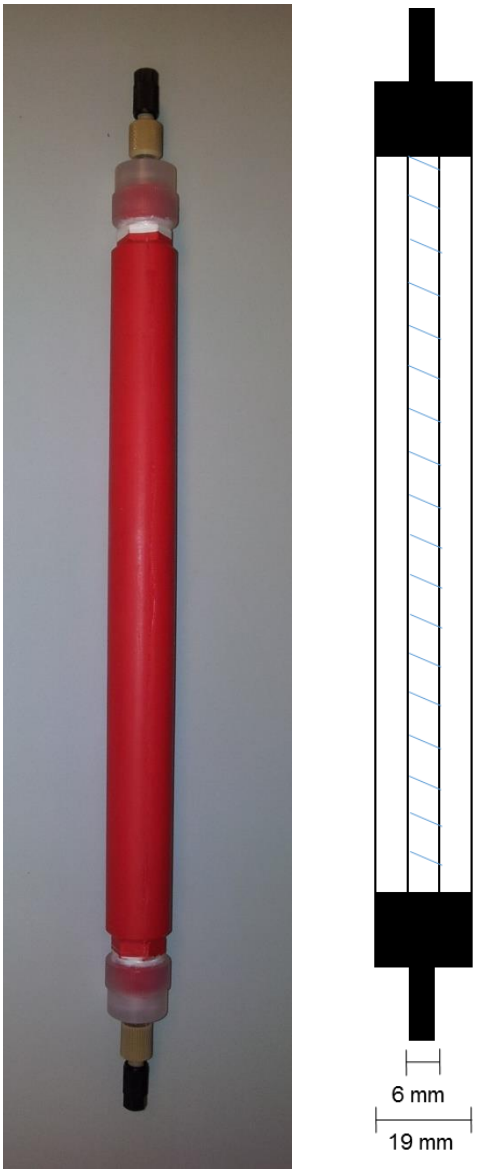

Figure 2.10 A 600 mm of MMCF membrane wrapped within a helical module.

2.3.6 Fluid flow and pressure drop flow studies

Pressure drop experiments were carried out according to Hornung et al. (Hornung et al., 2006) and briefly described here. The pressure drop across the microcapillary membranes was measured using the apparatus in **Figure 2.11.** The modules were connected via a three-way valve to a syringe pump. The pressure at the inlet of the microcapillary membrane module was measured using a pressure transducer (Dynisco, Heilbronn, Germany) and data was acquired via LabVIEW. The

microcapillary membrane module outlet was open to atmospheric pressure and fluid leaving the module was collected and weighed using a Sartorius (Surrey, UK) mass balance to determine the volumetric flow rate. The pressure drop in the rest of the apparatus was neglected due to the relatively large hydraulic diameters of the steel piping used compared to the capillary diameters. Deionised water was used as the test fluid for these studies. These tests were run in triplicate at each different syringe volumetric flow rate.

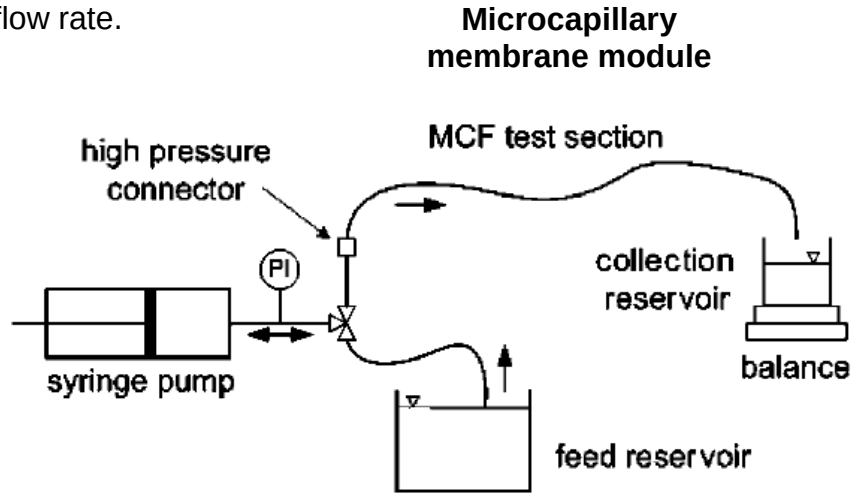

Figure 2.11 Schematic diagram of the apparatus used for pressure drop experiments on microcapillary membrane modules.

2.3.7 Qualitative tracer flow distribution study

The use of confocal laser scanning microscopy (CLSM) in membrane research originated from its novel application to the characterization of resin bead chromatography media. Hubbuch and Kula (Hubbuch & Kula, 2008) recently reviewed the use of CLSM as an analytical tool in chromatography research. CLSM has been used for various purposes such as to visualise protein binding within the chromatographic membrane structure (Reichert, Linden, Belfort, Kula, & Thömmes, 2002) (Wang & Ghosh, 2008), to characterize the morphology of microfiltration membranes (Charcosset, Cherfi, & Bernengo, 2000), as well as to characterize fouling

mechanisms in membranes (Ferrando, Rrzek, Zator, Lopez, & Guell, 2005). The distribution of a tracer dye through pores at flow conditions has been conducted previously (Ng, Kamali-Zare, Brismar, & Bergström, 2008). To date mostly commercial membrane chromatography materials have been examined using the CLSM technique (Reichert et al., 2002; Wang & Ghosh, 2008; Wickramsinghe et al., 2006).

7.5 mg of rhodamine 6G tracer dye was loaded into a straight MMCF module. Triplicate cross sections of 2 mm widths were taken at 1 cm, 8 cm, and 18 cm from the top of the column. The rhodamine 6G was excited at 530 nm and fluorescence emissions were recorded at 552 nm using a Leica TCS SP5 confocal microscope (Cambridge Material Imaging and Analysis Centre).

Figure 2.12 Schematic diagram of a straight MMCF module cross sections used for CLSM flow study.

2.3.8 Residence time distribution study

The residence time distribution study was conducted on a standard AKTA^{TM} Explorer system (GE Healthcare, Hatfield, UK). The system and tubing was firstly primed with deionised water. Fluid flow for the equilibration step was run in the same column direction as the main pulse efficiency test. The connecting tubing was minimal to reduce the external volume to 50 µl. The microcapillary membrane module was equilibrated in deionised water for 1.5 column volumes. The tracer substance and eluent conditions were selected such that chemical interactions with the microcapillary membrane and disturbances of the fluid flow were avoided. The tracer substance was also selected to allow full permeability into the porous structure of the microcapillary membrane medium was possible. The tracer used was 1% acetone in deionised water in a sample loop of 100 µl, with deionised water used as the eluent. The pulse efficiency test was conducted at the lowest possible volumetric flow rate of 0.5 cm h-1 on the microcapillary module. The elution was run till the entire peak had exited the column. The pulse efficiency tests were carried out in triplicates.

2.4 Results and Discussion

2.4.1 Production of microcapillary membranes and porosity characterisation

Low-cost polymers, for e.g. EVOH blends, are used to produce microfluidic devices that are being studied for the capture and adsorptive purification of a biomolecule by conjugation of a functional ligand to the surface of the polymer (Mandal, Townsend, Darton, Bonyadi, & Slater, 2014). The micro-structured film material used in the microfluidic device has a single capillary or multiple capillaries depending on the extruder dye chosen. The microcapillary membranes in this thesis are produced using similar extrusion parameters as by Bonyadi et al. (Bonyadi & Mackley, 2012), hence

proving the NIPS process using the CSPP platform to be reproducible. Each NIPS-based microporous membrane extrusion produced a batch length of up to 5 m. During the course of the PhD research this was repeated successfully four times. From SEM images as in **Figure 2.13**, the porosity studies show a similar macrovoid free and pore size distribution to previous studies.

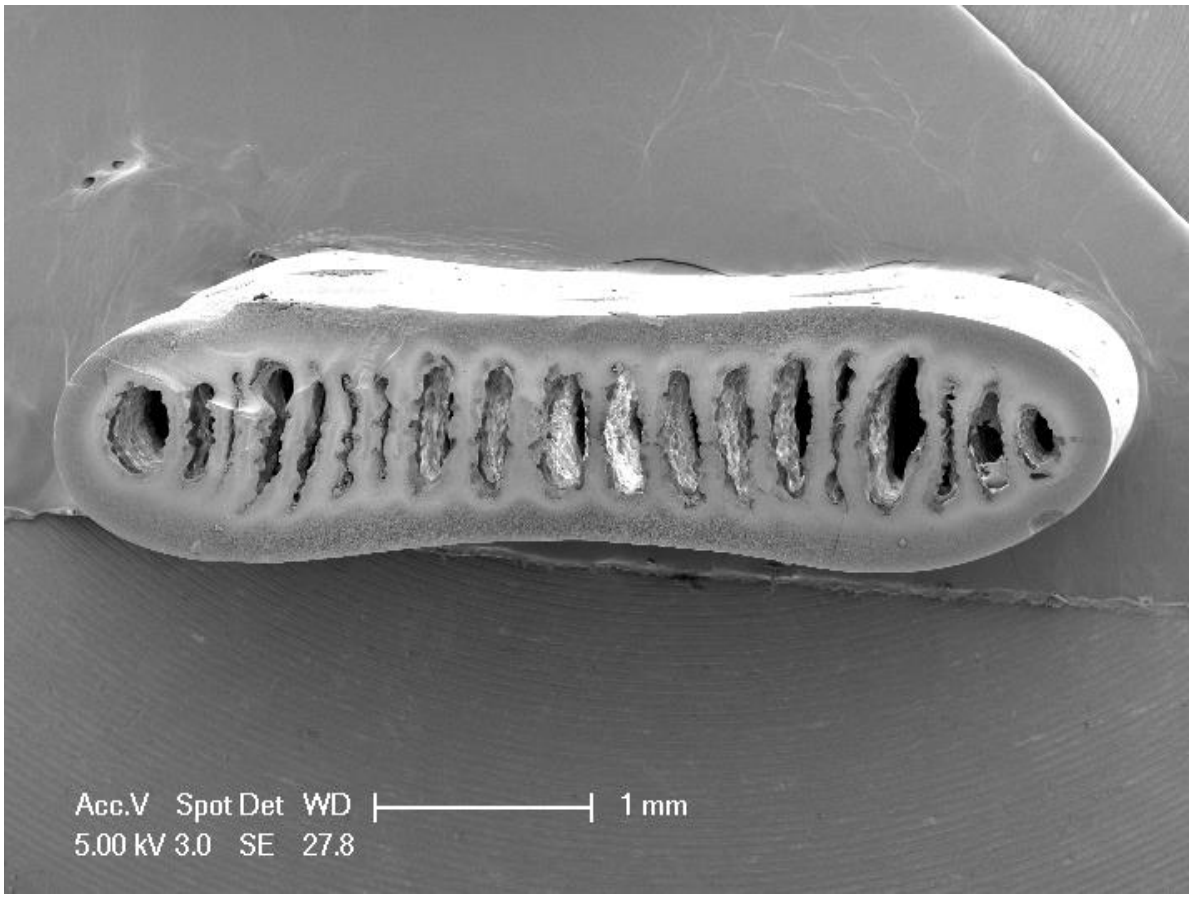

Figure 2.13 Scanning electron micrograph of a transverse cross section of a 19 capillary MMCF membrane.

It can be observed in **Figure 2.13** how the internal capillaries in the MMCF membrane are irregular and elliptical at times. This was also noticed by Bonyadi (Bonyadi, 2012) when increasing the air-gap distance, a larger number of capillaries deform into oval-like shapes. This occurs due to the compression of capillaries in the direction of extrudate width as a result of a compressive force causing extrudate necking.

A key limitation of previous studies using non-porous microcapillary films (NMCF) is the low capacity due to limited surface area. The surface area of the HFM and MMCF microcapillary membranes was measured using a BET analysis. HFM has a surface area of 230.0 m^2 g^{-1} whilst the MMCF has a surface area of 11.01 ± 0.59 m^2 g^{-1}. The MMCF surface area is ~ 425 fold higher than a 5 m NMCF (Darton et al., 2011). However, the BET surface area does not describe the effective surface area available under flow conditions during chromatography. The BET surface area is measured under the conditions of multilayer molecules adsorption, which may or not may not happen depending on the type of purification chemistry. The effective surface areas may be lower due to accessibility of molecules to the pore network (Leinweber & Tallarek, 2003).

2.4.2 Fluid flow studies on microcapillary membrane modules

A linear relationship is obtained between the pressure drop and the volumetric flow rate when the Hagen Pousielle equation is obeyed. Previous flow studies on non-porous microcapillary films (NMCF) show that the pressure drop increases linearly with volumetric flow rate, hence concluding that the fluid flow is laminar (Hornung et al., 2006). The fluid flow through a HFM is also found to be laminar with a Reynolds number of 1300 and pressure drop of 5 bar m^{-1} at a volumetric flow rate of 26.7 ml min^{-1}.

In the MMCF membrane fluid flow study, experimental measurements are compared with theoretical prediction based on **Equation 2.1** and shown in **Figure 2.14.** This study characterises the nature of fluid flow, and also scans for operating pressures and flow velocities the MMCF module tolerates. Deionised water of viscosity 8.94×10^{-4} Pa.s is used as the working fluid on a MMCF membrane length of 0.20 m. The

experimental best fit straight line does not cross through the origin, the pressure drop only kicks in after a threshold volumetric flow rate. This initial low pressure drop is a characteristic of the less pressure across the module due to the module and MMCF geometry. The pressure drop across the straight MMCF module is quite low up to 1.3 bar m^{-1} even at a high volumetric flow rate of 333 ml min^{-1}. For the theoretical prediction, some assumptions are made. Considering the linearity of the experimental measurements, it is assumed the flow is fully developed, laminar and Newtonian. The flow is assumed to be primarily through the diameter of each capillary and negligible flow in between capillaries.

Depending on the air-gap the internal capillaries can be more circular (**Figure 2.3**) or more elliptical (**Figure 2.13**). Multiple MMCF cross-sections were studied and the ones with the more homogenous circular capillaries were selected for further fluid flow and chromatography studies. The mean capillary diameter of 2.17×10^{-4} m is determined from SEM images through Image J analysis.

The theoretical prediction of pressure drop fits the experimental measurements well with a R^2 value of 0.973. A Reynolds number of 76 is calculated for straight MMCF module.

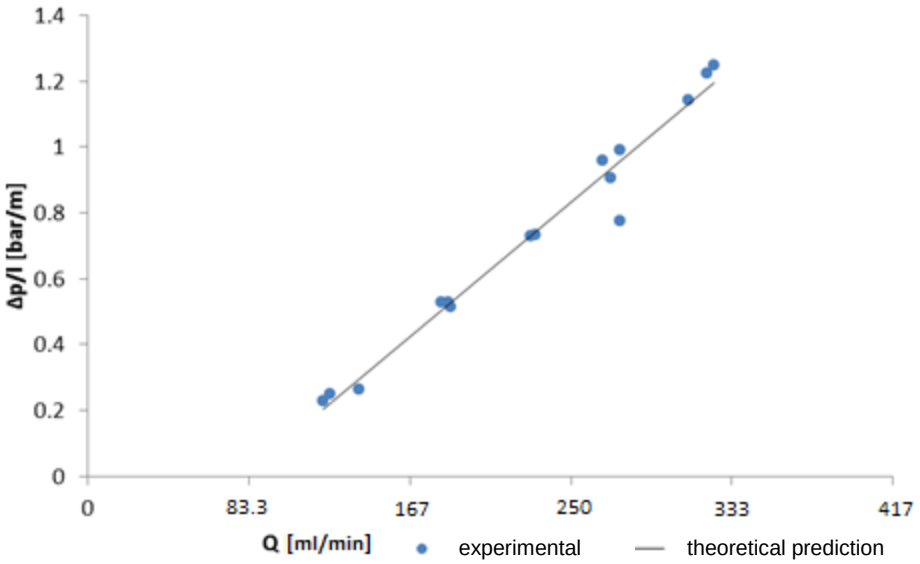

Figure 2.14 Experimental measurements and theoretical prediction of pressure drop, ∆p/l, in straight MMCF module for different volumetric flow rates Q (ml/min), using deionised water as the working fluid (R^2 fit=0.97). This data was modelled with triplicate sample points.

To investigate the effect of curvature on fluid flow, a helical MMCF membrane around a 6 mm polyurethane rod is studied in **Figure 2.15**. The pressure drop across the helical MMCF module is at 120 bar m^{-1}, 90 times higher, at a lower volumetric flow rate 26.7 ml min^{-1}, 12.5 times lower, compared to a straight MMCF module. In the helical MMCF module, at lower volumetric flow rate the pressure drop is much higher than the in the straight MMCF module. This is due to the high back pressure received from the three times longer length of the MMCF used, the helical wound instead of straight MMCF and the higher cross-sectional area of the polyurethane coating compared to the epoxy glue module. Helical MMCF module was produced and tested four times to study reproducibility.

Laminar flow modelling is adequate to predict the theoretical pressure response data. Similar flow and capillary dimensions are made as for the straight MMCF module. The theoretical prediction of pressure drop fits the experimental measurements with a R^2

value of 0.94. A Reynolds number of 99 is calculated for the helical MMCF module. The higher Reynolds number indicates Dean vortices are present. Dean vortices form a secondary flow through the helical MMCF module. A Dean number of 72 is calculated for the helical MMCF module. The dean number indicates the dean vortices are not too strong, and the ratio between the diameter of the rod over diameter of capillary may need to be optimised if the secondary flow needs to be increased. In comparison with other stationary phase materials, such as irregular Lichoprep beads or spherical Kovasil beads, the Reynolds number is four orders of magnitude lower in both straight and helical MMCF modules (Lottes et al., 2009).

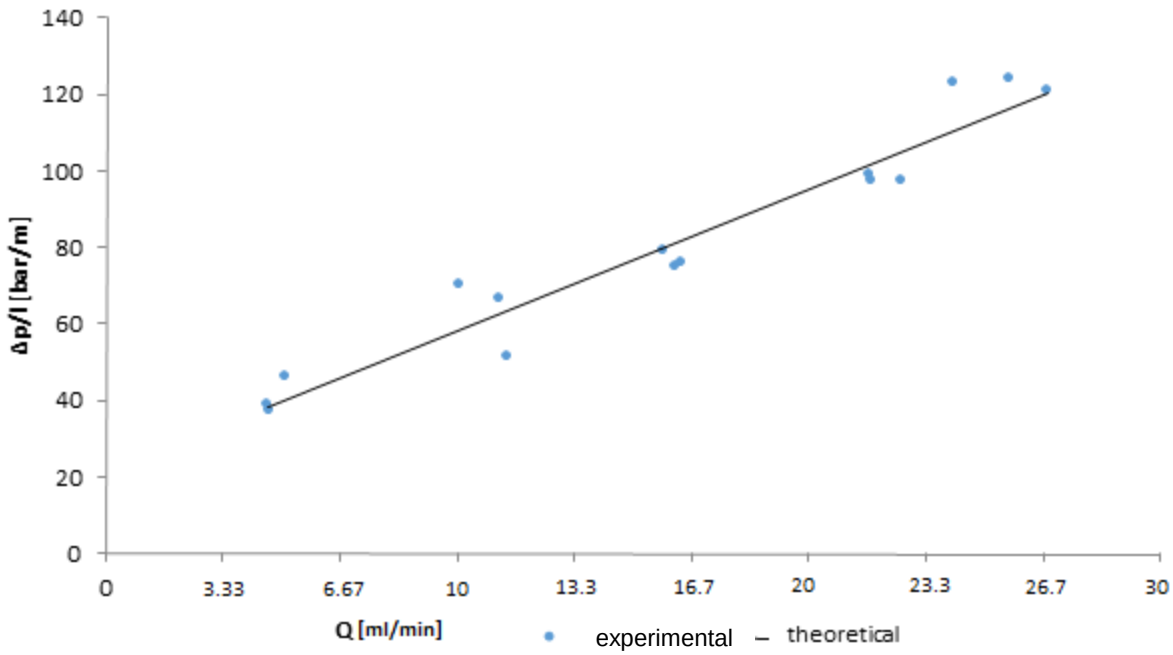

Figure 2.15 Experimental measurements and theoretical prediction of differential pressure, Δp, and pressure drop, $\Delta p/l$, in helical MMCF module for different volumetric flow rates, using deionised water as the working fluid (R^2= 0.94). This data was modelled with triplicate sample points.

2.4.3 Qualitative flow distribution study

Rhodamine 6G is used as a tracer dye to qualitatively monitoring the flow distribution across the 19 capillaries in the straight MMCF PDMS module. Module cross-sections

were imaged in triplicate and the most representative images were analysed. No channelling of flow is observed. The dye penetrates the pores homogenously and distributes over all 19 capillaries in the 1 cm and 8 cm cross sections as seen in **Figure 2.16**. However, when reaching the end of the column at the 18 cm cross section, the flow starts choosing a path of least resistance.

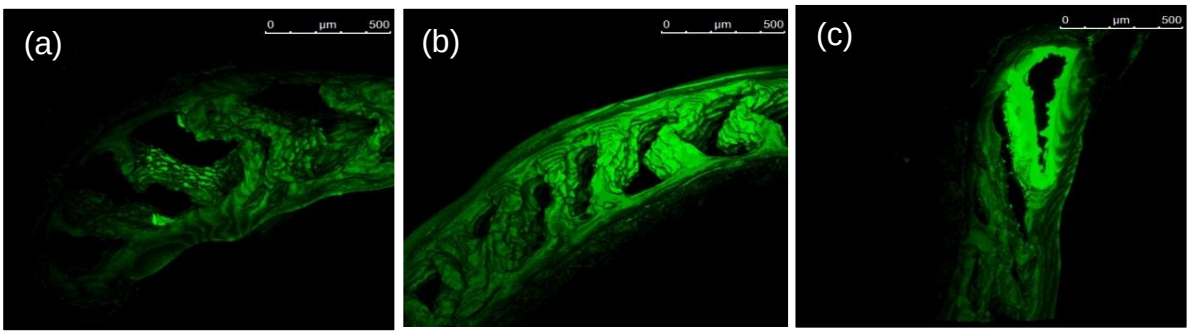

Figure 2.16 Fluorescence trace study of macro flow distribution through straight MMCF module. Rhodamine 6G is represented in green. (a) Cross section 1 cm from the top of the column. (b) Cross section 8 cm from the top of the column. (c) Cross section 18 cm from the top of the column.

2.4.4 Residence Time Distribution

The tracer pulse curves are presented for HFM, straight MMCF module and helical MMCF module (**Figure 2.17**) with key RTD parameters summarised in **Table 2.2**. The tracer pulse curves were obtained in triplicate. The ideal range of the reduced plate height is h ≤ 3 and only the straight MMCF module meets this criterion. High linear velocity led to shorter residence time and peak broadening due to limited diffusion in the HFM and helical MMCF module (GE Healthcare, 2010). The acceptable range for the asymmetry factor is $0.8 < A_S < 1.8$. All microcapillary membranes exceed this criterion and have peak tailing as the acetone tracer molecule is retained in the pores of the MMCF. Especially the helical MMCF module had a wide peak broadening, very high reduced plate height corresponding to a significantly high asymmetry factor. This

is best explained due to the difference in flow behaviour due to dean vortices that are affecting the tracer diffusion through the microcapillary membrane.

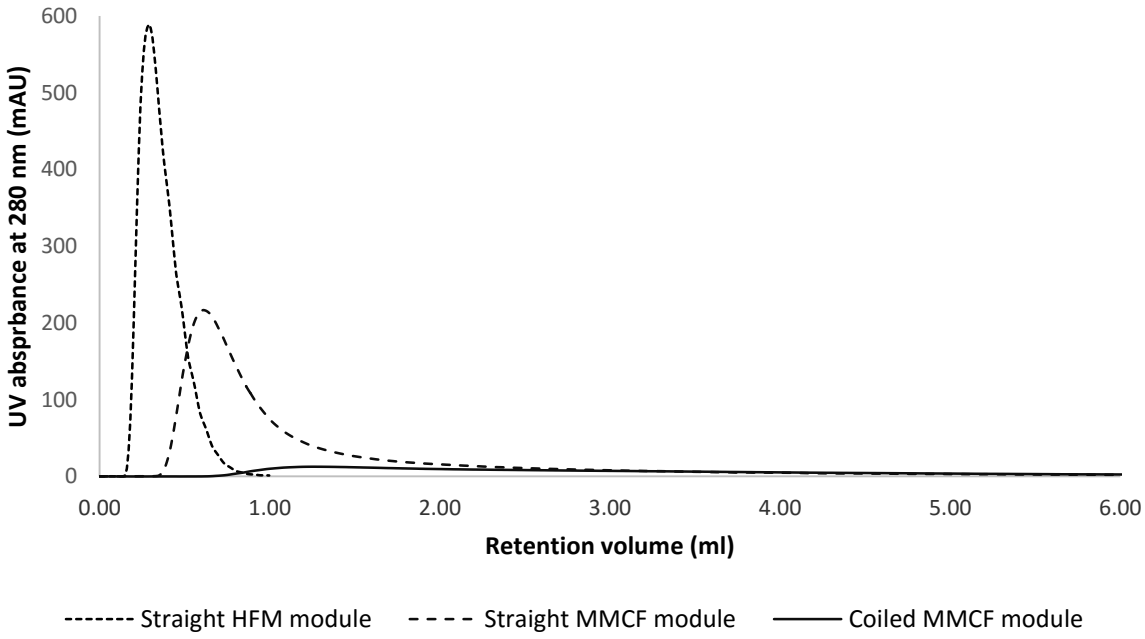

Figure 2.17 Pulse efficiency test on the straight HFM module, straight MMCF module and helical MMCF module using 1% acetone in water at a volumetric flow rate of 0.5 ml min^{-1}.

Table 2.2 Key column efficiency parameters and their comparison between different microcapillary membranes modules.

	Straight HFM module	Straight MMCF module	Helical MMCF module
Reduced plate height (*h*)	4.2 ± 0.5	1.7 ± 0.1	46.8 ± 4.9
Asymmetry factor (A_s)	3.1 ± 0.1	5.0 ± 0.2	12.4 ± 0.4

2.5 Conclusion

This chapter concludes having studied the reproducible production of microcapillary membranes, assembled them into straight and helical modules, and characterised their porosity and other flow behaviours.

Microcapillary membranes, HFMs and MMCFs were extruded from a NIPS process with similar process parameters as described in the literature before, proving it to be a reproducible process. The microcapillary membranes had a similar porosity profile across the outer wall cross-section of larger pores close to the capillary and smaller pores towards the outside wall. HFM BET surface area per unit mass was 230.0 m^2 g^{-1} and MMCF BET surface area per unit mass was 10.59 m^2 g^{-1}.

The microcapillary membranes were assembled into straight and helical modules. Flow studies were conducted on the various modules to understand the degree of laminar or turbulent behaviour with any secondary flows such as dean vortices. A straight MMCF module has a Reynolds number of pressure drop of 1.3 bar m^{-1}. A helical MMCF module had a Reynolds number of 99 and a dean number of 72 indicating dean vortices formation.

A qualitative tracer flow distribution found no channelling of flow with the dye distributed over all 19 capillaries except at the very end of the module. Residence time distribution studies showed that all microcapillary membranes had some degree of peak broadening and tailing.

CHAPTER 3: CATION-EXCHANGE CHROMATOGRAPHY IN MICROCAPILLARY MEMBRANES

3.1 Overview

The aim of this chapter is to develop and study microcapillary membrane modules for cation-exchange chromatography of model proteins. The microcapillary membranes surface chemistry is chemically functionalised with sulfonic acid groups for cation-exchange. A qualitative study of how a rhodamine dye tagged model protein lysozyme adsorbs onto the modified microcapillary membrane is studied. The cation-exchange modified microcapillary membrane modules- straight HFM, straight MMCF and helical MMCF modules, are characterised by their breakthrough curves, dynamic and equilibrium binding capacities. A model separation study is conducted on the straight MMCF membrane module between model proteins lysozyme and bovine serum albumin and analysed for purity of samples.

3.2 Background

3.2.1 Cation-exchange chromatography

In a cation-exchange resin the binding sites are negatively charged, hence only positively charged molecules selectively bind to the resin during loading. An example of a weak cation-exchanger group is carboxymethyl (CM) and a strong cation-exchanger group is sulpho-propyl (SP). In this chapter, SP-MMCF modules are studied against Amersham Biosciences SP Sepharose XL^{TM} adsorbent and Pall Mustang S^{TM} membranes. Sepharose XL^{TM} adsorbent is formed from a highly cross-linked bead formed of 6% agarose matrix. Dextran chains are coupled to the agarose matrix and SP groups are attached to this through stable ether bonds. The SP Sepharose XL^{TM} matrix requires column packing, operates between linear velocities 300 – 500 cm h^{-1} at a maximum pressure of 0.15 MPa and a dynamic binding capacity

at 10% breakthrough of 160 mg ml^{-1} lysozyme/ adsorbent volume. The Mustang S™ membrane has a polyethersulfone (PES) base modified with SP groups. The membrane requires no column packing, operates between a volumetric flow rate of 1 – 4 ml min^{-1} at a maximum pressure of 0.55 MPa and a dynamic binding capacity at 10% breakthrough of 47 mg ml^{-1} lysozyme/ membrane volume. With the high cost of Protein A, and monoclonal antibody titres in excess of 10 g L^{-1}, cation-exchange membranes are now also being studied as an alternative to Protein A affinity capture step for preparative scale downstream processing (Tao et al., 2014).

The methodology for developing ion-exchange chemistries is often proprietary to suppliers, and hence there is limited information in literature about surface chemistry synthesis of commercial membranes. Peterson and Sober directly introduced anion and cation exchanger groups onto a cellulose resin matrix (Peterson & Sober, 1956). The disadvantage with direct attachment is poor performance due to limited association between the ion-exchanger group and the protein. Müller describes attaching ionic groups indirectly through linear polymer chains grafted on the resin surface (Müller, 1990). Indirect attachment groups increase both capacity and selectivity, but involve complex intermediate chemistries. McCreath et al. incorporated charged ion exchanger groups using cyanuric chloride (McCreath, Owen, Nash, & Chase, 1997).

The McCreath et al. surface chemistry modification method was used in a non-porous microcapillary film (NMCF) device for SP and Q chemistries (Darton et al., 2012, 2011). The SP-NMCF device requires no column packing, operates between linear velocities 19800 – 99720 cm h^{-1} at a maximum pressure of 2.0 MPa and a dynamic binding capacity at 10% breakthrough of 0.001 mg ml^{-1} lysozyme/capillary volume (Darton et al., 2011). Although the NMCF device has a high throughput and can

tolerate a high pressure, its dynamic binding capacity is relatively low for applications in preparative scale chromatography.

HFM has been used for purification and concentration of lysozyme as an ultrafiltration system (Mayani, Filipe, & Ghosh, 2010). Ion-exchange resins were loaded into the polymer membrane itself (Avramescu, Borneman, & Wessling, 2008) and by surface modification (Camperi et al., 1999). HFMs have not yet been tested for protein chromatography.

3.2.2 Qualitative ligand distribution of ion-exchange chemistry

Once a novel matrix is modified for ion-exchange chromatography it is important to study the charged ligand distribution across it. A qualitative visualisation of the ion-exchange ligand distribution is possible through a dye tagged model protein binding to the novel matrix surface.

NHS-Rhodamine is an amine-reactive fluorescent labelling regent that has an excitation wavelength of 552 nm and emission wavelength of 575 nm. N-Hydroxysuccinimide (NHS)-ester labelling reagents are most commonly used for labelling proteins. NHS esters react efficiently with primary amino groups ($-NH_2$) in pH 7-9 buffers to form stable amine bonds. Proteins have several primary amines in the side chain of lysine residues that are available as targets for NHS-ester reagents.

Quantification of model protein and dye conjugation is essential for predicting the amount of probe necessary for an experiment and for controlling fluorescence intensity between experiments (Thermo Scientific, 2008a). The degree of labelling may be calculated by separately determining the protein and fluorophore molar concentrations of the conjugate based on absorbance measurements and then expressing these concentrations as a ratio. The ratio represents the average number of dye molecules

conjugated to each protein molecule; some individual protein molecules in the solution have greater than the average number of dye molecules and others will have less. Labelling reactions are influenced by the molar ratio of the reactants, contaminants, and the activity of the labelling agent.

A 1 cm path length cuvette is used to measure absorbance of the labelled rhodamine at 280 nm and 555 nm (Thermo Scientific, 2008a).

The concentration of the protein in the sample is calculated using:

- $\varepsilon_{protein}$= lysozyme molar extinction coefficient = 37500 M^{-1} cm^{-1} (Lundblad & Macdonald, 2010)
- A_{max}= A_{555}
- CF= Correction factor= $\frac{A_{280}}{A_{max}}$

$$Protein\ concentration\ (M) = \frac{A_{280} - (A_{\max} \times CF)}{\varepsilon_{protein}} \times dilution\ factor$$

(**Equation 3.1)**

The degree of labelling is calculated using:

- ε'= Rhodamine molar extinction coefficient= 80000M^{-1} cm^{-1}

$$Moles\ fluorophore\ per\ mole\ protein$$

$$= \frac{A_{max} of\ the\ labeled\ protein}{\varepsilon' \times protein\ concntration\ (M)} \times dilution\ factor$$

(**Equation 3.2)**

3.3 Materials and Methods

3.3.1 Chemicals

Sodium hydroxide (NaOH), cyanuric chloride, acetone, sodium phosphate (Na_2HPO_4), 3-amino-1-propanesulphonic acid (SP), tris(hydroxymethyl)aminomethane (Tris), hydrochloric acid (HCl), chick-egg lysozyme (pI 11, MW 14.3 kDa), BSA (pI 4.9, MW 67.0 kDa), Rhodamine 6G, phosphate buffered saline solutions (PBS, 135mM, pH 7.2), sodium chloride (NaCl) were all purchased from Sigma Aldrich (St. Louis, Missouri).

3.3.2 Surface modification of microcapillary membranes with sulfonic acid groups

The microcapillary membrane modules were functionalised for cation-exchange functionality by methods developed by McCreath et al. and Darton et al. (Darton et al., 2011; McCreath et al., 1997). Briefly, the microcapillary membrane was first activated by flowing 30 ml of ice cold NaOH (1 M) in an ice bath for 30 minutes using a high pressure liquid chromatography (HPLC) pump. This increased the nucleophilicity by introducing alkoxide groups on the vinyl alcohol on the plastic surface. Subsequently, 20 ml of ice cold cyanuric chloride (50 mM) in acetone was passed through the microcapillary membrane in an ice bath for 20 minutes to attach the linker onto the activated EVOH surface. The microcapillary membrane was then washed with 10 ml of ice cold deionised water in an ice bath for 10 minutes. For the covalent attachment of SP groups to the activated surface of microcapillary membrane, 20 ml of Na_2HPO_4 (1 M) containing 1 g 3-amino-1-propanesulphonic acid in a 40 ºC water bath was left circulating through the microcapillary membrane module overnight. Following this step, the water bath temperature was increased to 60 ºC for 5 hours, after which 20 ml of deionised water was flowed through the SP modified microcapillary membrane

module for 20 minutes. Finally, the module was washed with 20 ml of NaOH (0.4 M) for 20 minutes followed by 20 ml deionised water for another 20 minutes. The modified microcapillary module was stored at 4 ºC in 20 mM Tris–HCl pH 7.2 or 20% ethanol for long term storage (Darton et al., 2011; McCreath et al., 1997).

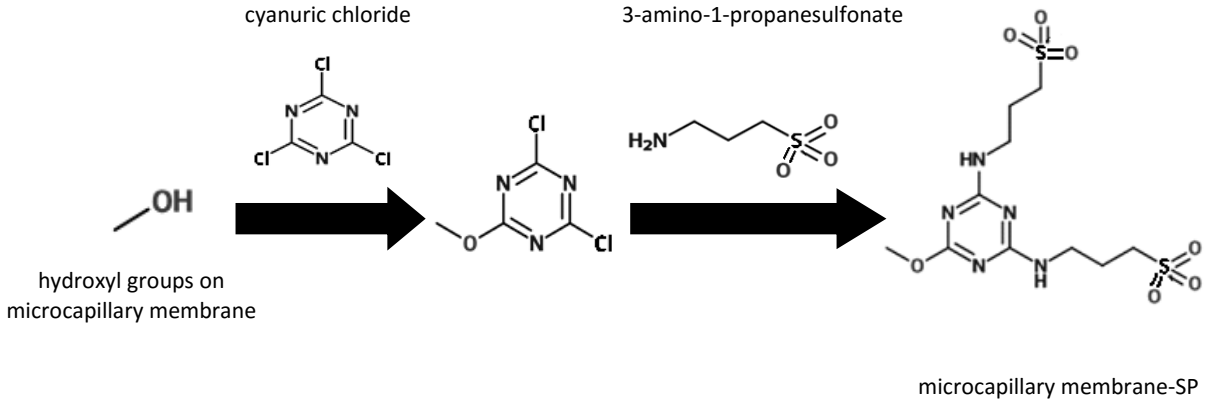

Figure 3.1 Schematic diagram showing the microcapillary membrane surface modification for SP cation-exchange chemistry (Darton et al., 2011; McCreath et al., 1997)

Modifications were made to the McCreath et al. method to allow the chemistry to interface appropriately from the solution chemistry to chemistry within the microcapillary modules. All the chemistry steps were undertaken of a HPLC pump at a volumetric flow rate of 1 ml min^{-1}. The final wash steps with distilled water and 0.4 M NaOH were all timed to 20 minutes each.

It was noticed that the cyanuric chloride in acetone was a rate limiting step. This is because acetone solvent is volatile at room temperature and would sometimes block off the HPLC pump and stall the flow of chemistry. The MMCF could not be exposed to acetone for an extended period of time as well as it easily dissolves EVOH matrix. To have better control of this chemistry linker step, the pump system was purged every 5 minutes.

Minor modifications for the helical MMCF module were made. The cyanuric chloride concentration was increased to 100 mM. The module was also washed for more than 10 min to wash out as much of the unreacted cyanuric chloride. The organic solvent also had to be changed from acetone to acetonitrile, as acetone was found to dissolve polyurethane. Control experiments were conducted between cyanuric chloride in acetone verses acetonitrile in a straight MMCF module and no loss of capacity was found.

The HPLC pump was also run at a range of volumetric flow rates between 0.1 ml min^{-1} to 1 ml min^{-1} to study if the lower volumetric flow rates, aid better diffusion of chemical molecules and improved capacity. Significant changes in capacity were not noted.

Many of the derivatisation steps between the NMCF and MMCF were kept consistent, for comparable analysis only dependent on level of porosity and surface area.

3.3.3 Qualitative ligand distribution study

A study of the distribution of the cation-exchange surface chemistry across the pore surfaces of the MMCF module was conducted using a qualitative dye tagged model protein distribution study. The labelling experiment was conducted according to the NHS-Rhodamine instruction manual (Thermo Scientific, 2008b). NHS-Rhodamine, dimethyl sulfoxide (DMSO), PBS buffer as conjugation buffer, Zeba Spin Desalting Columns were all purchased from Thermo Scientific (Rockford, USA).

1 mg ml^{-1} of model protein lysozyme in PBS buffer was prepared. The NHS-Rhodamine was equilibrated at room temperature before opening. It was dissolved at a concentration of 10 mg ml^{-1} in DMSO. 3.5 µl of NHS-Rhodamine was added to 1 ml of the 1 mg ml^{-1} lysozyme solution. The reaction was incubated at room temperature

for 1 hour. The non-reacted excess NHS-Rhodamine was removed using a Zeba spin desalting column according to the instruction manual (Thermo Scientific, 2012). The column's bottom closure was twisted off and the cap was loosened. The column was placed in a 15 ml falcon collection tube. The column was centrifuged at 1000 × g for two minutes to remove storage solution. A mark was placed on the side of the column where the compacted resin was slanted upward. The column was placed in the centrifuge with the mark facing outward in all subsequent centrifugation steps. 2.5 ml of ultrapure water was added to the column. The column was then centrifuged at 1000 × g for two minutes. The last two steps were repeated three more times. The column was placed in a collection tube, the cap was removed and the reaction solution was added to the centre of the compact resin bed. 100 µl of ultrapure water stacker was added to the resin bed after the reaction sample was fully adsorbed, to ensure maximal rhodamine tagged lysozyme recovery. The column was centrifuged at 1000 × g for two minutes to collect the sample. The rhodamine labelled lysozyme was stored at 4°C and protected from light.

The dye tagged protein was loaded onto a straight MMCF module made in PDMS coating. Cross sections were taken 10 mm (top), 50 mm (middle) and 80 mm (bottom) from one end of the module, in triplicate. Confocal laser scanning microscopy (CSLM) was conducted using a Leica TCS SP5 confocal microscope (Cambridge Material Imaging and Analysis Centre).

3.3.4 Quantitative binding capacity analyses

3.3.4.1 Frontal analysis, dynamic binding capacity, saturation binding capacity studies

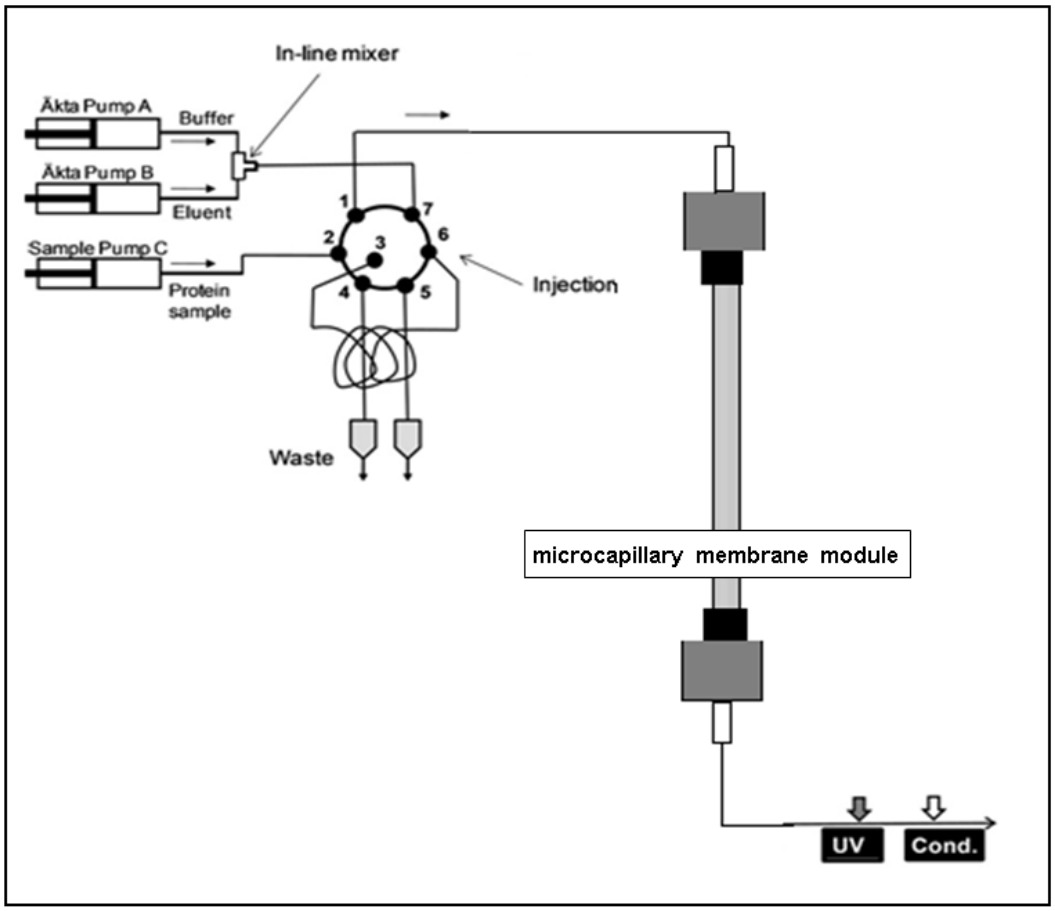

Figure 3.2 Experimental setup used for frontal analysis experiments on AKTA^{TM} FPLC liquid chromatography system with a microcapillary membrane module. A HPLC sample pump C was used for continuously feeding protein samples into the microcapillary membrane module. UV absorbance was measured at 280 nm. Conductivity was recorded in mS cm^{-1}.

Frontal analysis was carried out according to methods described by Darton et al. (Darton et al., 2011). Briefly, the microcapillary membrane module was connected to an AKTA FPLC liquid chromatography system (GE Healthcare Bioscience, Uppsala, Sweden) as illustrated in the experimental setup in **Figure 3.2**. Using this configuration, it was possible to control the continuously fed sample volume

and buffer gradients for different salt concentrations. The module was first pre-equilibrated with running buffer 20 mM Tris-HCl pH 7.2 for at least two capillary volumes. 5.0 mg ml^{-1} lysozyme was continuously fed into the microcapillary membrane module using sample pump C till near 100% breakthrough was reached. The module was then washed with running buffer for 40 capillary volumes. An elution buffer consisting of 0.5 M NaCl in running buffer was passed through for 50 capillary volumes to elute bound protein completely. The module was re-equilibrated using seven capillary volumes of running buffer. These tests were conducted in duplicate.

The void volume was measured in a non-modified microporous membrane module in the above setup by measuring the volume to breakthrough.

3.3.4.2 Saturation binding capacity studies

The mass of lysozyme bound at different flow velocities was calculated from frontal analysis studies. To calculate the mass of protein bound, the module was continuously loaded with a lysozyme concentration, C_{inj} of 5.0 mg ml^{-1} in running buffer with a sample pump C. Frontal chromatograms tests were carried out at volumetric flow rates of 0.5, 1.0, 2.0, 3.0, 4.0 and 5.0 ml min^{-1}. These tests were conducted in duplicate. Integrals were obtained by numerical integration of the data using the trapezoid approximation in MATLAB®.

3.3.4.3 Ligand density modelling and equilibrium binding capacity studies

The linear velocity with the highest mass bound was selected to saturate the microcapillary membrane module with a range of lysozyme protein concentrations and this data was then modelled to study the nature of the adsorption isotherm. These tests were conducted in duplicate.

3.3.5 Cation-exchange separations via frontal analysis

Bio-separation tests using frontal analysis were conducted in the same experimental setup as shown in **Figure 3.2**. The experiment was conducted at a linear velocity of 10,800 cm h^{-1}. The running buffer 20 mM Tris-HCl pH 7.2 was pre-equilibrated through the straight MMCF module for at least two capillary volumes. 15 ml of protein sample was continuously fed using HPLC Pump C. Protein solutions used were 5.0 mg ml^{-1} lysozyme, 5.0 mg ml^{-1} BSA and a mixture of 5.0 mg ml^{-1} lysozyme and 5.0 mg ml^{-1} BSA, all dissolved in running buffer. The module was then washed with running buffer for 40 capillary volumes. A 0.5 M NaCl in running buffer was passed through for 50 capillary volumes for eluting bound protein. The module was re-equilibrated using seven capillary volumes of running buffer. These tests were conducted in duplicate.

3.3.6 SDS-PAGE and Coomassie staining

The sample fractions collected from the frontal analysis experiment of the mixture of 5.0 mg ml^{-1} lysozyme and 5.0 mg ml^{-1} BSA were analysed by sodium dodecyl sulphate polyacrylamide gel electrophoresis (SDS-PAGE). The samples were diluted ten times, with 1.3 µl of original fraction, prepared with denaturing agent and sample buffer and loaded in NuPAGE Novex Bis-Tris 4-12% Pre-Cast Gel (Invitrogen, Paisley, UK) using instruction guide recommendations. Invitrogen's Novex Sharp Pre-Stained Protein Standard was used for molecular weight markers. The gel was run on Invitrogen's XCell SureLock™ Mini-Cell electrophoresis system using appropriate running buffers at 200 V for 35 minutes. The gel was then Coomassie stained using SimplyBlue SafeStain™ (Invitrogen, Paisley, UK) using instruction guide recommendations. Gels were photographed on G:BOX Chemi XT4 (Syngene, Cambridge, UK).

3.4 Results and Discussion

3.4.1 Qualitative ligand distribution study

The degree of labelling of rhodamine-6G dye was 10.4 moles rhodamine-6G dye per mole of lysozyme. Rhodamine 6G dye was used to label protein and qualitatively monitor the flow distribution across the 19 capillaries in the straight MMCF PDMS module. Module cross-sections were imaged in triplicate and the most representative images were analysed. No channelling of flow was observed. The cation-exchange chemistry penetrates the pores homogenously and distributes over all 19 capillaries in the 1 cm, 5 cm and 8 cm cross sections as seen in **Figure 3.3**. However, a stronger fluorescence intensity can be observed near the inner and outer capillary walls consistently across all the cross-sections, corresponding to smaller pore sizes between 0.1-0.5 µm.

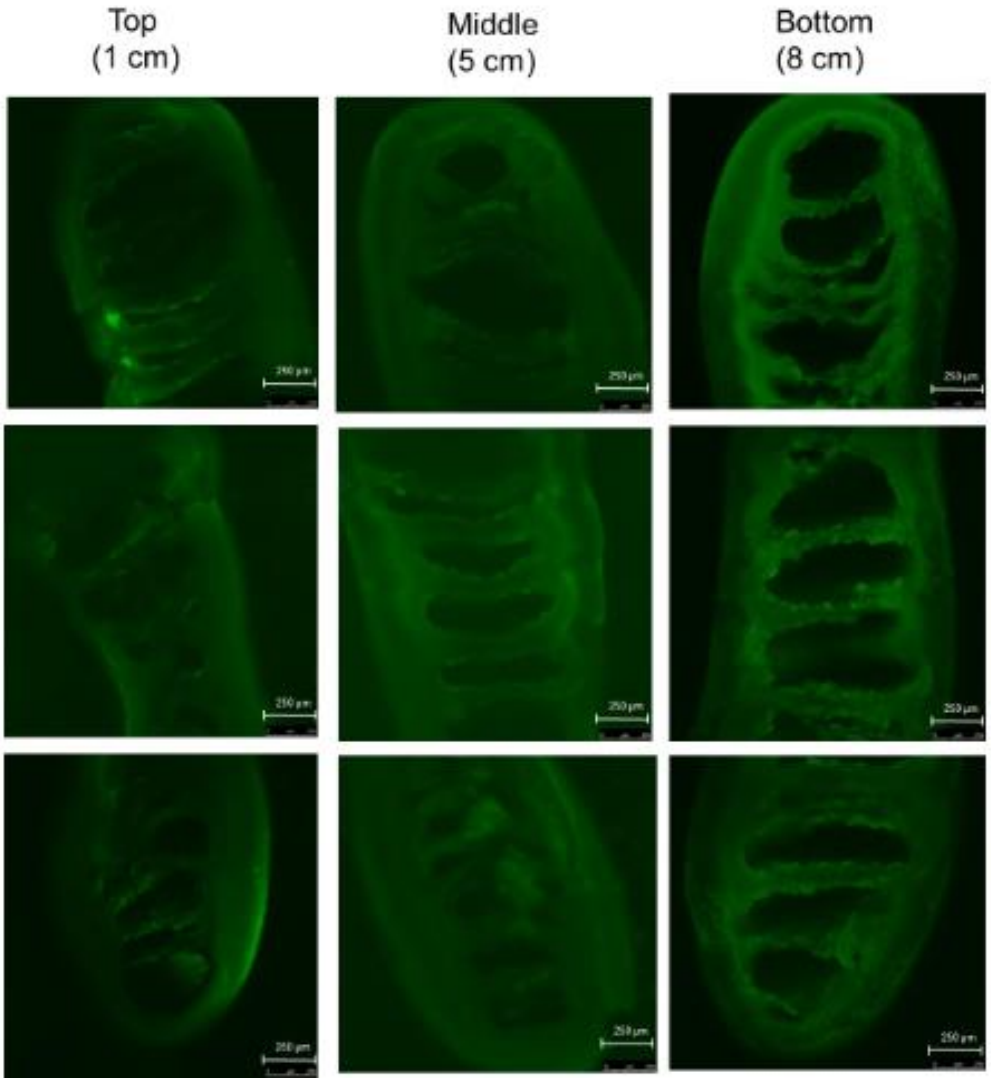

Figure 3.3 Fluorescence ligand distribution study of lysozyme binding in a SP modified straight MMCF module. Rhodamine 6G-lysozyme was represented in green. Cross sections from 10 mm, 50 mm and 80 mm from the top of the column shown.

3.4.2 Frontal chromatogram analysis and dynamic binding capacity of microcapillary membrane modules

The capillary volume is defined as the total internal volume within capillaries. The adsorbent volume of microcapillary membranes is the total volume of the microcapillary membranes excluding the capillary volume.

3.4.2.1 Straight HFM module

The breakthrough curve for the straight HFM module (**Figure 3.4**) showed the binding and elution profile using 5.0 mg ml^{-1} lysozyme solution at 378,000 cm h^{-1}. The MMCF

module displayed a sharp breakthrough even though it has a microporous wall. The dynamic binding capacity of HFM module at 10% breakthrough was 3.14 mg lysozyme/ ml adsorbent volume.

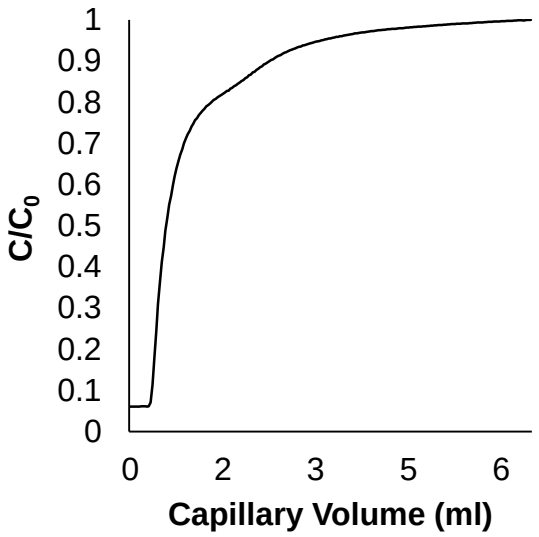

Figure 3.4 Lysozyme loading and elution profile on straight HFM module. Frontal analysis experiment with 0.2 mg ml^{-1} lysozyme solution loaded onto 100 mm MMCF module at a linear velocity of 378,000 cm h^{-1}. On Y axis C/C_0 was the relative UV absorbance of the running lysozyme concentration by the initial feed lysozyme concentration.

3.4.2.2 Straight MMCF module

The high capacity of the MMCF module required an increase in protein loading concentration from 0.2 mg ml^{-1} lysozyme used for NMCF device capacity studies to 5.0 mg ml^{-1} lysozyme to reach near 100% breakthrough (Darton et al., 2011). The breakthrough curve for the straight MMCF module (**Figure 3.5)** showed the binding and elution profile using 5.0 mg ml^{-1} lysozyme solution at a linear velocity of 10,800 cm h^{-1}. The MMCF module displayed a sharp breakthrough even though it has a microporous wall.

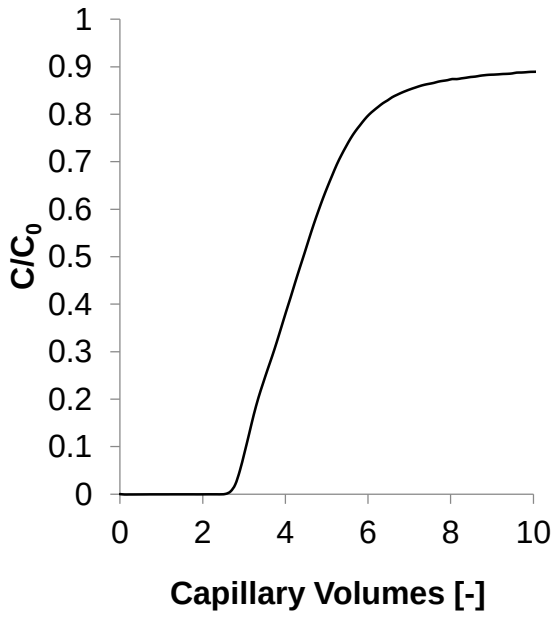

Figure 3.5 Lysozyme loading and elution profile on straight MMCF module. Frontal analysis experiment with 5.0 mg ml^{-1} lysozyme solution loaded onto 200 mm straight MMCF module at a linear velocity of 10,800 cm h^{-1}. On X axis one capillary volume of the straight MMCF module is 1.55 ml. On Y axis C/C_0 is the relative UV absorbance of the running lysozyme concentration by the initial feed lysozyme concentration.

The dynamic binding capacity of MMCF module at 10% breakthrough was 13.8 mg lysozyme/ ml adsorbent volume was of a similar magnitude to commercial packed bed columns (160 mg lysozyme/ ml adsorbent volume GE SP Sepharose XL®) and membranes (47 mg lysozyme/ ml adsorbent volume Pall Mustang S modified Supor ®).

3.4.2.3 Helical MMCF module

The high capacity of the helical MMCF module required an increase in protein loading concentration from 5.0 mg ml^{-1} lysozyme used for straight MMCF module capacity studies to 15.0 mg ml^{-1} lysozyme to reach near 100% breakthrough. The breakthrough curve for the helical MMCF module (**Figure 3.6)** showed the binding and elution profile using 15.0 mg ml^{-1} lysozyme solution at a linear velocity of 10,800 cm h^{-1}. The MMCF module displays a sharp breakthrough even though it has a microporous wall. The

dynamic binding capacity of the helical MMCF module 10% breakthrough was 13.8 mg lysozyme/ ml adsorbent volume, similar to the straight MMCF module.

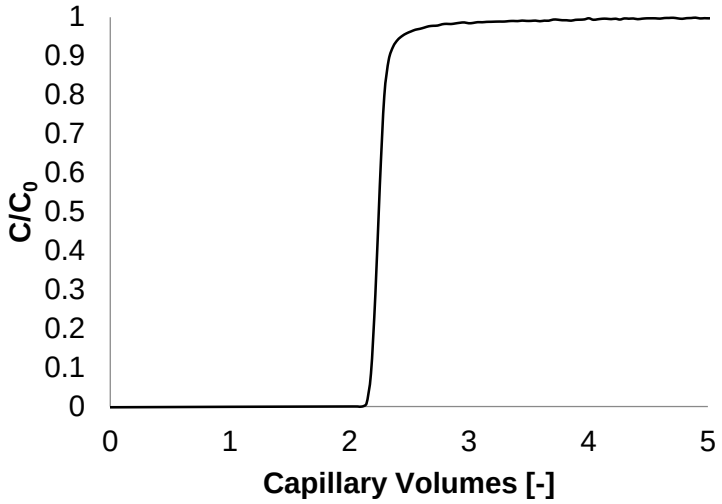

Figure 3.6 Lysozyme loading and elution profile on helical MMCF module. Frontal analysis experiment with 15.0 mg ml^{-1} lysozyme solution loaded onto 600 mm helical MMCF module at a linear velocity of 10,800 cm h^{-1}. On X axis one capillary volume of the helical MMCF module was 4.48 ml. On Y axis C/C_0 was the relative UV absorbance of the running lysozyme concentration by the initial feed lysozyme concentration.

3.4.3 Effect of flow velocities on breakthrough curve and saturation binding capacity

3.4.3.1 Straight HFM module

A series of frontal analysis experiments using the model protein lysozyme allowed the DBC of SP straight HFM module to be determined for a range of linear velocities 189,000 cm h^{-1} to 1,520,000 cm h^{-1}. **Figure 3.7** shows the breakthrough curves for various linear velocities through the straight HFM module. A sharper breakthrough was seen at higher linear velocities. Linear velocities also had an effect on the pressure drop across the module and dynamic binding capacities. Results of the binding capacity analyses with lysozyme for a range of linear velocities shown in **Figure 3.8**.

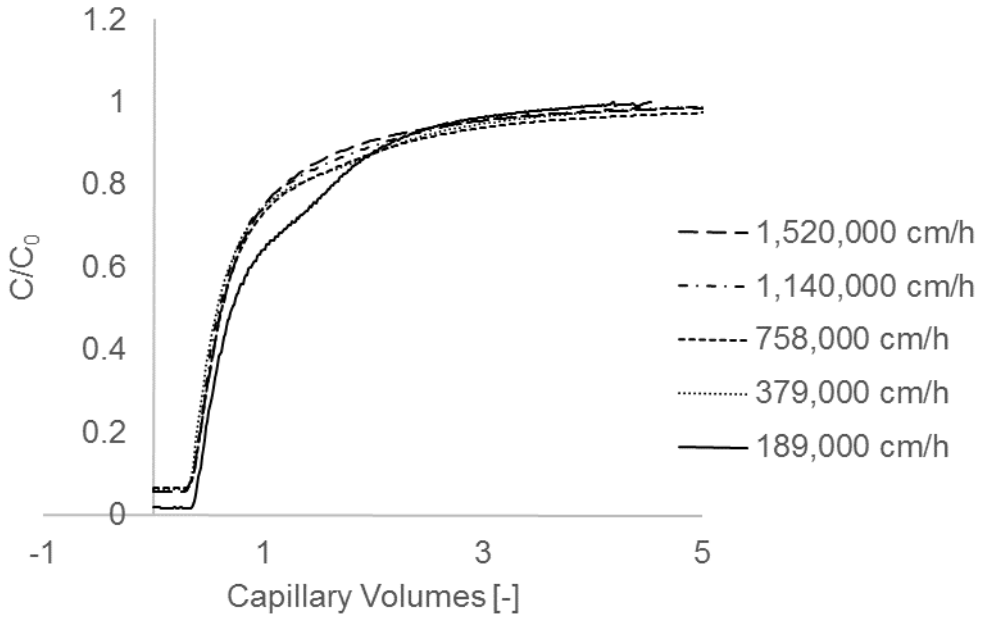

Figure 3.7 Frontal analysis breakthrough curves using 0.2 mg ml^{-1} lysozyme to near 100% breakthrough at linear velocities of 189,000 cm h^{-1} to 1,520,000 cm h^{-1} through 100 mm straight HFM module. C/C_0 was the relative UV absorbance of the running lysozyme concentration by the initial feed lysozyme concentration.

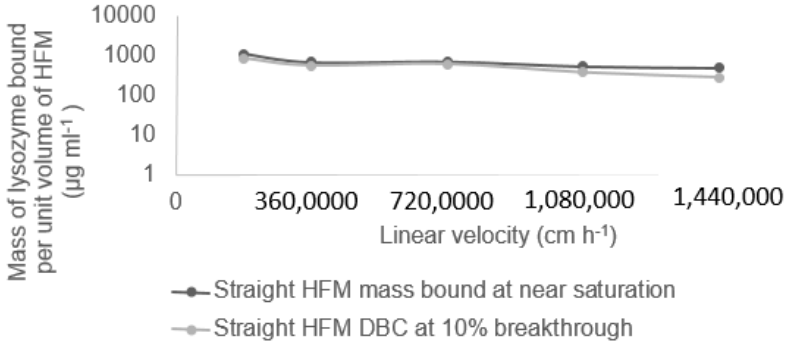

Figure 3.8 Effect of linear velocity on binding capacity of straight HFM module. The mass of lysozyme bound is shown as per unit adsorbent volume of HFM. These tests were conducted in duplicate and the data points indicate averages. The smooth line was used to indicate the trend.

3.4.3.2 Straight MMCF module

A series of frontal analysis experiments using the model protein lysozyme allowed the DBC of SP MMCF module to be determined for a range of linear velocities 5,400 – 54,000 cm h^{-1}. When loaded to near saturation 41.4 mg lysozyme was bound and on subsequent elution 40.1 mg lysozyme was recovered. This corresponds to a

binding density of 228 ng lysozyme/ cm^2 adsorbent surface area, in the same magnitude but lower than NMCF device at 314 ng lysozyme/ cm^2 adsorbent surface area (Darton et al., 2011). In terms of length this corresponds to 2.05 mg lysozyme per cm of MMCF, much higher than 266 ng lysozyme per cm of NMCF. **Figure 3.9** shows the breakthrough curves for various linear velocities through the straight MMCF module. A sharper breakthrough was seen at higher linear velocities. Linear velocities also have an effect on the pressure drop across the module and dynamic binding capacities. As linear velocity increases, pressure drop across the straight MMCF module also increases. For the highest linear velocity tested (54,000 cm h^{-1}) the pressure drop across the straight MMCF module was 0.65 MPa. Hence as with the NMCF device, the straight MMCF module can operate at high linear velocities experiencing low pressure drops, enabling its high throughput behaviour.

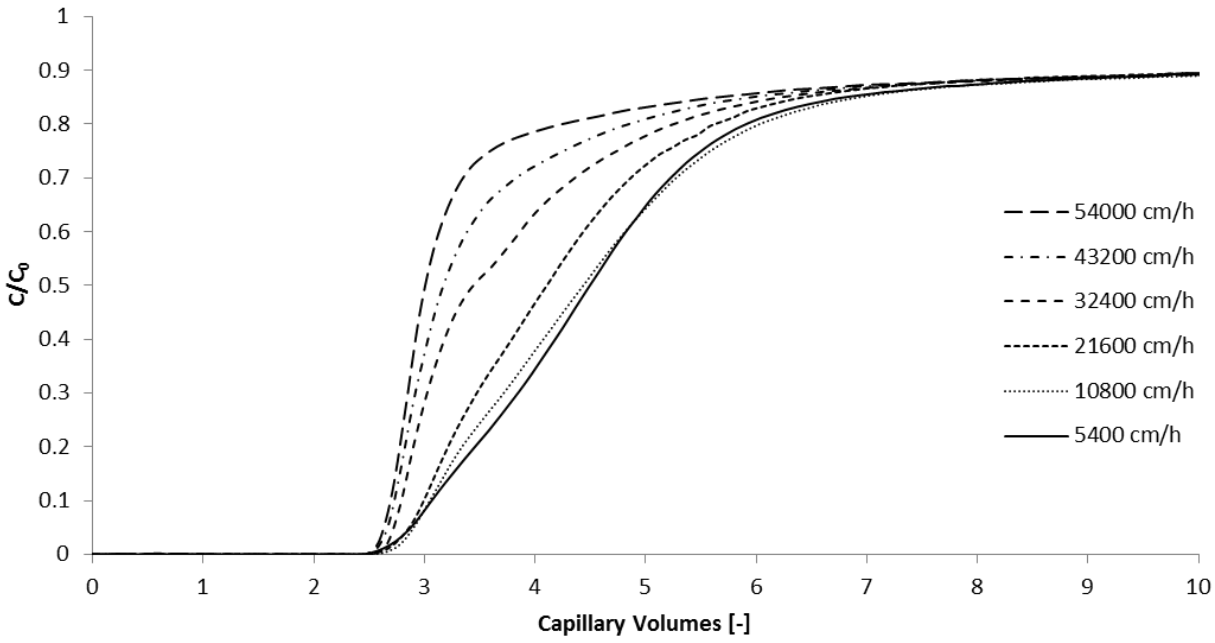

Figure 3.9 Frontal analysis breakthrough curves using 5.0 mg ml^{-1} lysozyme to near 100% breakthrough at linear velocities of 5,400 cm h^{-1} to 54,000 cm h^{-1} through 200 mm straight MMCF module. 1 capillary volume of the straight MMCF module is 1.55 ml. C/C_0 was the relative UV absorbance of the running lysozyme concentration by the initial feed lysozyme concentration.

Results of the binding capacity analyses with lysozyme for a range of linear velocities are shown in **Figure 3.10**. The binding capacity at near saturation of the straight MMCF module is 10^4 times higher than the NMCF device.

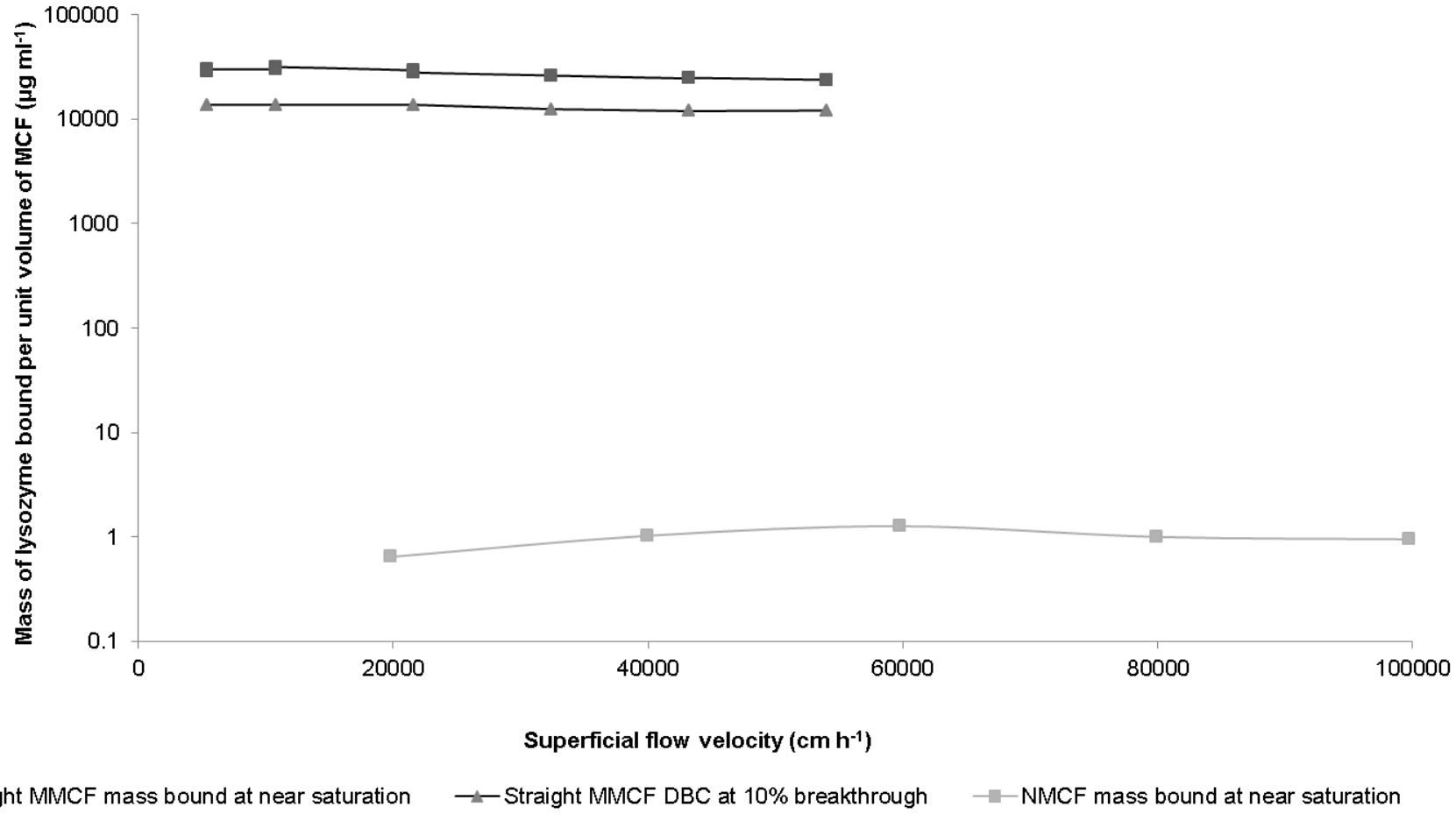

Figure 3.10 Effect of linear velocity (superficial flow velocity) on binding capacity of straight MMCF module (black lines) and NMCF device (grey line). The mass of lysozyme bound is shown as per unit adsorbent volume of MCF. These tests were conducted in duplicate and the data points indicate averages. The smooth line was used to indicate the trend.

With conventional packed bed chromatography, the linear velocities that can be used are limited by relatively low intraparticle mass transfer rates for adsorbates (Albanese, Blehaut, Chochois, Colin, & Guillerm, 2011) and by the compressibility of gels that causes pressure drops to increase. Commonly, DBC's fall with increasing flow velocities for protein adsorption in conventional beads (Darton et al., 2011). By contrast, the DBC for the MMCF is relatively invariant with linear velocity (**Figure 3.10**).

3.4.3.3 Helical MMCF module

Figure 3.11 shows the breakthrough curves for various linear velocities through the helical MMCF module. A sharper breakthrough was seen at higher linear velocities.

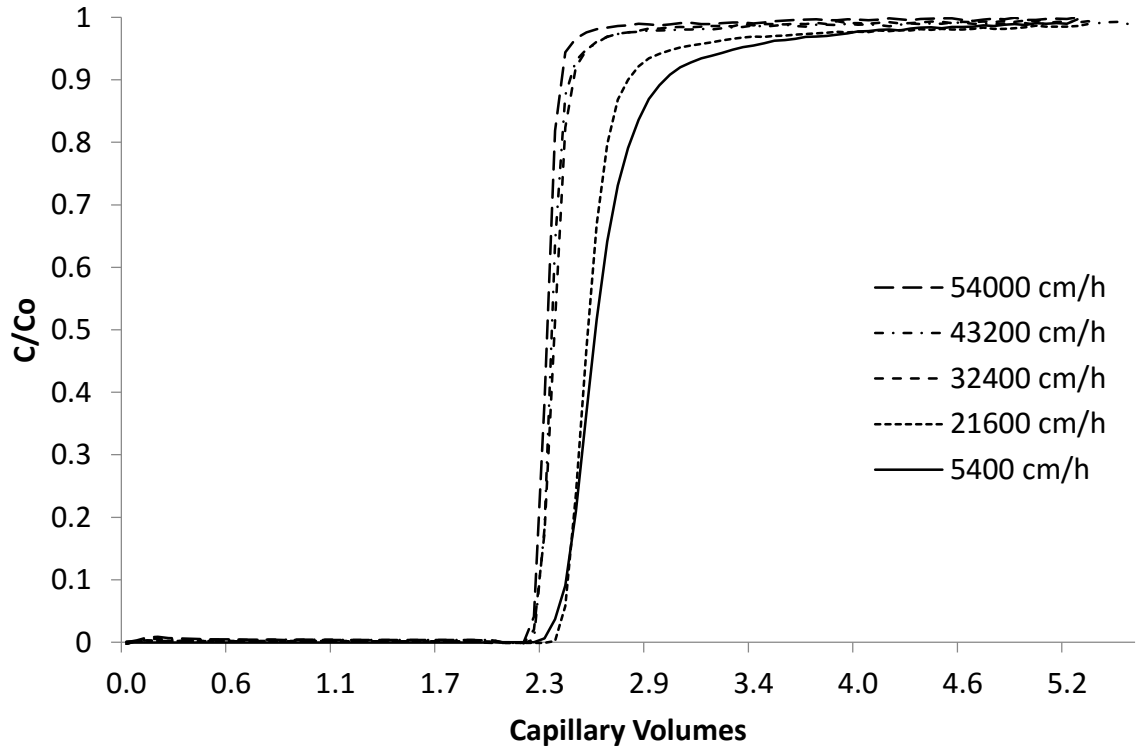

Figure 3.11 Frontal analysis breakthrough curves using 5.0 mg ml^{-1} lysozyme to near 100% breakthrough at linear velocities of 5,400 cm h^{-1} to 54,000 cm h^{-1} through 600 mm helical MMCF module. 1 capillary volume of the helical MMCF module was 4.48 ml. C/C_0 was the relative UV absorbance of the running lysozyme concentration by the initial feed lysozyme concentration.

The helical MMCF module has binding capacity of 36.4 mg ml^{-1} lysozyme/ adsorbent volume at near saturation which is 15% increase in 100% breakthrough, saturation

binding capacity, than a straight MMCF module. The binding capacity at near saturation for the helical MMCF is relatively invariant with linear velocity (**Figure 3.12**).

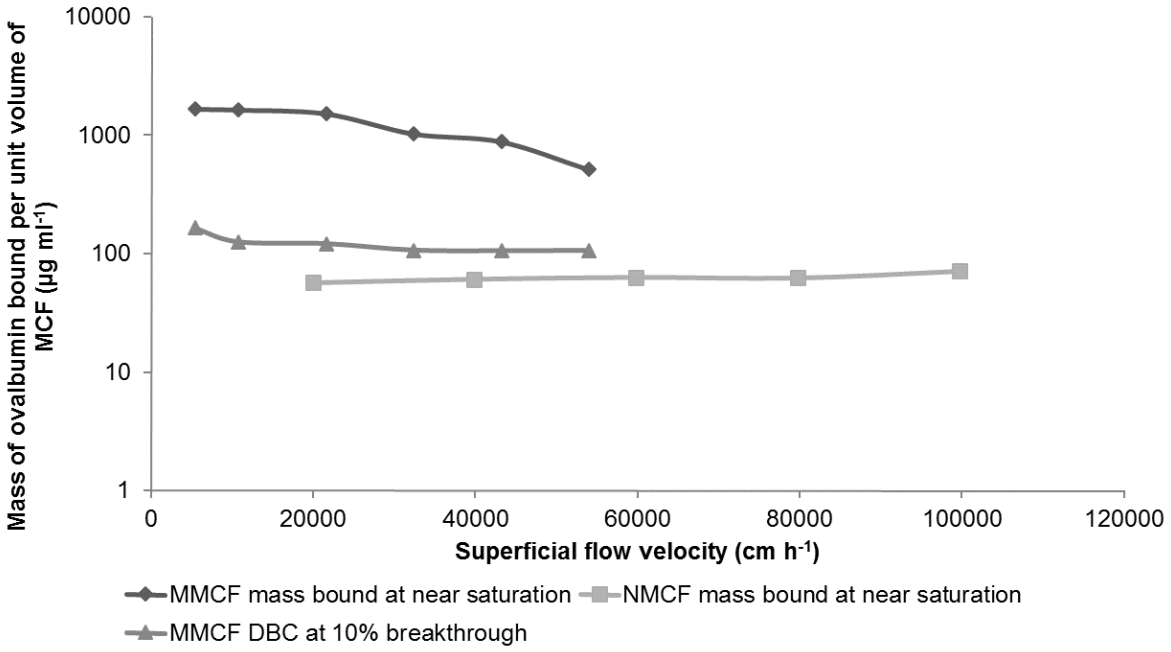

Figure 3.12 Effect of linear velocity (superficial flow velocity) on the saturation binding capacity of helical MMCF module (black lines). The mass of lysozyme bound was shown as per unit adsorbent volume of MMCF. These tests were conducted in duplicate and the data points indicate averages. The smooth line was used to indicate the trend.

Overall as both HFM and MMCF microcapillary membranes are porous materials, as protein adsorption takes place, they deviate from the ideal column breakthrough model. As flow velocity increases, there is a lower residence time for protein to be adsorbed and the breakthrough curve mimics the ideal column breakthrough model again.

Further binding model studies and cation-exchange studies were only performed using straight MMCF modules. It was analysed from the binding capacity studies in this section that the DBC at 10% breakthrough was similar. From residence time distribution studies from Chapter 2, it was seen that the asymmetry factor for helical MMCF modules was too high. This would affect the resolution of the elution peaks.

3.4.4 Ligand binding model and equilibrium binding capacity of the straight MMCF module

A volumetric flow rate of 1.0 ml min^{-1} corresponding to a linear velocity of 10,800 cm h^{-1} was used for subsequent surface ligand binding density studies. **Figure 3.13** shows the mass of lysozyme bound calculated from frontal analysis experiments at different protein concentrations (*C*). The solid black line models the Langmuir isotherm equation which fits the data with a R^2 value of 0.9503. The fit of the Langmuir plot with the experimental data indicates that the lysozyme binds to the MMCF in a monolayer. **Figure 3.13** shows the mass of lysozyme bound at equilibrium per unit volume of MMCF as a fraction of lysozyme concentration in the supernatant. The EBC of the MMCF module was 479 ng lysozyme/ cm^2 adsorbent surface area and 64.7 mg lysozyme/ ml adsorbent volume. This EBC was higher than what was achieved on PVA beads using similar surface chemistry modification methodology which was 31.8 mg lysozyme/ ml adsorbent volume. The EBC was limited by the surface area of the resin that is sterically available via the SP ligand density and contact with the solute (Albanese et al., 2011). The molar equilibrium binding capacity of the MMCF matrix is 4.4 µM lysozyme/ ml adsorbent volume, which is a more accurate representation of the number of charged groups per unit volume available for binding to the MMCF volume.

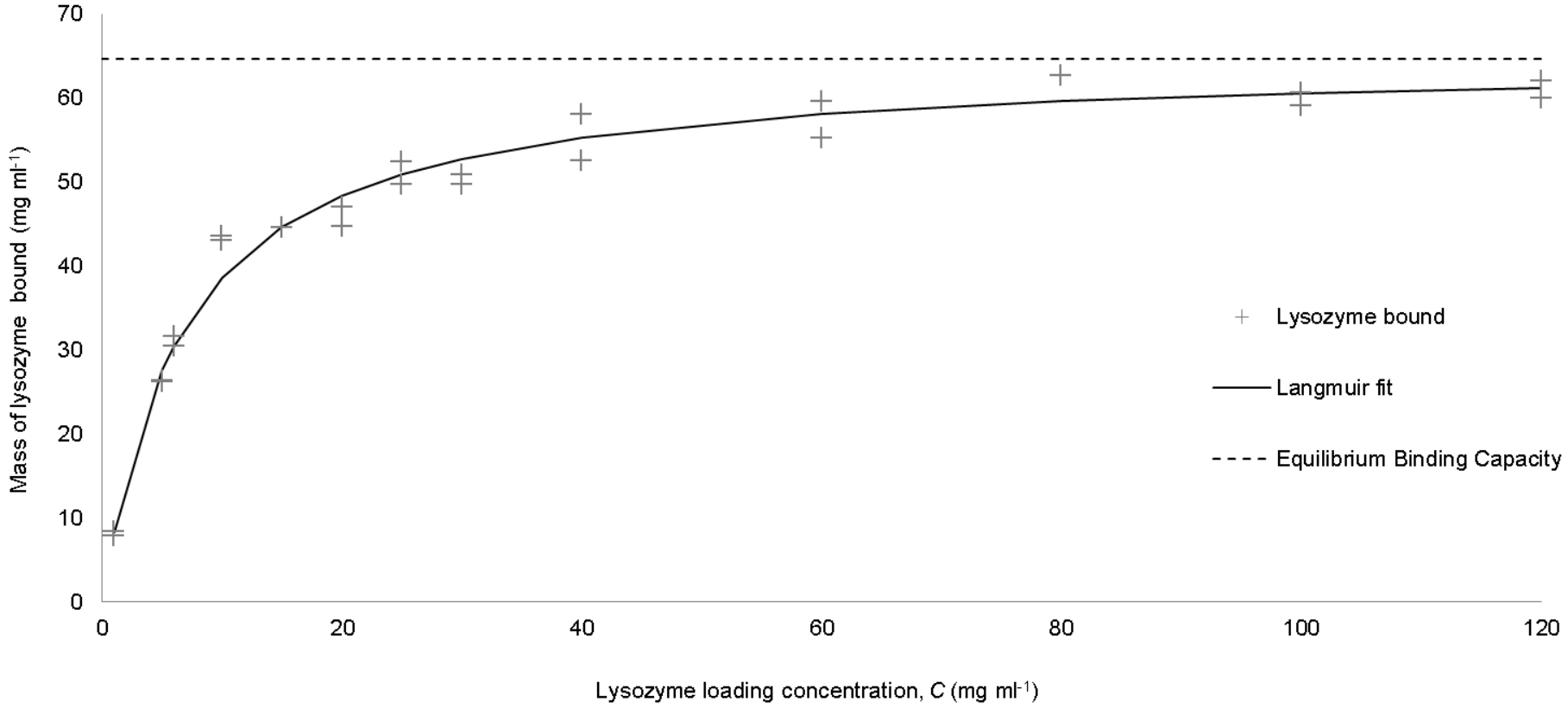

Figure 3.13 Ligand density model of straight MMCF module. The values of lysozyme mass bound were measured at different lysozyme loading concentrations, *C*, have been plotted (crosses). The experiments were conducted in duplicate. The solid line represents the Langmuir isotherm equation and has a good fit with the data ($R^2 = 0.9503$) and gives an equilibrium binding capacity of 64.7 mg lysozyme/ ml adsorbent volume (shown as dotted line).

3.4.5 Cation-exchange studies on straight MMCF module via frontal analysis and SDS-PAGE

Figure 3.14 shows frontal analysis plots for lysozyme (5.0 mg ml^{-1}), BSA (5.0 mg ml^{-1}) and mixtures of these two model proteins. Comparison between the lysozyme plot and BSA plot indicate that the BSA front was less steep as it reached saturation, indicating non-specific adsorption. From the mixed protein samples, 41.0 mg of lysozyme and 0.5 mg of BSA were eluted. Hence at elution 98.8% of the total sample eluted was the target protein lysozyme with only 1.2% impurity BSA. SDS-PAGE analysis (**Figure 3.15**) of 1.0 ml sample fractions collected from **Figure 3.14(c)** confirm that both lysozyme and BSA flow through the saturated straight MMCF module at the frontal analysis loading step (lanes 3, 4 and 5) and the elution fractions consist of lysozyme predominantly (lanes 8 and 9).

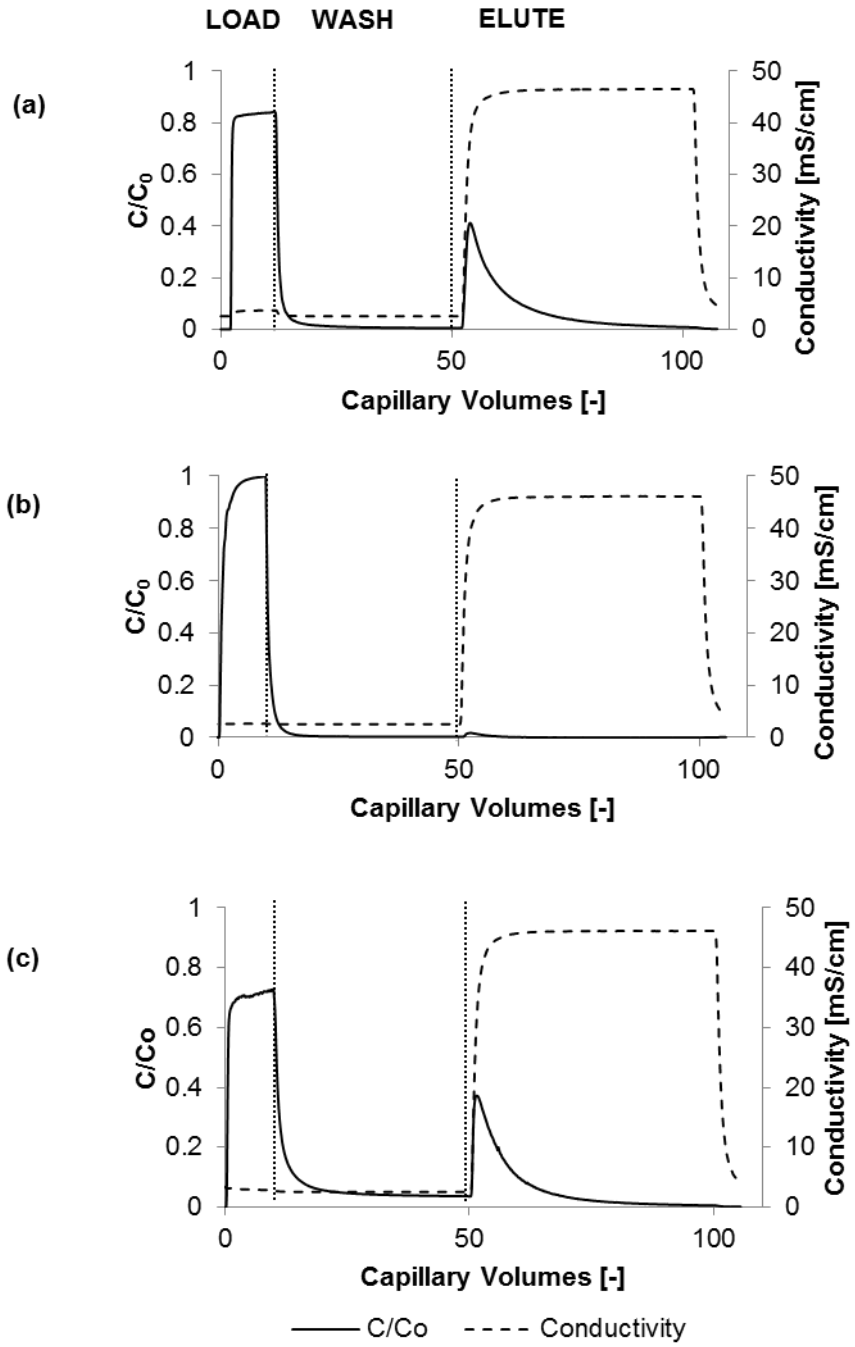

Figure 3.14 Application of straight MMCF module as a cation-exchange separation medium. Frontal analysis loading experiments of lysozyme, BSA and mixtures of these two proteins were tested at a linear velocity of 10,800 cm h^{-1}. On X axis one capillary volume of the MMCF module is 1.55 ml. On Y axis C/C_0 was the relative UV absorbance of the running protein concentration by the initial feed protein concentration. (a) Frontal analysis study of 5.0 mg ml^{-1} lysozyme, 41.0 mg lysozyme was eluted (b) Frontal analysis study of 5.0 mg ml^{-1} BSA, 0.49 mg BSA was eluted (c) Frontal analysis study of a mixture of 5.0 mg ml^{-1} lysozyme and 5.0 mg ml^{-1} BSA, samples from this experiment were analysed on SDS-PAGE in Figure 3.15.

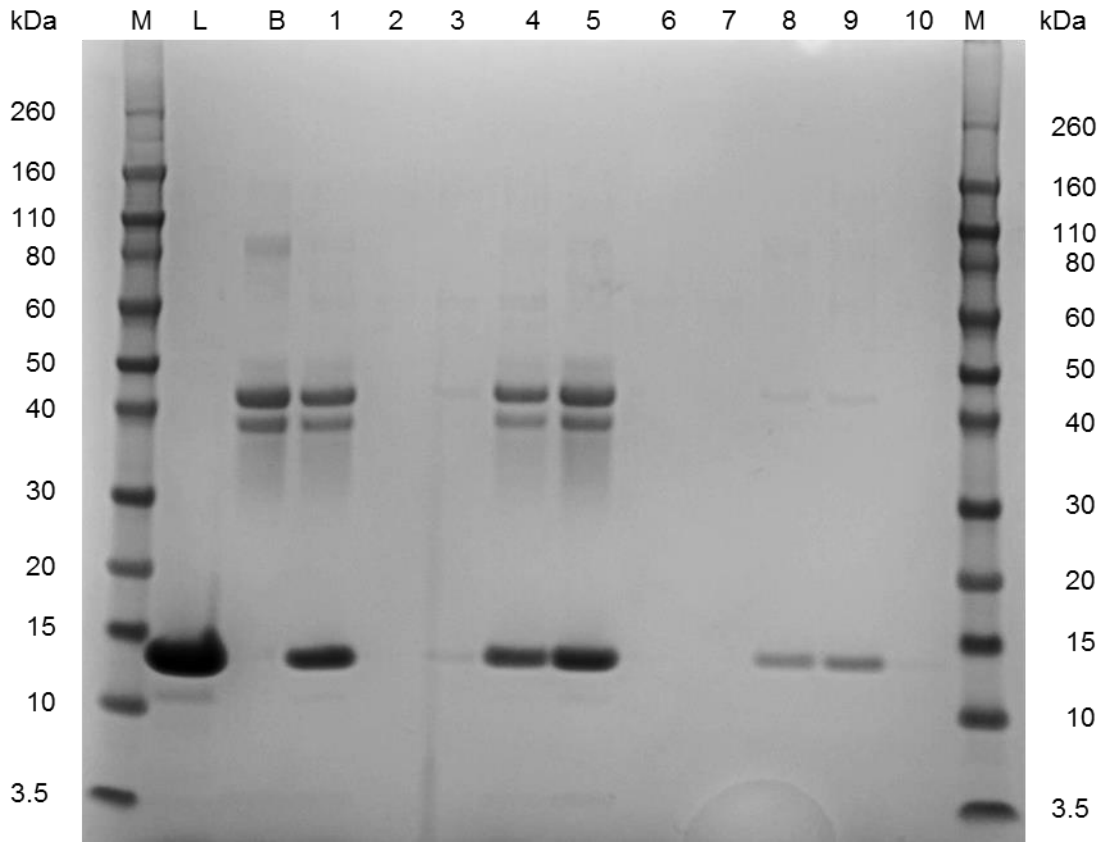

Figure 3.15 Coomassie stained SDS-PAGE analysis of 1.3 µl samples from Figure 3.16(c) frontal analysis experiment mixture of 5.0 mg ml^{-1} lysozyme and 5.0 mg ml^{-1} BSA, loaded in a NuPAGE Novex Bis-Tris 4-12% Pre-Cast Gel. Lanes M on the far left and right mark the Novex Sharp Pre-Stained Protein Standard ladder. Lane L consists of pure 5.0 mg ml^{-1} lysozyme. Lane B consists of pure 5.0 mg ml^{-1} BSA. Lane 1 has the loading mixture of 5.0 mg ml^{-1} lysozyme and 5.0 mg ml^{-1} BSA, Lane 2 has a sample of the fraction from the equilibrium step. Lanes 3, 4 and 5 have samples from the fractions of the sample loading step. Lanes 6 and 7 have samples from the fractions of the wash step. Lanes 8 and 9 have samples from the fractions of the elution step. Lane 10 has a sample of the fraction from the re-equilibration step.

Table 3.1 Comparison of straight MMCF module against NMCF device and current commercial packed bed and membrane media.

	Chromatography medium			
	Microporous beads (GE SP Sepharose XL®)	Membrane (Pall Mustang S modified Supor®)	Nonporous MCF device [11]	Microporous MCF module
Packing requirement	Yes	No	No	No
Superficial flow velocity Volumetric flow rate	300-500 cm h^{-1} 2 – 10 ml min^{-1}	N/A 1 – 4 ml min^{-1}	19800 - 99720 cm h^{-1} 1- 5 ml min^{-1}	5400 – 54000 cm h^{-1} 1- 5 ml min^{-1}
Maximum pressure	0.15 MPa	0.55 MPa	2.0 MPa	>1.5 MPa
Typical operating Dynamic Binding Capacity	160 mg lysozyme/ ml adsorbent volume	47 mg lysozyme/ ml adsorbent volume	0.001 mg lysozyme/ ml capillary volume	13.8 mg lysozyme/ ml adsorbent volume 11.8 mg lysozyme/ ml capillary volume

Table 3.1 compares typical operating parameters for a conventional packed bed adsorber and a membrane adsorber with NMCF and a straight MMCF module. Notably, **Table 3.1** shows that MMCF's can be operated at much higher linear velocities than packed beds, which reduces film mass transfer resistance. MMCF's require no packing which avoids validation of packing integrity and can be operated up to higher pressures. The DBC of the prototype MMCF was about 12-fold lower than the conventional packed bed comparator, but only about 4-fold lower than that of the membrane adsorber. Compared with NMCF, the MMCF has substantially higher DBC yet retains similar ability to operate at high superficial velocities and pressures.

In this study the extent of derivatisation was controlled by studying concentrations of linker groups, measured using qualitative rhodamine ligand binding study for distribution, and quantitative frontal binding capacity. Further characterisation of these matrices is being conducted using titration of ion-exchanger groups and Fourier transform infra-red attenuated total reflectance (FTIR-ATR) to optimise the chemistry and improve the capacity of these matrices

Scale-up of MMCF module separations is similar to the linear scale-up of membrane processes. Whereas conventional columns are operated with low linear velocities between 300-500 cm h^{-1}, MMCF modules can be run with superficial velocities up to 180-fold higher since no matrix compression occurs. High dynamic binding capacities are obtainable when operated at high throughput. The material chemicals cost for the MMCF used in this work is estimated to be only a few pence as the cost of extrusion is low. A major proportion of scale-up cost is likely to lie in the materials and labour expenses for the chemical functionalization and other pilot scale-up production requirements. Overtime the need for monitoring leachables against the amount of intact surface chemistry would be a quality validation study.

3.5 Conclusion

Functionalised microcapillary membrane modules have been developed as a module for cation-exchange separation of proteins. Residence time distribution and capacity studies between the straight HFM, straight MMCF and helical MMCF modules concluded straight MMCF modules ideal for bio-separations in terms of resolution and capacity. A straight MMCF module has been operated on a standard AKTA^{TM} chromatography system at linear velocities up to 54,000 cm h^{-1}. The dynamic binding capacity of the straight MMCF module at 10% breakthrough was 13.8 mg lysozyme/ ml adsorbent volume, which is comparable to the capacity of current commercial adsorbents. Frontal analysis studies using a mixture of lysozyme and bovine serum albumin (BSA) have shown that lysozyme can be isolated free of BSA to the limit of detection of the SDS gel assay used. 98.8% of the total sample eluted was the target protein lysozyme with only 1.2% BSA impurity. MMCF may thus be a viable chromatographic medium for preparative protein chromatography.

CHAPTER 4: ANION-EXCHANGE CHROMATOGRAPHY IN STRAIGHT MMCF MODULE

4.1 Overview

In Chapter 3 after having studied the different types of microcapillary membrane modules in cation-exchange chromatography, the high performance straight MMCF module is chosen in this chapter for opposite surface chemistry studies. Overall this chapter explores the thesis goal of versatility of surface chemistries that can be modified onto this microcapillary membrane for a wide range of biological macromolecule separations. The aim of this chapter is to develop and study straight MMCF modules for anion-exchange chromatography of model proteins. The MMCF membrane surface chemistry is chemically functionalised with quaternary amine groups (Q) for anion-exchange chromatography. The MMCF-Q module is characterised on its breakthrough curve, dynamic and saturation binding capacities. A model separation study is conducted on the MMCF-Q module between model proteins lysozyme and bovine serum albumin and analysed on a gel for purity of samples.

4.2 Background

4.2.1 Anion-exchange chromatography

An anion-exchanger is positively charged oftentimes with amine groups attached to the resin matrix. Anion-exchange chemistry is used widely in industry as a polishing step to remove impurities such as deoxyribonucleic acid (DNA) and viruses from the target biomolecule. Negatively charged molecules selectively bind to positive amine groups. An example of a weak anion-exchanger group is diethylaminoethyl (DEAE) and a strong anion-exchanger is quaternary amines (Q). In this chapter, MMCF-Q

studies have been compared against Amersham Biosciences Q Sepharose XL™ adsorbent and Pall Mustang Q™ membranes. In Q Sepharose XL™, the dextran groups are attached to strong quaternary amine groups. The Q Sepharose XL™ matrix requires column packing, operates between linear velocities of 300 – 500 cm h^{-1} linear velocities at a maximum pressure of 0.15 MPa and a dynamic binding capacity at 10% breakthrough of 130 mg BSA/ ml adsorbent volume. The Mustang Q membrane has a polyethersulfone (PES) base modified with quaternary amine groups. The membrane requires no column packing, operates between volumetric flow rate 1 – 4 ml min^{-1} volumetric flow rate at a maximum pressure of 0.55 MPa and a dynamic binding capacity at 10% breakthrough of 70 mg BSA/ ml membrane volume.

McCreath et al. incorporated charged anion-exchanger groups into a poly(vinyl alcohol) (PVA) coated perfluoropolymer (FEP) support using cyanuric chloride and diaminohexane (McCreath et al., 1997). The McCreath et al. Q chemistry modification method has been used in a non-porous microcapillary film (NMCF) device for lentivirus capture (Darton et al., 2012). These studies on NMCF-Q for lentivirus capture found elution of ~40% of bound lentivirus or 2.5×10^6 infectious units. Although the NMCF device has a high throughput and can tolerate a high pressure, its binding capacity is very low for applications in preparative scale chromatography.

4.3 Materials and Methods

4.3.1 Chemicals

Sodium hydroxide (NaOH), cyanuric chloride, acetone, sodium phosphate (Na_2HPO_4), tris(hydroxymethyl)aminomethane (Tris), hydrochloric acid (HCl), chick-egg lysozyme (pI 11, MW 14.3 kDa), BSA (pI 4.9, MW 67.0 kDa), ovalbumin (pI 4.5, 45.0 kDa), sodium chloride (NaCl) were all purchased from Sigma Aldrich (St. Louis, Missouri).

4.3.2 Surface modification of straight MMCF module with quaternary amine groups

The straight MMCF module was functionalised for anion-exchange functionality by methods developed by McCreath et al. and Darton et al. (Darton et al., 2012; McCreath et al., 1997). Briefly, the MMCF module was attached to a HPLC pump. 30 ml of ice cold NaOH (1M) was then recycled though the MMCF for 30 min using the pump. This increased the nucleophilicity by introducing alkoxide groups on the vinyl alcohol present on the MMCF surface. Then 20 ml ice cold cyanuric chloride (50mM) in acetone was recycled through the MMCF in an ice bath for 20 min followed by a wash with 10 ml ice cold MilliQ water for 10 min. Next a linker, 1,6-diamino hexane, was introduced onto the cyanuric chloride functionalised MMCF. In this step 4 g of 1,6-diamino hexane in a 20 ml solution of 1M $NaHCO_3$ (pH 12.0) was passed through the MMCF at a volumetric flow rate of 1 ml min^{-1} at 40 °C overnight (17 h) in a water bath. The temperature of the water bath was then increased to 60 °C for a further 5 h. The MMCF was then washed with MilliQ water for 20 min followed by a second wash with 20 ml 0.1 M Na_2CO_3 (pH 10.0) for 20 min. The quaternary amine functional groups were added next by passing glycidyl trimethylammonium chloride diluted (1:1) with 0.1 M Na_2CO_3 (pH 10.0) through the MMCF at 40 °C in a water bath for 44 h. Due to the high viscosity of the amine solution this step was performed at a lower volumetric flow rate of 0.1 ml min^{-1}. Three successive wash steps were then performed with; 20 ml MilliQ water for 20 min; then 20 ml NaOH (0.4 M) for 20 min; and finally 20 ml MilliQ water for 20 min. The resulting MMCF-Q anion exchange material was stored at 4 °C in 20 mM Tris-HCL buffer (Darton et al., 2012; McCreath et al., 1997).

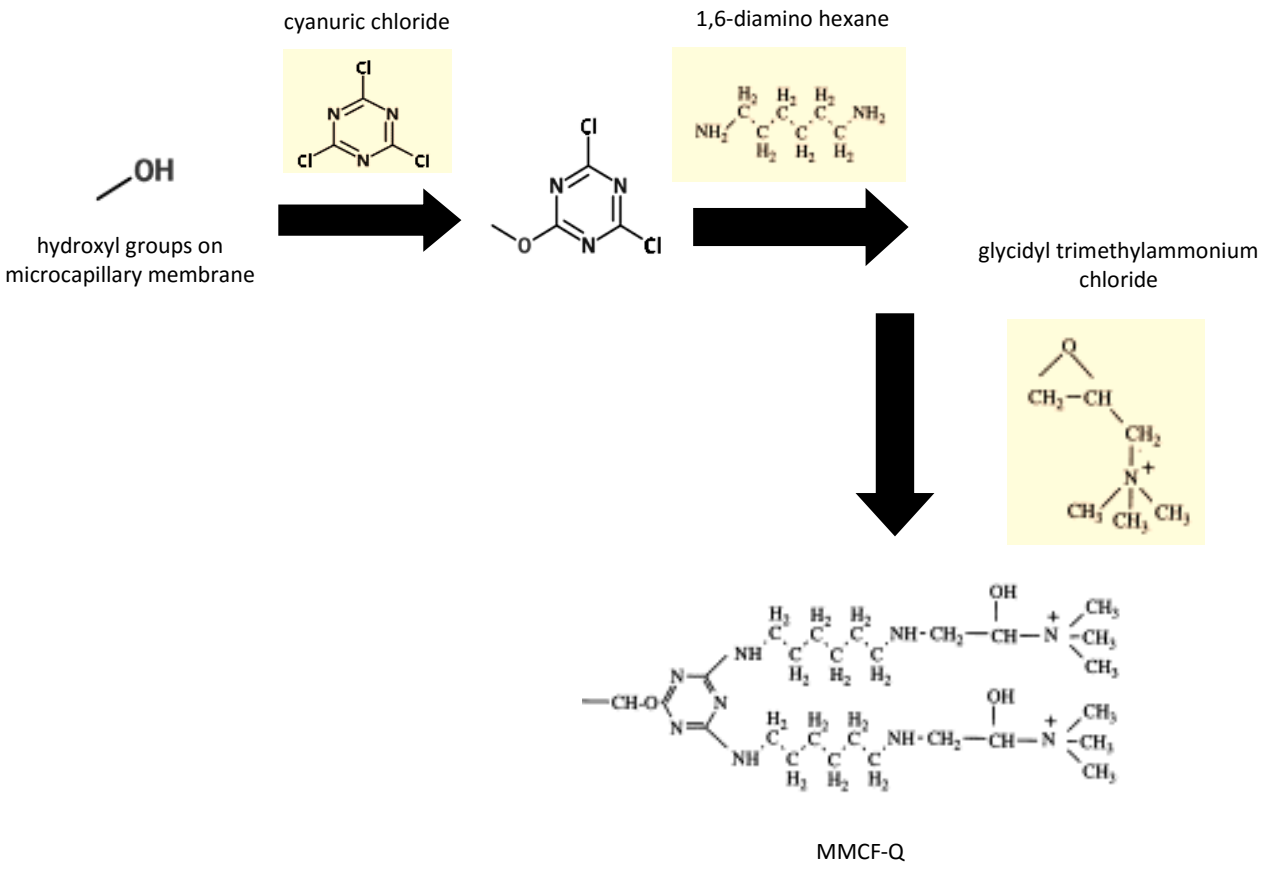

Figure 4.1 Schematic diagram showing the MMCF surface modification for Q anion-exchange chemistry (McCreath et al., 1997).

Modifications were made to the McCreath et al. method to allow the chemistry to interface appropriately from the solution chemistry to chemistry within the microcapillary modules. All the chemistry steps were undertaken of a HPLC pump at a volumetric flow rate of 1 ml min^{-1}. The 1,6 diaminohexane was dissolved in higher concentration in a lower volume of $NaHCO_3$ 20 ml. Each of the wash steps were decreased from 200 ml to 20 ml.

Glycidyl trimethylammonium chloride was diluted with sodium carbonate at various fold concentrations (1:10 and 1: 20) and run at a low volumetric flow rate. This was done to decrease the viscosity of the solution for better permeability of the chemical through the microporous membrane. The incubation time was also increased by another 24 hr to increase diffusion time. These optimisations have a much higher binding capacity of the Q-MMCF column.

Many of the derivatisation steps between the NMCF and MMCF were kept consistent, for comparable analysis only dependent on level of porosity and surface area.

4.3.3 Frontal analysis and dynamic binding capacity studies

Frontal analysis was carried out according to methods described by Darton et al. (Darton et al., 2011). Briefly, the microcapillary membrane module was connected to an AKTA^{TM} FPLC liquid chromatography system (GE Healthcare Bioscience, Uppsala, Sweden) as illustrated in the experimental setup in **Figure 4.2**. Using this configuration, it was possible to control the continuously fed sample volume and buffer gradients for different salt concentrations. The module was first pre-equilibrated with running buffer 20 mM Tris-HCl pH 7.6 for at least two capillary volumes. 5.0 mg ml^{-1} ovalbumin was continuously fed into the microcapillary membrane module using sample pump C till near 100% breakthrough was reached. The module was then washed with running buffer for 40 capillary volumes. An elution buffer consisting of 0.5 M NaCl in running buffer was passed through for 50 capillary volumes to elute bound protein completely. The module was re-equilibrated using seven capillary volumes of running buffer. These tests were conducted in duplicate.

The void volume was measured in a non-modified microporous membrane module in the above setup by measuring the volume to breakthrough.

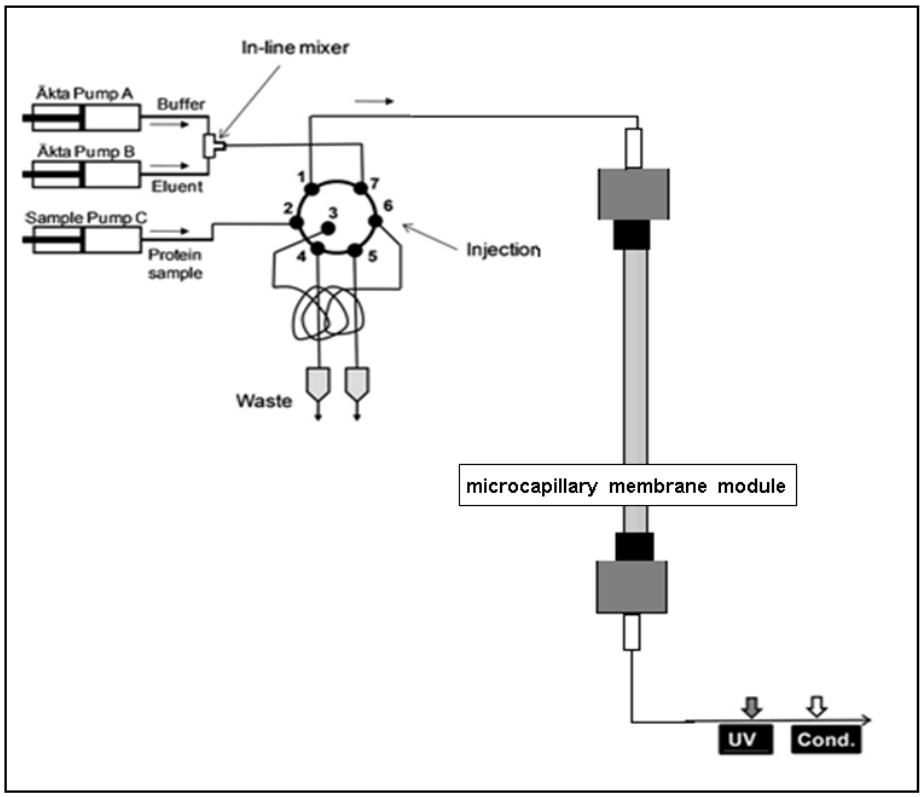

Figure 4.2 Experimental setup used for frontal analysis experiments on AKTA FPLC liquid chromatography system with a microcapillary membrane module. A HPLC sample pump C was used for continuously feeding protein samples into the MMCF module. UV absorbance was measured at 280 nm. Conductivity was recorded in mS/cm.

4.3.4 Saturation binding capacity studies

The mass of ovalbumin bound at different flow velocities was calculated from frontal analysis studies. To calculate the mass of protein bound, the module was continuously loaded with an ovalbumin concentration, C_{inj} of 5.0 mg ml^{-1} in running buffer with a sample pump C. Frontal chromatograms tests were carried out at volumetric flow rates of 0.5, 1.0, 2.0, 3.0, 4.0 and 5.0 ml min^{-1}. These tests were conducted in duplicate. Integrals were obtained by numerical integration of the data using the trapezoid approximation in MATLAB®.

4.3.5 Ligand density modelling

The linear velocity with the highest mass bound was selected to saturate the column with a range of BSA protein concentrations of 1.0, 5.0, 10, 20, 40, 60, 80, 100 and 120 mg ml^{-1} and this data was then modelled to study the nature of the adsorption isotherm. These tests were conducted in duplicate.

4.3.6 Anion-exchange studies via frontal analysis

Bio-separation tests using frontal analysis were conducted in the same experimental setup as shown in **Figure 4.2**. The experiment was conducted at a linear velocity of 10,800 cm h^{-1}. The running buffer 20 mM Tris-HCl pH 7.6 was pre-equilibrated through the module for at least two capillary volumes. 15 ml of protein sample was continuously fed using HPLC Pump C. Protein solutions used were 5.0 mg ml^{-1} lysozyme, 5.0 mg ml^{-1} BSA and a mixture of 5.0 mg ml^{-1} lysozyme and 5.0 mg ml^{-1} BSA, all dissolved in running buffer. The module was then washed with running buffer for 40 capillary volumes. A 0.5 M NaCl in running buffer was passed through for 50 capillary volumes for eluting bound protein. The module was re-equilibrated using seven capillary volumes of running buffer. These tests were conducted in duplicate.

4.3.7 SDS-PAGE, Coomassie and silver staining

The sample fractions collected from the frontal analysis experiment of the mixture of 5.0 mg ml^{-1} lysozyme and 5.0 mg ml^{-1} BSA were analysed by sodium dodecyl sulphate polyacrylamide gel electrophoresis (SDS-PAGE). The samples were diluted ten times, with 1.3 µl of original fraction, prepared with denaturing agent and sample buffer and loaded in NuPAGE Novex Bis-Tris 4-12% Pre-Cast Gel (Invitrogen, Paisley, UK) using instruction guide recommendations. Invitrogen's Novex Sharp Pre-Stained Protein Standard was used for molecular weight markers. The gel was run on Invitrogen's

XCell SureLock™ Mini-Cell electrophoresis system using appropriate running buffers at 200 V for 35 minutes. The gel was then Coomassie stained using SimplyBlue SafeStain™ (Invitrogen, Paisley, UK) using instruction guide recommendations. Silver staining was conducted using the SilverXpress® Silver Staining Kit using the instruction guide recommendations. Gels were photographed on G:BOX Chemi XT4 (Syngene, Cambridge, UK).

4.4 Results and Discussion

4.4.1 Frontal chromatogram analysis and dynamic binding capacity

The breakthrough curve for the MMCF-Q module (**Figure 4.3)** shows the binding profile using 5.0 mg ml^{-1} ovalbumin solution at a linear velocity of 10,800 cm h^{-1}. The MMCF-Q module displays a sharper breakthrough than the MMCF-SP module in Chapter 3, indicating a lower amount of protein mass bound. The dynamic binding capacity of MMCF-Q module at 10% breakthrough is 1.26 mg ovalbumin/ ml adsorbent volume. This shows a two-fold exponential reduction than commercial packed bed columns (130 mg bovine serum albumin/ ml adsorbent volume GE Q Sepharose XL ®) and membranes (70 mg bovine serum albumin/ ml adsorbent volume Pall Mustang Q modified Supor ®). Variables of the Q surface chemistry modification procedure such as linker concentrations, incubation times and pump volumetric flow rates were changed step wise to choose the optimal conditions for highest surface chemistry density. This dynamic binding capacity of the Q-MMCF module is comparatively lower than that of the SP-MMCF module. The Q surface chemistry itself is more complex the SP surface chemistry with stepwise loss of charged groups depending on the success of the covalent attachment of the linker steps. The bulkier quaternary amine chemistry

may also be adding to stearic resistance in the pores for the right orientation of the higher molecular weight protein ovalbumin to be bound quickly.

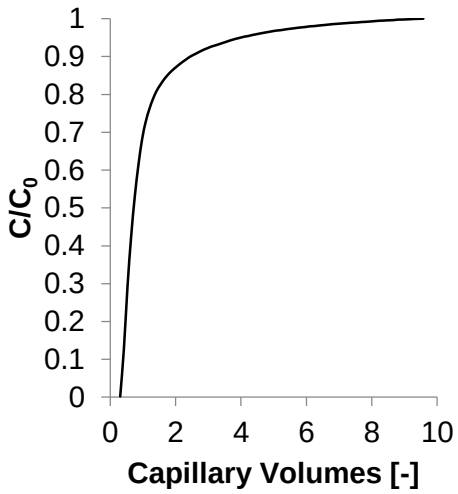

Figure 4.3 Ovalbumin loading profile on straight MMCF-Q module. Frontal analysis experiment with 5.0 mg ml^{-1} ovalbumin loaded onto 200 mm MMCF-Q module at a linear velocity of 10,800 cm h^{-1}. On X axis one capillary volume of the MMCF module is 1.55 ml. On Y axis C/C_0 is the relative UV absorbance of the running ovalbumin concentration by the initial feed ovalbumin concentration.

4.4.2 Effects of flow velocities on breakthrough curve and saturation binding capacity

A series of frontal analysis experiments using the model protein ovalbumin allowed the saturation binding capacity of MMCF-Q module to be determined for a range of linear velocities 5,400 – 54,000 cm h^{-1}. When loaded to near saturation 1.86 mg ovalbumin was bound. This corresponds to a binding density of 10.3 ng ovalbumin/ cm^2 adsorbent surface area or 0.093 mg ovalbumin per cm of MMCF. **Figure 4.4** shows the breakthrough curves for various linear velocities through the straight MMCF-Q module. A sharper breakthrough is seen at higher linear velocities.

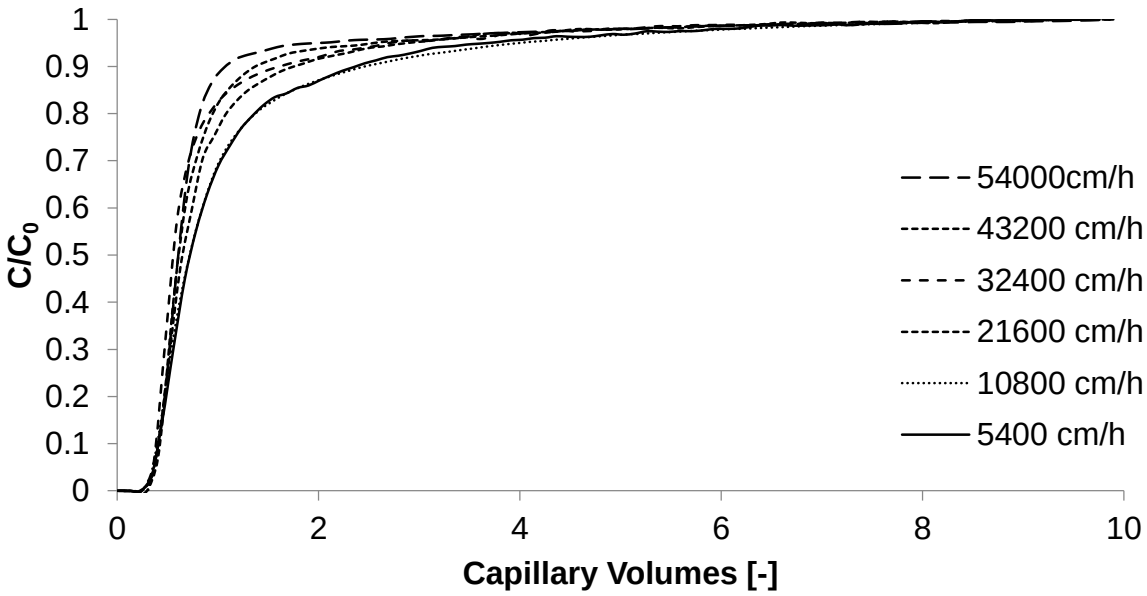

Figure 4.4 Frontal analysis breakthrough curves using 5.0 mg ml^{-1} ovalbumin to near 100% breakthrough at linear velocities of 5,400 cm h^{-1} to 54,000 cm h^{-1} through 200 mm straight MMCF-Q module. 1 capillary volume of the straight MMCF-Q module is 1.55 ml. C/C_0 is the relative UV absorbance of the running ovalbumin concentration by the initial feed ovalbumin concentration.

Results of the saturation binding capacity analyses with ovalbumin for a range of linear velocities are shown in **Figure 4.5**. The saturation binding capacity of MMCF-Q is variant with linear velocity, dropping at higher velocities. This is different from the NMCF-Q saturation binding trend which doesn't vary noticeably on the exponential scale with increasing linear velocities (Townsend, 2015). The binding capacity at near saturation of the MMCF module is on average 22 times higher than the NMCF device.

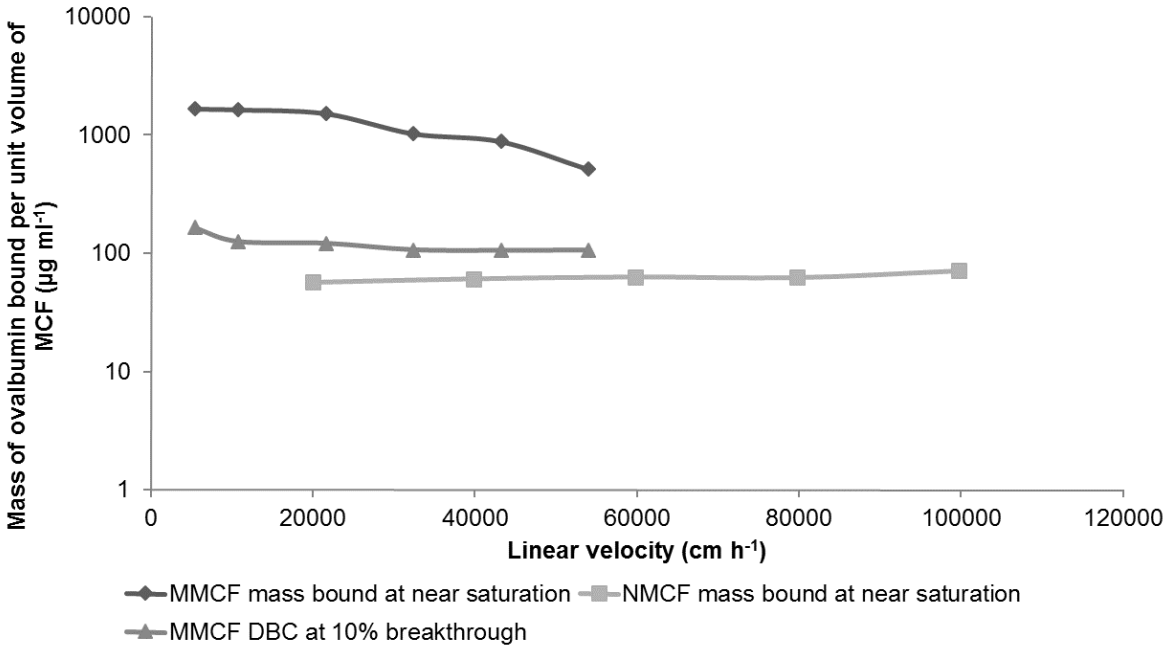

Figure 4.5 Effect linear velocity on the saturation binding capacity of the straight MMCF-Q module (black line) and NMCF-Q module (grey line). The mass of ovalbumin bound was shown as per unit adsorbent volume of MCF. These tests were conducted in duplicate and the data points indicate averages. The smooth line was used to indicate the trend.

4.4.3 Ligand binding model

A volumetric flow rate of 1.0 ml min^{-1} corresponding to a linear velocity of 10,800 cm h^{-1} was used for subsequent surface ligand binding density studies. **Figure 4.6** shows the mass of ovalbumin bound calculated from frontal analysis experiments at different protein concentrations (*C*). The solid black line models the linear isotherm equation which fits the data with a R^2 value of 0.955. The equilibrium disassociation constant, K_d, was found to be 0.316. The deduced ligand binding model was not an ideal adsorption isotherm for a chromatography medium as it was not convex in shape as in the MMCF-SP Langmuir model but linear, affecting maximal capture of target protein or biomolecule from solution.

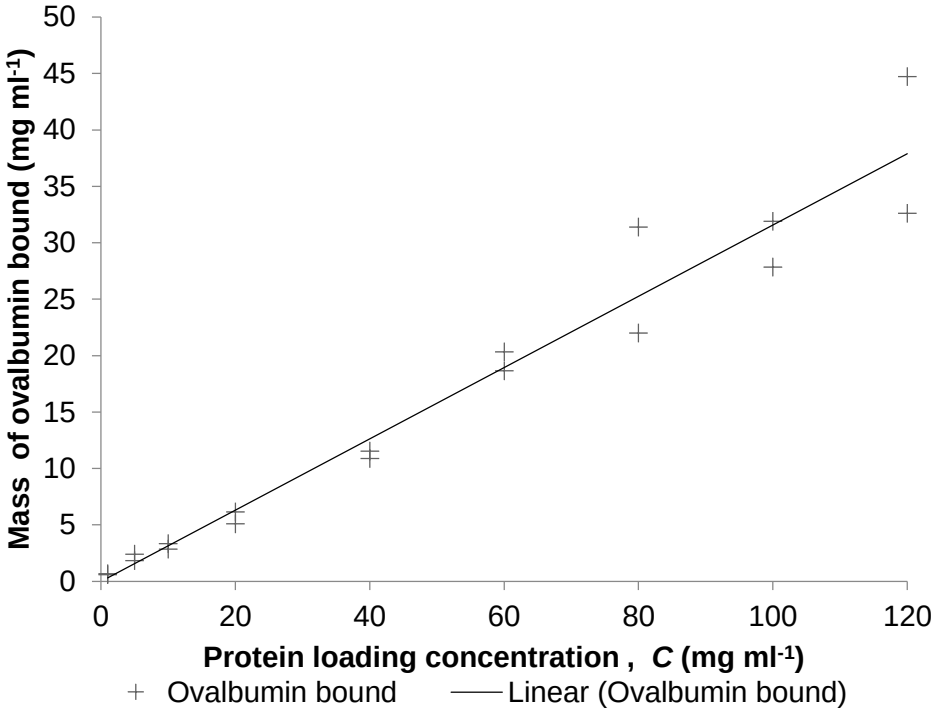

Figure 4.6 Ligand density model of straight MMCF-Q module. The values of ovalbumin mass bound were measured at different ovalbumin loading concentrations, *C*, have been plotted (crosses). The experiments were conducted in duplicate. The solid line represents the Linear isotherm equation and has a good fit with the data (R^2 = 0.955).

4.4.4 Anion-exchange studies via frontal analysis

Figure 4.7 shows frontal analysis plots for BSA (5.0 mg ml^{-1}), lysozyme (5.0 mg ml^{-1}) and mixtures of these two proteins. From the mixed protein samples, 1.86 mg of BSA was bound. SDS-PAGE analysis (**Figure 4.8**) of 1.0 ml sample fractions collected from **Figure 4.7(c)** confirm that both lysozyme and BSA flow through the saturated straight MMCF module at the frontal analysis loading step (lanes 1, 2 and 3) and the elution fractions consist of BSA predominantly (lanes 7 and 8).

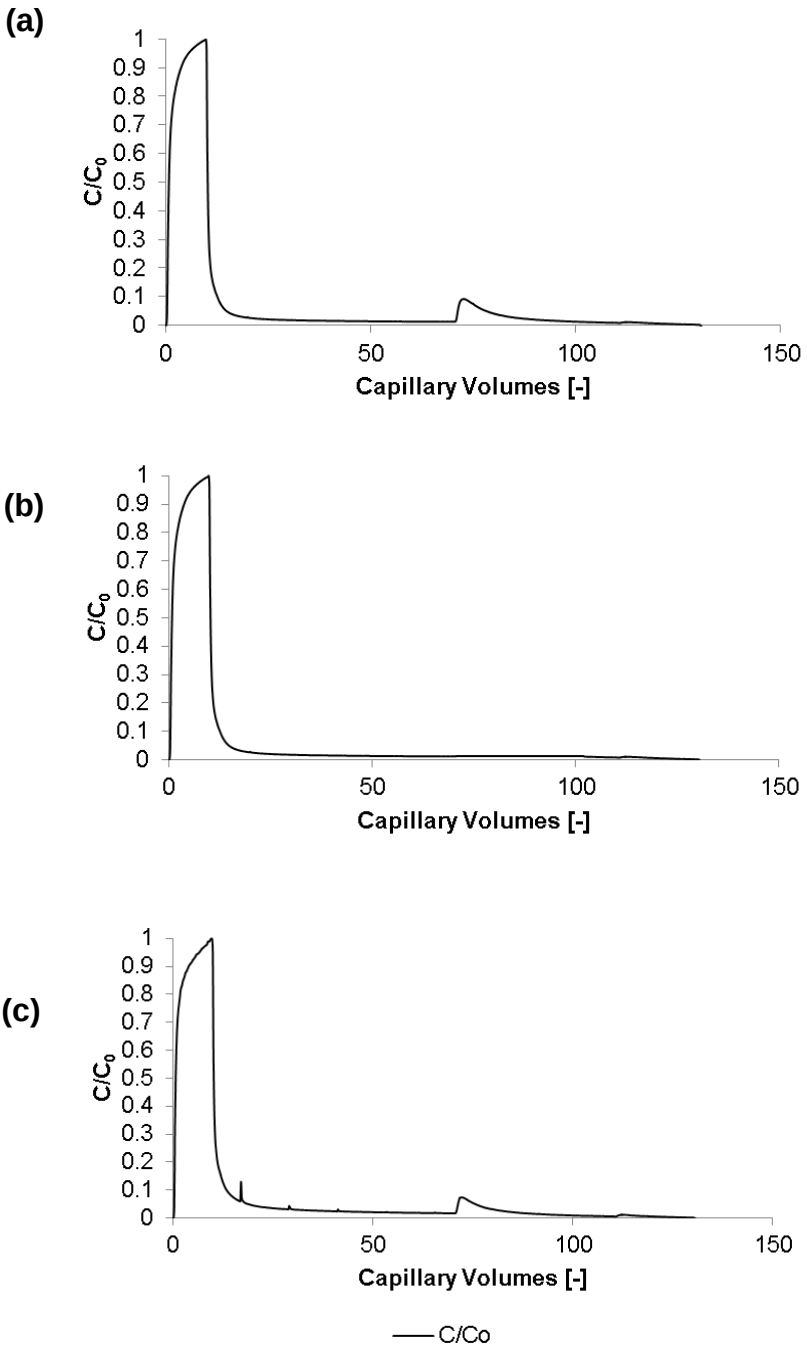

Figure 4.7 Application of a straight MMCF module as an anion-exchange medium. Frontal analysis loading experiments of BSA, lysozyme and mixtures of these two proteins were tested at a linear velocity of 10,800 cm h^{-1}. On the X axis one capillary volume of the MMCF module is 1.55 ml. On the Y axis C/C_0 is the relative UV absorbance of the running protein concentration by the initial feed protein concentration. (a) Frontal analysis study of 5.0 mg ml^{-1} BSA, 1.86 mg BSA was bound (b) Frontal analysis study of 5.0 mg ml^{-1} lysozyme (c) Frontal analysis study of a mixture of 5.0 mg ml^{-1} BSA and 5.0 mg ml^{-1} lysozyme, samples from this experiment were analysed on SDS-PAGE in Figure 4.8.

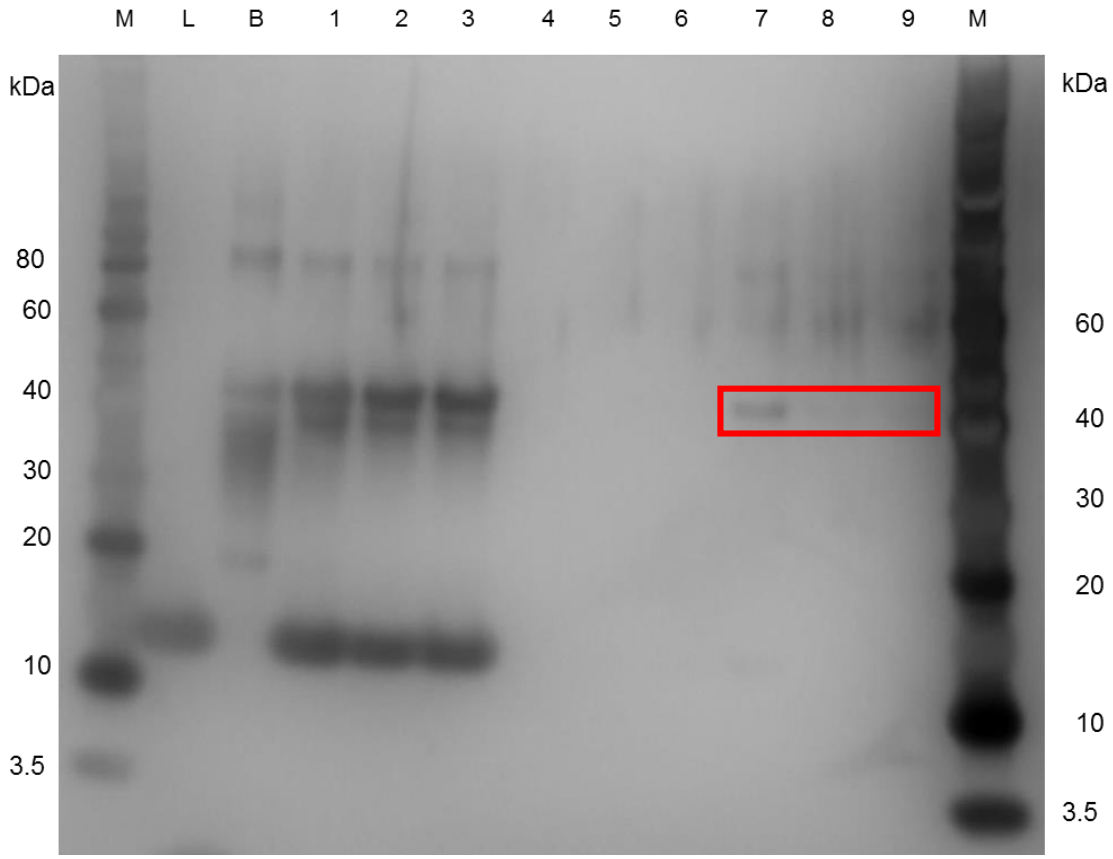

Figure 4.8 Silver stained SDS-PAGE analysis of 1.3 µl samples from Figure 4.9(c) frontal analysis experiment mixture of 5.0 mg ml^{-1} BSA and 5.0 mg ml^{-1} lysozyme, loaded in a NuPAGE Novex Bis-Tris 4-12% Pre-Cast Gel. Lanes M on the far left and right mark the Novex Sharp Pre-Stained Protein Standard ladder. Lane L consists of pure 5.0 mg ml^{-1} lysozyme. Lane B consists of pure 5.0 mg ml^{-1} BSA. Lane 1 has the loading mixture of 5.0 mg ml^{-1} lysozyme and 5.0 mg ml^{-1} BSA, Lanes 2 and 3 have samples from the loading step. Lanes 4, 5 and 6 have samples from the fractions of the wash step. Lanes 7, 8 and 9 have samples from the fractions of the elution step. The red box highlights the key BSA band highlighting target protein purity in the elution fractions.

4.5 Conclusion

An anion-exchange functionalised, straight microporous walled micro-capillary film (MMCF), has been developed as a module. The dynamic binding capacity of MMCF module 10% breakthrough is 1.26 mg ovalbumin/ ml adsorbent volume, which is two-folds exponentially lower in capacity than current commercial adsorbents but 22 times higher than NMCF-Q. Frontal analysis studies using a mixture of lysozyme and bovine serum albumin (BSA) have shown that BSA can be isolated free of lysozyme to the limit of detection of the SDS gel assay used.

CHAPTER 5: ACTIVATED CARBON IN HOLLOW FIBER MEMBRANES AS MIXED-MATRIX MEMBRANES

5.1 Overview

The aim of this chapter is to study activated carbon adsorption of impurities, in a high flow-through membrane geometry. Mixed-matrix membranes (MMM) are extruded using previously described (Chapter 2) non-solvent induced phase separation process, incorporating activated carbon into a hollow fibre membrane (HFM) geometry in membranes of different wt. % compositions. The porosities of the various AC-HFM-MMM's extruded are analysed by scanning electron micrographs and mercury porosimetry to study the effect of mixed composition on pore sixes across the capillary and overall surface area. Binding capacity studies are conducted with a model dye, methylene blue and a waste water pollutant, humic acid.

The topic of forming mixed-matrix membranes and the experimental strategy was developed by me. The data for analysis of this project was collected during supervisory projects of Part IIB students Michael Carson and Jackson Lippold, and MPhil student Yongjun Kwon. Additional repeats on the batch uptake data for the methylene blue and humic acid studies were conducted after the projects. The data analysis and discussion reported in this chapter was conducted by me.

5.2 Background

Hollow fiber membranes (HFMs) are a good starting model for producing mixed-matrix membranes due to their simpler capillary geometry and extrusion parameters. In previous chapters, HFMs have been extruded, flow and residence time characterised, and studied for cation-exchange dynamic binding capacity. In this chapter a proof-of-

concept of incorporating an inorganic particle to HFMs is being developed, to form a novel type of mixed-matrix membrane, and study its microstructure and adsorption of different types of chemicals.

5.2.1 Mixed-matrix membranes

Membranes which have homogenously interpenetrating polymeric matrices and functional particles are defined as mixed-matrix membranes (MMM). A schematic representation of the MMM technology platform is presented in **Figure 5.1**. Successful development of MMM requires homogenous distribution of the functional particles to fully utilise the unique characteristics of the filler. Functional particles based on materials such as clays, zeolites, carbon nanotubes, metals and oxides have been explored in polymeric membranes (Guillen et al., 2011). The function of the binder polymer is to be highly porous and hence allowing for a high degree of pore interconnectivity but also possessing surface properties that do not bind to the desired product (Avramescu et al., 2003).

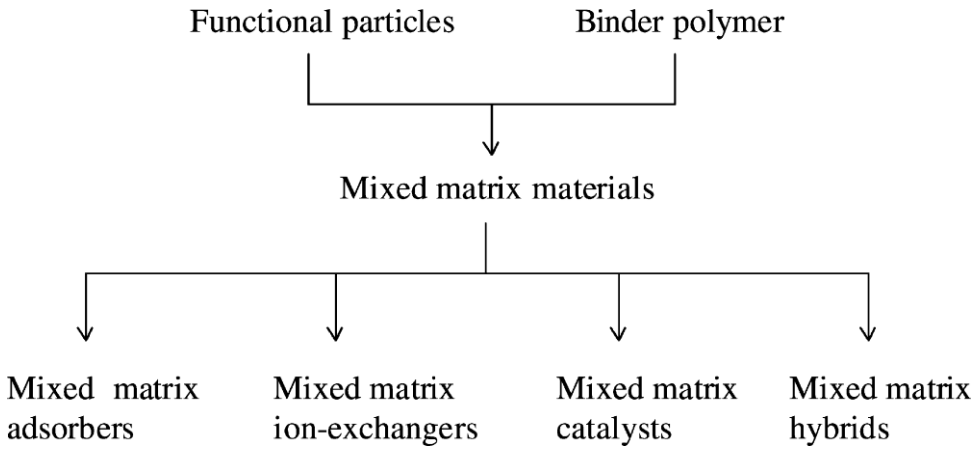

Figure 5.1 Schematic representation of the Mixed Matrix Membrane (MMM) technology platform (Avramescu et al., 2003).

MMMs were developed as mixed matrix ion-exchangers by Avramescu et al. (2003) in a flat membrane format using Lewatit type ion-exchanger particles in EVOH for

both cation and anion exchange (Avramescu et al. 2003a, 2003b; Avramescu et al., 2003; Borneman & Wessling, 2006). Normally a membrane chromatography material is chemically activated and coupled with ligands. With such chemical modification, undesirable and irreversible changes in the membrane structure can be prevented. For mixed-matrix ion-exchangers an adsorptive resin is incorporated into a membrane polymer solution prior to membrane fabrication. The polymer has been casted into flat sheet membranes or HFM geometries. Studies have also been conducted with SP Sepharose and D061 cation-exchange resins for lysozyme binding capacity (Saufi & Fee, 2011; Zhang et al., 2009).

5.2.2 Activated carbon and its use as an adsorber

Activated carbon is an inexpensive material with non-specific adsorption properties. Powdered activated carbon (AC) has been studied to adsorb a diverse range of molecules including dyes such as methylene blue (Avom et al., 1997; Potgieter, 1991) and small molecule humic substances (Daifullah et al., 2004; Summers & Roberts, 1988). Humic acid is a small biomolecule usually formed from the biodegradation of dead organic matter and creates a problem in the water treatment industry since these acids inhibit the chemical disinfection process (Libecki & Dziejowski, 2008).

Due to its non-specificity, AC applications in high performance protein purification have not been explored till recently where AC has been used to separate protein from impurities in a non-adsorption mode (Ishihara, 2014). AC has been incorporated in commonly used industrial polymers such as acrylonitrile-butadiene-styrene (Anson, Marchese, Garis, Ochoa, & Pagliero, 2004a) and polysulfone (Ballinas, Torras, Fierro, & Garcia-Valls, 2004a) in flat sheet membrane geometry. In HFM geometry polyethersulfone has been used with carbon nanotubes (Gallagher et al., 2013) and activated carbon (Tijink et al., 2013). EVOH has not been used with AC before but is

of interest due to biocompatibility. AC particle size has been found to affect the membrane pore structure (Ballinas, Torras, Fierro, & Garcia-Valls, 2004b). In the study by Ballinas et al. AC particles were ground to specific sizes between 8 to 45 microns. However another study by Anson et al. uses commercial grade AC particles without milling before use (Anson, Marchese, Garis, Ochoa, & Pagliero, 2004b).

5.3 Materials and methods

5.3.1 Chemicals and materials

EVOH copolymer supplied by Kuraray (Hattersheim, Germany) was used as the base polymer for the mixed-matrix membrane. N-methyle-2-pyrrolidone (NMP) was used as a solvent for the EVOH beads and polyvinyl-pyrrolidone (PVP) was used as a pore forming agent. NMP, PVP, methylene blue, humic acid, sodium hydroxide were purchased from Sigma Aldrich (St. Louis, Missouri). AC was purchased under the brand name of Activated charcoal DARCO® KB-G from Sigma Aldrich (St. Louis, Missouri). These AC particles had a 90% upper bound population of 40 µm.

5.3.2 Preparation of polymer-activated carbon solutions

The base polymer solution composition was modified from a previous method developed for HFM EVOH extrusion (Bonyadi & Mackley, 2012). EVOH and PVP were dissolved in NMP in a three-neck round bottom flask in the ratio of 75/10/15 wt. % NMP/PVP/EVOH respectively. In addition, 0%, 0.5%, 1%, 2% or 4% AC by mass in solution was also added. The polymer-AC solution was stirred in the three-neck round-bottomed flask, which was suspended in an oil bath at 80 °C for 24 h, to form a homogenous solution.

5.3.3 Extrusion of mixed-matrix membranes

The mixed-matrix membrane extrusions were based on the non-solvent induced phase separation process (NIPS) (Bonyadi & Mackley, 2012) briefly described here with some modifications made to the original method for the modification in polymer-AC composition. Pressure from a compressed air cylinder forces the polymer-AC solution through an annular die. The pressure was adjusted so that the polymer-AC solution mass flow rate from the annular die was approximately 1.5 g min^{-1}. A bore fluid consisting of an 80:20 NMP/distilled water ratio, at a volumetric flow rate of 0.5 ml min^{-1}, using a Chemix Nexus 6000 syringe pump was co-extruded through the annular die. On exiting the die the solution passed through a 5 mm air gap and into the water bath where phase separation occurred and the membrane began to form. The nascent polymer-AC solution was fed onto a rotating motor haul-off drum.

For post-solution processing, the mixed-matrix membranes were immersed in distilled water for three days to complete the NIPS process. For long term storage they were then immersed in a glycerol solution for 24 hours and then air dried to prevent the pores in the membrane from collapsing.

The mass percentage of activated carbon with respect to EVOH in the polymer solution, assuming that the ratio of these components was maintained post-extrusion in the capillary, was calculated using **Equation 5.1**:

$$membrane\ wt\% = \frac{m_{AC}}{m_{AC} + m_{EVOH}} \times 100\%$$

(**Equation 5.1**)

Where m_{AC} is the mass of activated carbon in the polymer solution and m_{EVOH} is the mass of EVOH in the polymer solution.

5.3.4 Scanning electron micrograph imaging

SEM imaging was used as a qualitative way of investigating porosity of the AC-HF-MMMs. SEM images of AC-HF-MMM cross-sections at different magnifications are taken in order to observe the nature and size of the pores, the AC particles within the structure and whether the porous nature varies across the wall cross-section. The microstructure of the membranes was examined using a FEI Philips Scanning Electron Microscope. Samples of each AC membrane wt. % were frozen in liquid nitrogen and fractured to give a sharp cross section. For each sample images were obtained at different magnifications with the aim of characterizing regions of varying porosity.

Three images were taken of the inner region, centre region and outer region of the capillary wall. From each image, the diameter of 10 randomly chosen pores was measured. The SEM images were analysed using Image J software to measure the pore sizes.

5.3.5 Mercury Porosimetry

Mercury porosimetry was performed using AutoPore IV 9500 (Micromeritics, Hexton). The instrument measures the volume of mercury that penetrates the membrane structure as a function of the applied pressure. Mercury was first forced into the pores in the structure by an applied pressure (intrusion) before the pressure is slowly reduced, causing the mercury to vaporise and leave the pores (extrusion). In turn this gives a quantitative analysis of the total surface area within the fibre and a pore size distribution.

5.3.6 Methylene blue adsorption studies

The methylene blue adsorption studies were modified from a method initially developed by Potgieter (Potgieter, 1991). Different masses of each AC-HF-MMM sample was weighed out and then cut into approximately 1 cm lengths. These were placed in jars containing a measured volume of a 25 mg L^{-1} analytical grade methylene blue in distilled water solution. A calibration curve using ≤ 25 mg L^{-1} methylene blue was found to obey the Beer-Lambert law as shown in **Figure 5.2**. Every 24 hours, a 1 ml sample was taken from each jar and a spectrophotometric measurement at a wavelength of 630 nm was carried out using a UV-Vis spectrophotometer (Thermo Electron Corporation, Loughborough), before the sample was returned to its jar. The measurements were taken until the absorbance readings reached equilibrium. A control reading of the dye without any membrane was also taken with every set of measurements to obtain an approximate error for the measurements and to ensure that there was no change in the dye absorbance due to light exposure. These tests were conducted in duplicate.

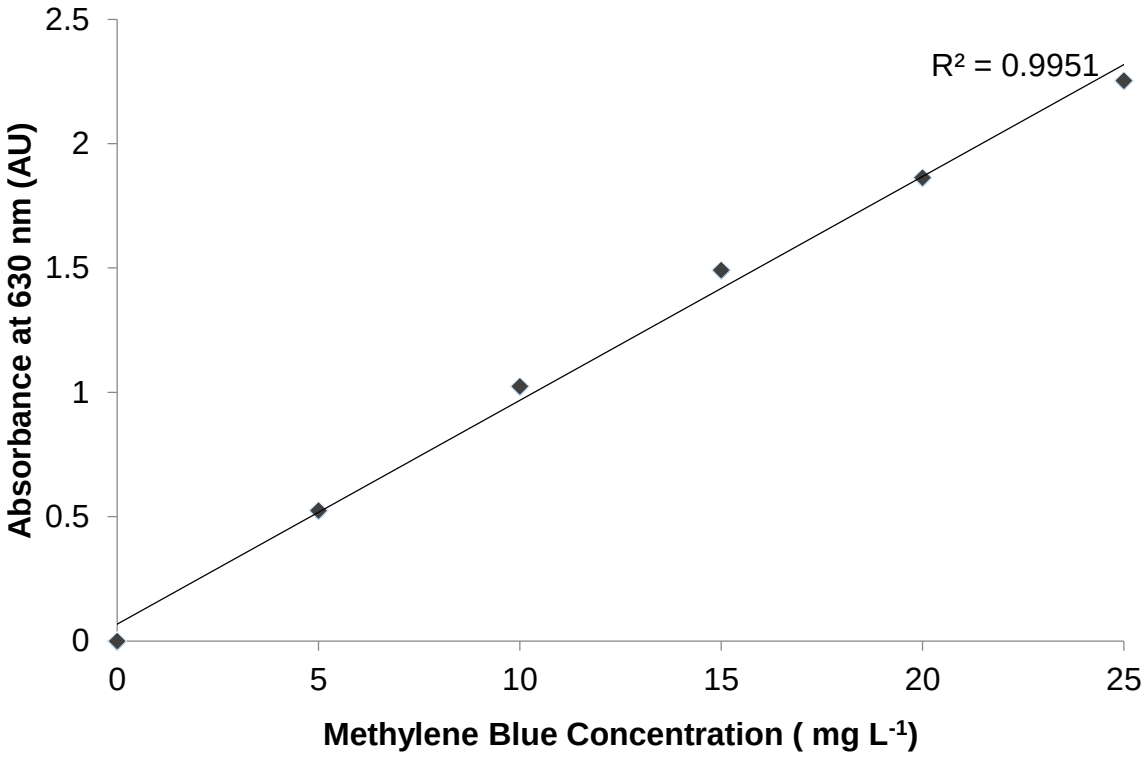

Figure 5.2 Calibration curve using ≤ 25 mg L^{-1} methylene blue was found to obey the Beer-Lambert law (R^2= 0.9951).

5.3.7 Humic acid adsorption studies

The humic acid adsorption studies were modified from studies by Rauthula and Srivastava (2011). AC-HF-MMMs were soaked in a 10 g L^{-1} humic acid solution, and the solution concentration was measured periodically with a UV spectrophotometer at 337 nm. Different masses of membranes were prepared according to their AC mass compositions. Membranes were cut to approximately 1 cm and soaked in the humic acid solutions contained in 15 ml test tubes. The test tubes were kept in the orbital shaker at a speed of 150 rpm. UV absorbance readings were taken every 15 minutes for the first hour of membrane introduction, and then they were taken every hour for the next four hours. After five hours of membrane introduction to the humic acid solution, the absorbance readings were taken every 24 hours, and the measurements were continued until equilibrium was reached. These tests were conducted in

duplicate. A standard calibration curve (**Figure 5.3)** was used to calculate the corresponding solution concentration from the absorbance reading.

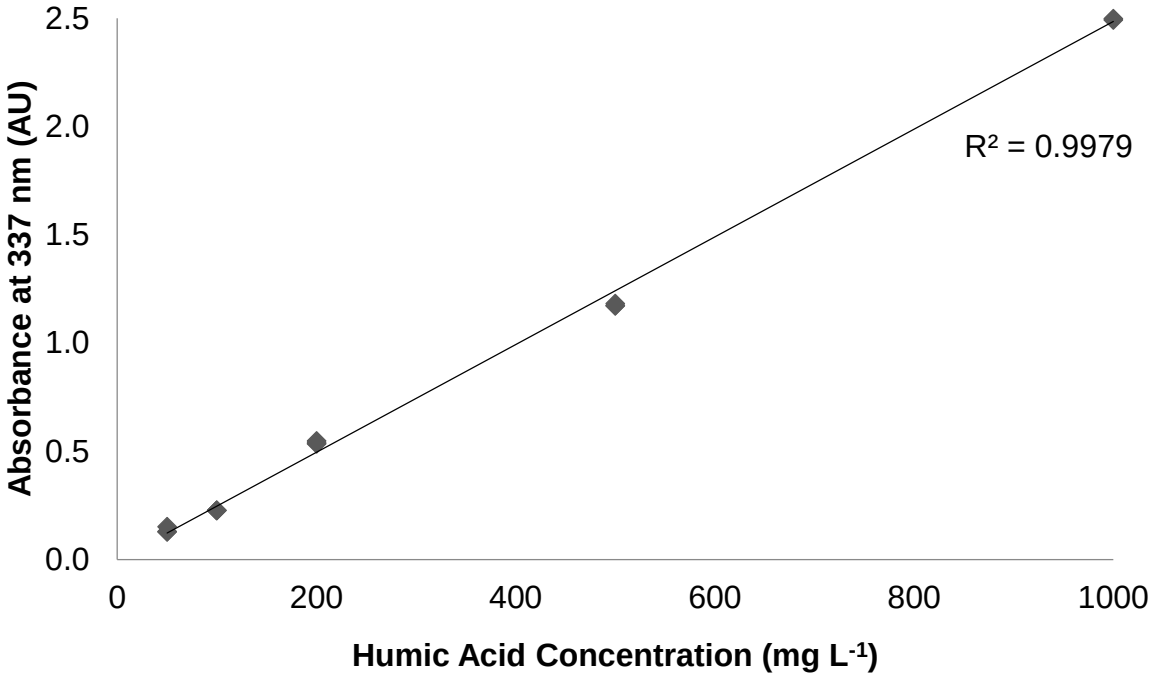

Figure 5.3 Calibration curve using ≤ 1000 mg L^{-1} humic acid was found to obey the Beer-Lambert law (R^2= 0.9979).

5.4 Results and Discussion

5.4.1 Activated carbon characterisation and mass compositions in mixed-matrix membranes

Each NIPS-based mixed-matrix microporous membrane extrusion produced a batch length of up to 5 m. During the course of the PhD research this was repeated successfully twice. The activated carbon (AC) particles used have a surface area of 1700 m^2 g^{-1}. The lower bound 10% population size was 5 µm, the median particle size for these AC particles was 20 µm and the 90% upper bound size was 40 µm. This range of AC particle size is typically used in literature (Ballinas et al., 2004b) without milling (Anson et al., 2004b). The presence of AC micropores substantially influences

its adsorption properties because the amount adsorbed on the membrane surface is negligible in comparison to that within the AC micropores (Avom, Mbadcam, Noubactep, & Germain, 1997). Post-processing the AC-HF-MMMs have carbon compositions of 0.0 %, 0.7 %, 3.2 %, 6.3 %, 11.8 % and 21.1% of AC by membrane mass as shown in **Figure 5.4**.

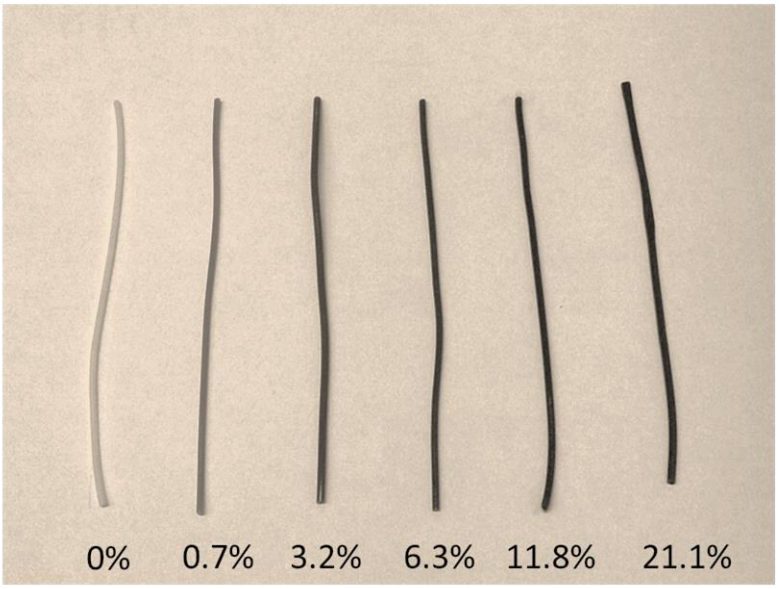

Figure 5.4 Photographs of 10 cm lengths of post-extrusion AC-HF-MMMs.

5.4.2 Porosity studies on AC-HF-MMMs

5.4.2.1 Scanning electron micrographs

Figure 5.5 presents SEM images of the different AC-HF-MMM compositions of 0.7, 3.2, 6.3, 11.8 AC membrane wt. %. Images are presented of the whole fibre cross-section, a whole wall cross section, as well as images of the inside edge, centre section and outer edge of the wall at higher magnifications. The AC particles appear evenly dispersed throughout the cross-section of the mixed-matrix membranes. AC particles were found to range between 5 µm and 25 µm. At the lower size range it is difficult to observe the activated carbon due to the scale of the SEM images. The AC

particles close to 10 μm can be seen as irregular shaped particles, especially in the whole wall and outer edge of the wall cross-sections. It was also observed in the presence of larger AC particles; local porosity was disrupted with small voids around the particles.

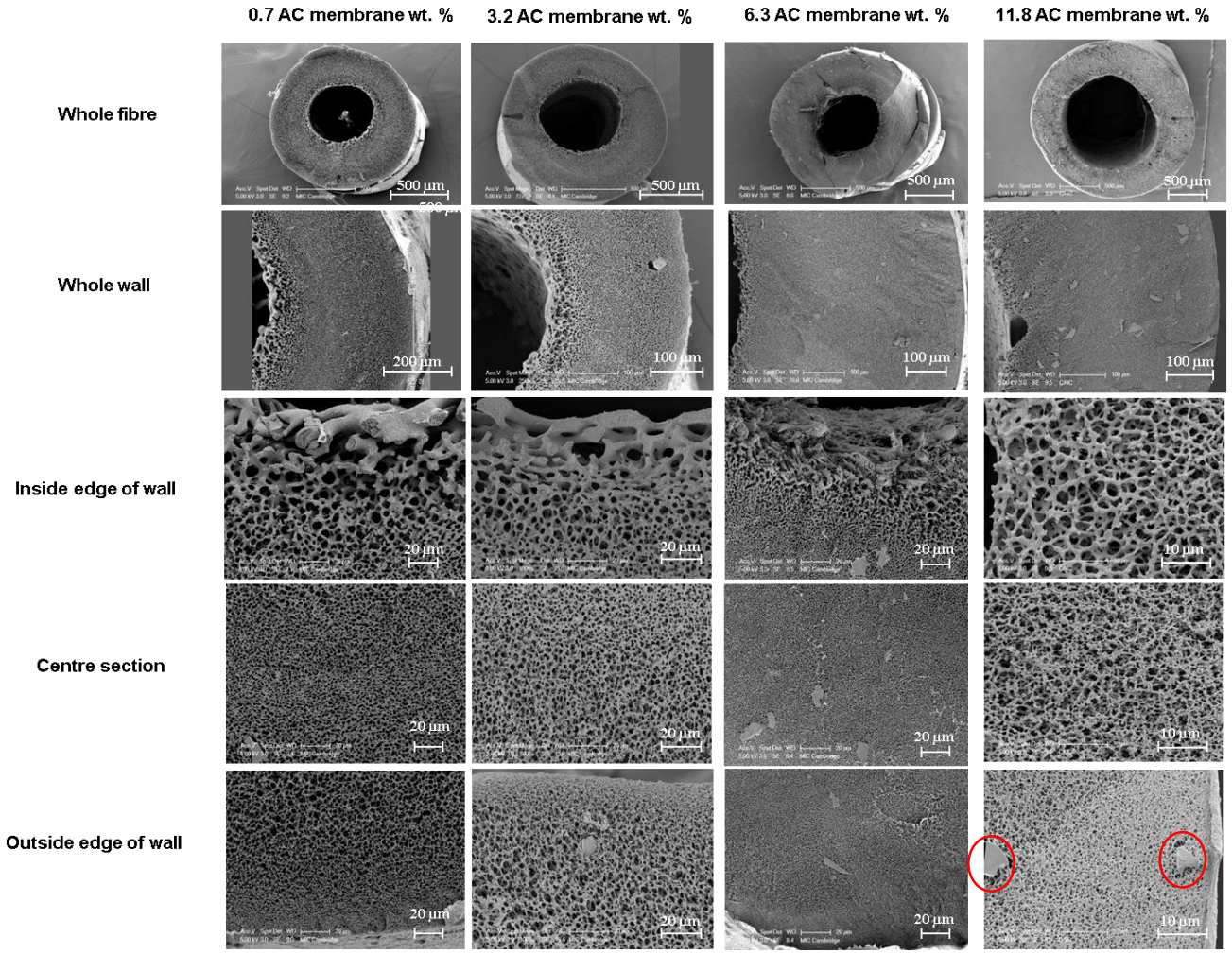

Figure 5.5 Scanning electron micrographs showing different magnifications of the cross-sectional microstructure of 0.7, 3.2, 6.3, 11.8 AC membrane wt. % mixed-matrix membranes. The red circles are examples of the irregularly shaped AC particles incorporated in the mixed-matrix membrane.

The AC-HF-MMM with the highest carbon mass fraction of 21.1 AC membrane wt. %, as shown in **Figure 5.6**, lost its porosity completely indicating a limit to AC particle composition.

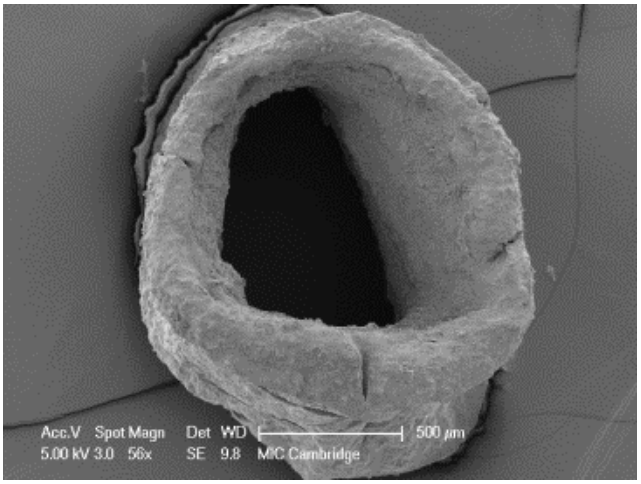

Figure 5.6 Scanning electron micrograph showing the 21.1 AC membrane wt. % mixed matrix membrane which has completely lost its membrane porosity.

Figure 5.7 compares the average pore sizes of the different AC-HF-MMMs across the inner capillary wall, middle section and outer capillary wall. The standard error of the average pore size measurements accounts for the pores not having ideal cylindrical shapes but structured as an interconnected network. Firstly, it was observed that as AC membrane wt. % increased, the average pore size of the inner capillary wall decreased. A significant trend for the average pore sizes for the middle section and outer capillary walls was not observed as the AC membrane wt. % increased. As in the control 0 AC membrane wt. %, for each composition the general trend is for the average pore sizes to be decreasing from the inner to the outer capillary wall.

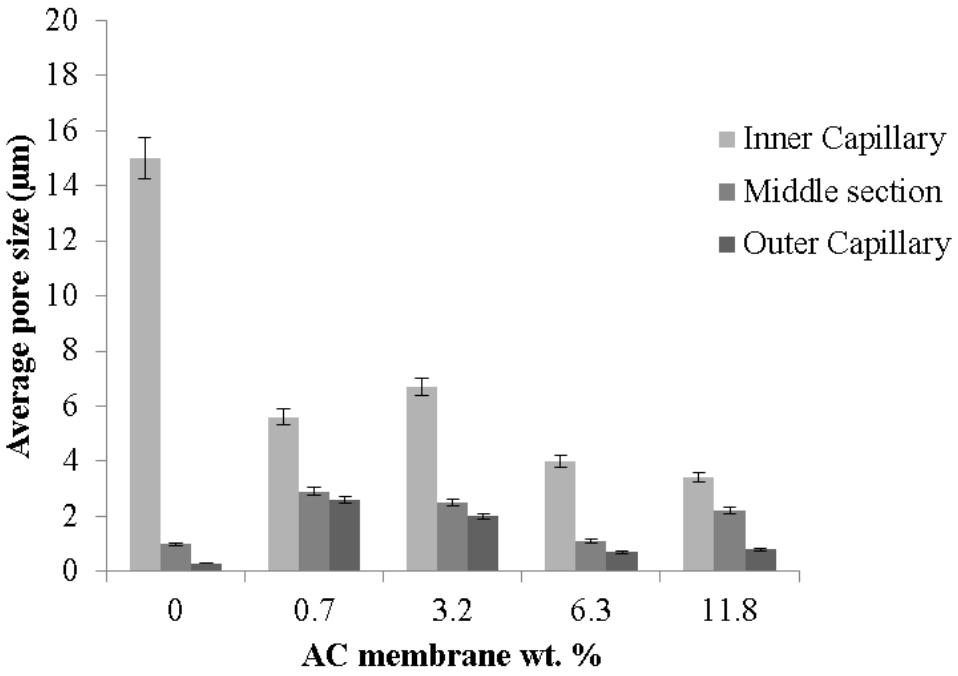

Figure 5.7 Pore size distributions across inner to outer capillary wall of different AC membrane wt. % mixed-matrix membranes. Average pore size across the inner capillary wall, middle capillary section and outer capillary wall are shown with the standard error across ten measurements.

5.4.2.2 Mercury porosimetry

The total surface area for the different AC-HFMs was calculated from mercury porosimetry studies. The porosimetry studies conclude that there were few closed pores across the capillary i.e. there was high inter-connectivity between the pores. Low AC membrane wt. % AC-HF-MMMs of 0.0 % — 6.3 % did not have a significant change in surface area, which was an average of 0.027 $m^2\ g^{-1}$. At 11.8 AC membrane wt. % there is a slight decrease in surface area to 0.024 $m^2\ g^{-1}$. At 21.1 AC membrane wt. %, there is a dramatic decrease in pore area to 0.013 $m^2\ g^{-1}$. This is expected since the SEM images for these AC-HF-MMMs show an almost complete loss of porosity. It was deduced with the decreasing average pore sizes over higher AC-HF-MMS there is also a decrease in surface area.

5.4.3 Methylene blue adsorption studies

Methylene blue was used as a model dye to study the adsorption characteristics of the mixed-matrix membrane. An increase in the amount of activated carbon in the fibres caused an increase in the mass of methylene blue adsorbed as shown in **Figure 5.8**. After 72 hours, the lower AC membrane wt. % membranes have comparatively darker blue solutions highlighting a high amount of unabsorbed methylene blue in solution. Overall as hypothesised, the control 0.0% AC membrane wt. % membrane absorbs the least dye and the 21.1% AC membrane wt. % membrane absorb the most.

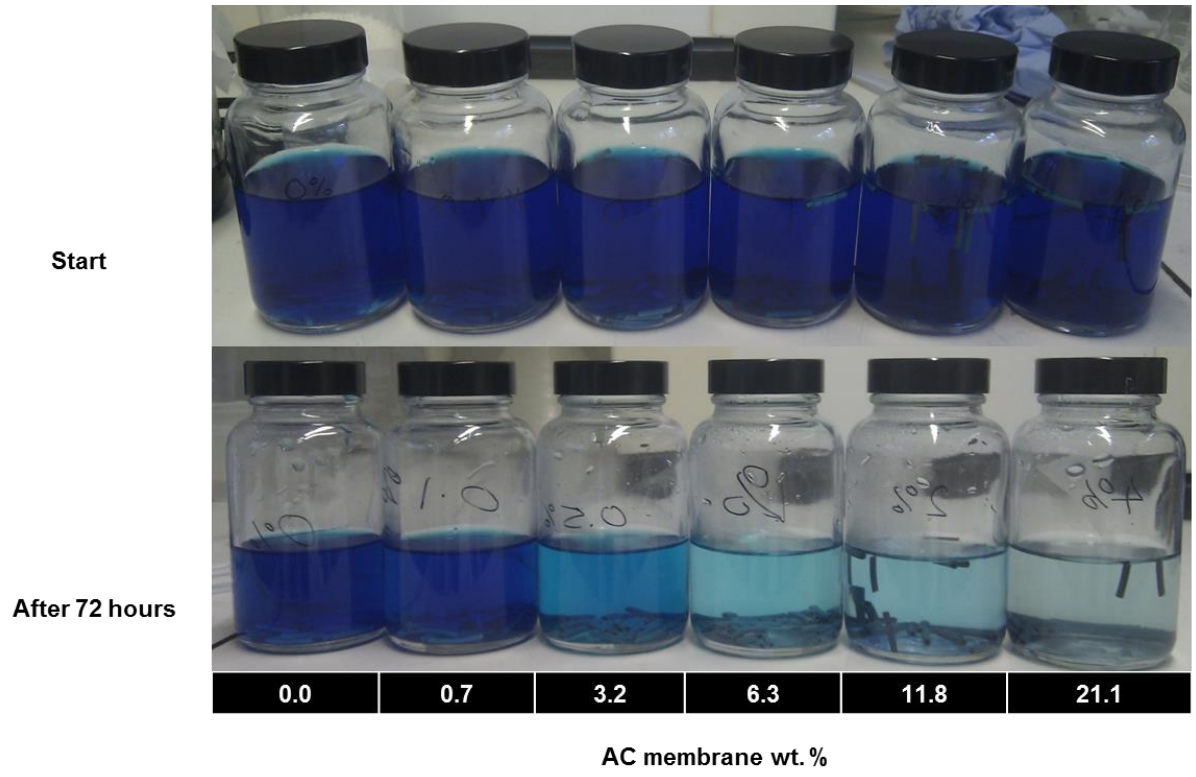

Figure 5.8 Qualitative study of methylene blue adsorption at equilibrium after 72 hours in 1g of AC-HF-MMMs of compositions of 0.0, 0.7, 3.2, 6.3, 11.8, 21.1 AC membrane wt.%.

For quantitative analysis, the concentration of the methylene blue in solution was measured during the experiment using spectrophotometry and Beer-Lambert law and presented in **Figure 5.9**. The quantitative adsorption studies complements result from the qualitative analysis of increase in methylene blue adsorption in increasing AC

compositions in AC-HF-MMMs. The standard deviation for the 11.8 and 21.1 AC membrane wt. % was especially high, this is deduced due to the interference of the activated carbon free particles to the UV readings.

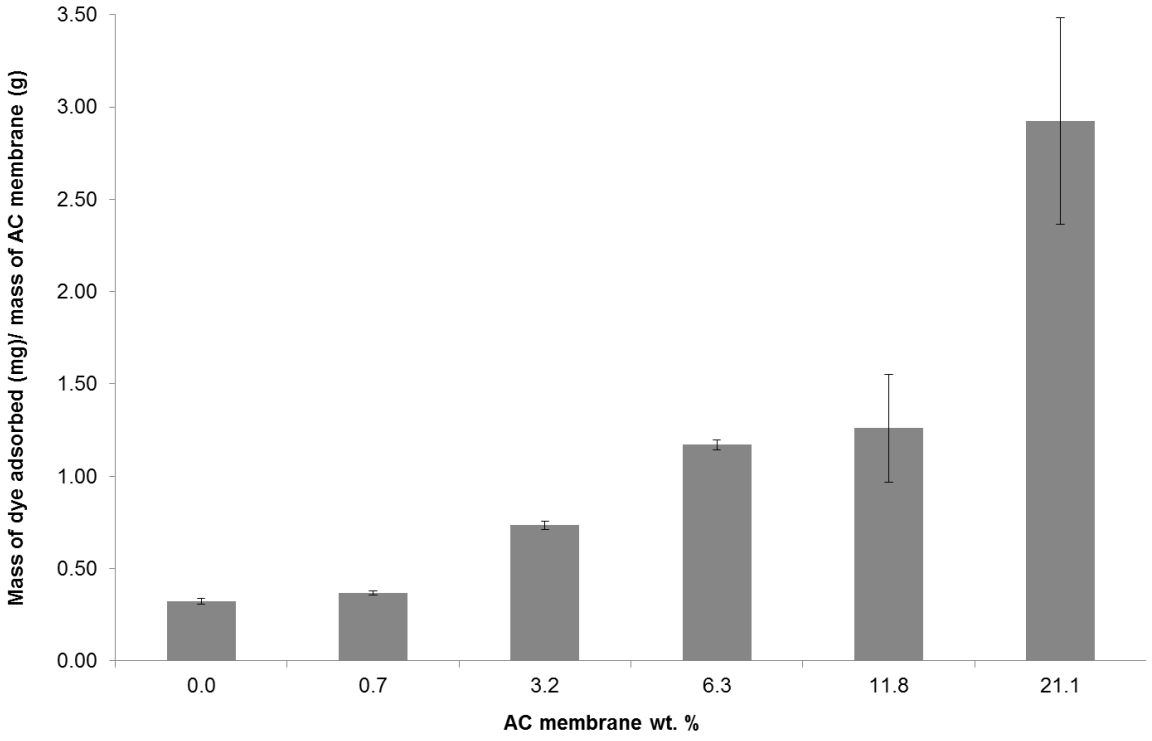

Figure 5.9 Amount of methylene blue dye absorbed per unit mass of AC-HF-MMM (mg methylene blue/ g membrane) to different compositons of AC membrane wt.% membranes. The error bars account for the standard error associated with UV-Vis readings.

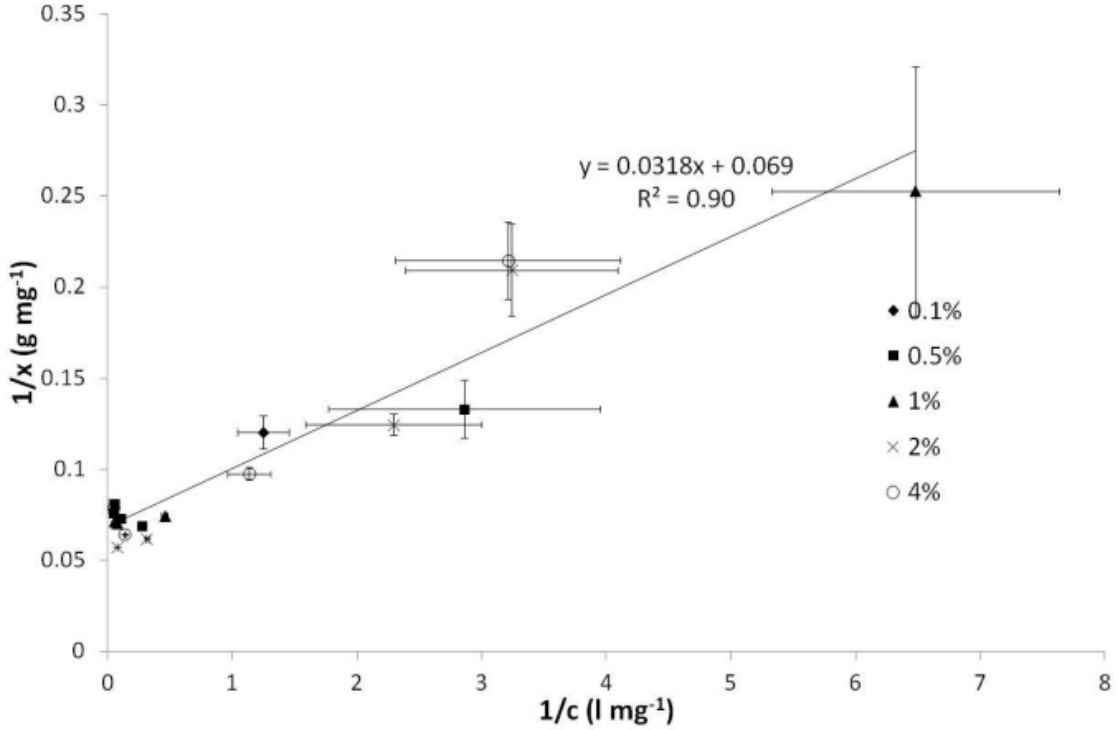

Figure 5.10 The Langmuir isotherm was the best fit for the methylene blue dye adsorption data on AC-HFM mixed-matrix membranes. In this figure x represents the mass of dye adsorbed per mass of carbon, and c the final concentration of dye in the solution.

Figure 5.10 shows a reasonable agreement for all carbon fibres. Regardless of the carbon fraction of fibre, the carbon has approximately constant chemical activity. For a stronger correlation a higher R^2 value than of 0.90 would normally be observed. This is most likely due to less adsorption in the higher carbon fraction fibres. From the porosity analysis this could be due to the reduced porosity leading to some of the AC particles becoming inaccessible to the dye.

5.4.4 Humic acid adsorption studies

Humic acid is a common pollutant that needs to be removed from wastewater. It is a small biomolecule usually formed from the biodegradation of dead organic matter and creates a problem in the water treatment industry since these acids inhibit the chemical disinfection process. After having characterised the AC-MMCF mixed matrix

membranes for its adsorption characteristics using model methylene blue, this study characterises its adsorption properties for humic acid.

Figure 5.11 shows humic acid adsorption at equilibrium in the highest three AC composition membranes, 6.3, 11.8 and 21.1 AC membrane wt. % AC-HFMs respectively. Overall the mass of humic acid adsorbed increases with humic acid concentration. The membranes could not adsorb more humic acid at maximum binding capacity at 500 mg L^{-1} and 1000 mg L^{-1} humic acid solution concentrations.

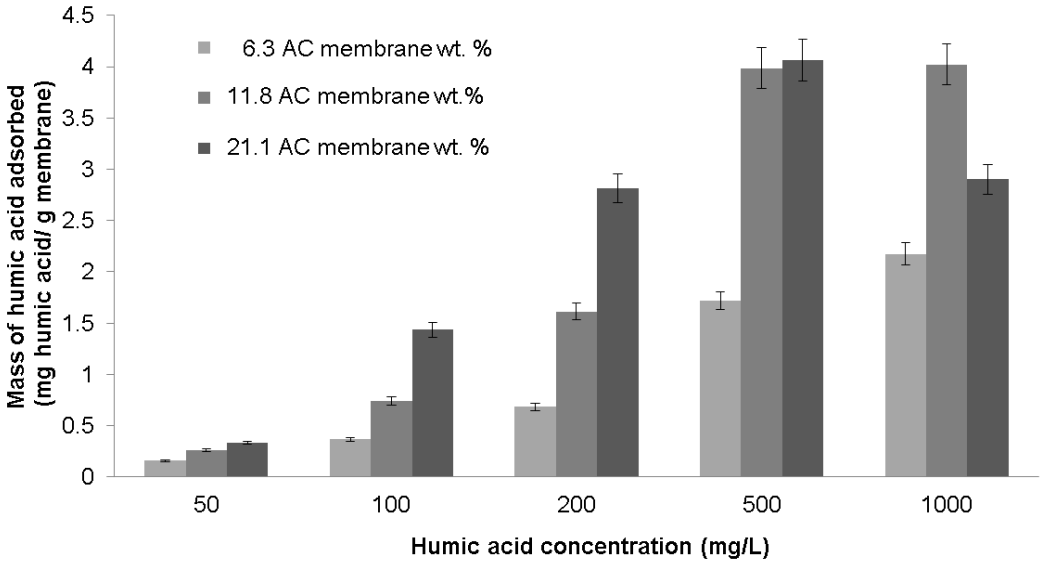

Figure 5.11 Amount of humic acid bound (mg humic acid/g membrane) to 3 different AC membrane wt. % membranes. The error bar account for the standard error associated with UV-Vis readings.

5.5 Conclusion

Mixed matrix membranes of activated carbon (AC) embedded in ethylene-vinyl alcohol were co-extruded to study the effect of the hollow fibre membranes (HFMs) on humic acid adsorption. Post-processing the AC-HF-MMMs had carbon compositions of 0.0, 0.7, 3.2, 6.3, 11.8 and 21.1 AC membrane wt. % by membrane mass. Overall as the

AC membrane wt. % composition increased the average pore size decreases. The higher AC membrane wt. % AC-HFMs adsorbed more methylene blue and humic acid. The mixed matrix membranes reached their maximum binding capacity at humic acid solution concentrations of 500 mg/L and 1000 mg/L. Future studies would focus on investigating the humic acid adsorption from wastewater samples and extrusion of AC-HFMs in a multi-capillary geometry.

CHAPTER 6 OVERALL CONCLUSIONS & FUTURE WORK

6.1 Overall Conclusions

In this thesis microcapillary membranes were characterised for separation of biomolecules and studied against existing separation processes in bioprocessing. This overall conclusions section summarises the problems or challenges in separations of biomolecules, the objectives this thesis has met, key original contributions made and the limitations of this study.

In processing of biopharmaceuticals, upstream processing has improved production yields and created a bottleneck for downstream purification steps. This is especially a problem in the first capture step that needs to bind a high concentration of the target biomolecule and allow flowthrough of cell debris and impurities. A decrease in processing time to reduce loss of biomolecule viability post-extraction is needed. Biomolecules can be broadly categorised as larger protein and antibody biomolecules, or small biological metabolites. Traditional chromatography columns have been developed for isolation of small chemical molecules and are not optimised for the complex nature of larger biomolecules. Two types of matrix geometries are most commonly used in the industry: bead-based and membrane-based. Although the bead based chromatography columns have the highest binding capacity, their flow throughput is slow due to the diffusion dependent mass transfer between and within beads. Membranes have much better flow behaviour and higher throughput but have a lower binding capacity due to a reduced surface area. Overall, there are problems in current biomolecule separation technologies of pressure tolerance, flow throughput, packaging requirements, sterilisation and disposability. The hypothesis of this thesis is to explore the novel matrix geometry of microcapillary membranes for large protein

biomolecules and small biomolecule separations and understand where they fit in key chromatographic parameters with other chromatographic media.

The thesis studied three key objectives:

- Investigated the physical nature of microporous capillary membranes, designed separation modules and tested various flow characteristics.
- Studied macromolecular biomolecule purifications via ion-exchange chromatography techniques of cation and anion-exchange chromatography.
- Altered the chemical composition of microporous microcapillary membranes through incorporating an inorganic particle and studied how the novel mixed-matrix membrane adsorbed small organic biomolecules.

These thesis objectives were studied using standard experiments that were conducted to study these novel chromatography matrices. These experiments were conducted according to industrial standards, to enable a comparison between the microcapillary membranes and appropriate commonly used chromatography media. Key characterisation experiments were pressure and flow tolerance, residence time distribution, dynamic binding capacity, ligand binding density and bio-separation studies.

Firstly, the two types of microcapillary membranes, hollow fibre membranes (HFM) and microporous walled microcapillary film (MMCF) membranes were reproduced using a non-solvent induced phase separation (NIPS) process. BET surface areas were measured to be 230.0 m^2 g^{-1} for HFM and 10.59 m^2 g^{-1} for MMCF. The 19 capillaries in the MMCF membranes instead of the one central capillary in the HFM and the difference in pore structure both contributed to the decrease in surface area

for MMCF membranes. Overall the surface area of the microcapillary membranes was higher than that of non-porous versions previously studied. A 20 cm MMCF membrane had a 425-fold higher surface area than a 5 m non-porous microcapillary film (NMCF).

Flow studies were conducted on the various modules to understand the degree of laminar or turbulent behaviour with any secondary flows such as dean vortices, due to the change from straight to helical module geometry. Fluid flow behaviour through the HFM and MMCF membranes was laminar as would be expected from the parallel capillary nature. More turbulent flow was measured once the module geometry for the MMCF was switched from a straight to a helical set-up. Residence time distribution studies through all the microcapillary membrane modules found tailing due to the porous nature of the membranes and high asymmetry factors increasing from HFM to straight MMCF to helical MMCF modules.

The microcapillary membranes were then tested for separation of biological macromolecules using both cation and anion exchange chemistry.

The two different types of microcapillary membranes and two different types of MMCF modules were studied for their performance in cation-exchange chemistry. The dynamic binding capacity (DBC) was an important parameter as in downstream bioprocessing under flow conditions a significant proportion of the theoretical capacity is not accessed. DBC of the HFM module was 3.14 mg lysozyme/ ml adsorbent volume, DBC of the MMCF straight module was 13.8 mg lysozyme/ ml adsorbent volume and DBC of the MMCF helical module was also 13.8 mg lysozyme/ ml adsorbent volume.

The DBC of the straight SP-MMCF module was also compared against Amersham Biosciences SP Sepharose XL adsorbent (160 mg lysozyme/ ml adsorbent volume)

and Pall Mustang S membranes (47 mg lysozyme/ ml adsorbent volume). The straight MMCF can operate at much higher linear velocities than conventional media. DBC of the MMCF is 12-fold lower than the conventional packed bed comparator, but only about 4-fold lower than that of a membrane adsorber. The DBCs fell with increasing flow velocities for protein adsorption in conventional beads, but was relatively invariant in MMCFs. The MMCF straight module was chosen as the module for further ligand density and equilibrium studies as it had altogether the best residence time distribution, DBC, pressure tolerance and flow velocities.

On the straight MMCF module, a homogenous distribution of the cation-exchange chemistry was found using a fluorescent tagged protein of rhodamine 6G-lysozyme across the 19 capillaries of the MMCF, except a concentration of surface chemistry was found within the smaller pore sizes between 0.1-0.5 µm. Using a Langmuir isotherm fit model, the molar equilibrium binding capacity of the MMCF module was calculated to be 4.4 µM lysozyme/ml adsorbent volume. This corresponds to a binding density of 228 ng lysozyme/cm^2 adsorbent surface area, in the same magnitude but lower than an NMCF device at 314 ng lysozyme/cm^2 adsorbent surface area. In large biomolecules separation of the total sample eluted, 98.8% was purified as the target protein lysozyme over 1.2% of the impurity BSA.

In the anion-exchange study, the straight MMCF module was modified to the opposite surface chemistry, a positively charged surface to attract negatively charged large biomolecules. The surface chemistry for the anion-exchange had additional chemical steps, to add two linkers before adding the quaternary amines, which may have reduced final quaternary amine density. The MMCF-Q module displayed a sharper breakthrough than the MMCF-SP module, indicating a lower amount of protein mass bound. The dynamic binding capacity of the MMCF-Q module at 10% breakthrough

was 1.26 mg ovalbumin/ ml adsorbent volume. This showed a two-fold lower magnitude than commercially packed bed columns (130 mg bovine serum albumin/ ml adsorbent volume GE Q Sepharose XL ®) and membranes (70 mg bovine serum albumin/ ml adsorbent volume Pall Mustang Q modified Supor ®). The saturation binding capacity of MMCF-Q was variant with linear velocity, dropping at higher velocities. The binding capacity at near saturation of the MMCF module was on average 22 times higher than the NMCF device. BSA was purified to the detection level of a silver stain of a solution of lysozyme and BSA.

A mixed-matrix membrane (MMM) was also developed for the study of adsorption of small biomolecules. Since the composition of the polymer solution in the NIPS process was modified to incorporate different wt. % of activated carbon (AC), the simpler HFM microcapillary membrane geometry was chosen for this study. Post-processing the AC-HF-MMMs had carbon compositions of 0.0 %, 0.7 %, 3.2 %, 6.3 %, 11.8 % and 21.1 % of AC by membrane mass. The AC particles were evenly dispersed throughout the cross-section of the mixed-matrix membranes. Porosity was lost at the AC-HF-MMM composition of 21.1 AC membrane wt. %. As the AC membrane wt. % increased, the average pore size of the inner capillary wall decreased. Decreasing the average pore sizes over higher AC-HF-MMMs was found to correspond with surface area. Two small molecules were chosen for the adsorption studies: the model chemical dye methylene blue and humic acid found from biodegraded organic matter. The control 0.0 % AC membrane wt. % membrane absorbs the lowest amount of methylene blue dye and the 21.1 % AC membrane wt. % membrane absorb the greatest amount. The highest amount of humic acid the higher AC-HF-MMM fibres could bind was ~ 4 mg humic acid/ g membrane.

Overall this thesis made key contributions in the understanding of microcapillary membranes. As hypothesised from the outset, the increase in surface area of microcapillary membranes facilitates up to 10^4 folds higher DBC in particular chemistries. Microcapillary membranes were used for the separation of both small molecule metabolites and large protein biomolecules. Mass transfer through microcapillary membrane was predominantly convection based (from aqueous phase to surface of the membrane) but also diffusion dependent (through pores, linear velocity dependent decrease in dynamic binding capacity) as seen in SP and Q dynamic binding capacity changes over flow velocities. The MMCF membrane was found to be the best suited for biomolecules separation in terms of its DBC, pressure tolerance, high-throughput behaviour, reproducibility and disposability. A simpler linker chemistry of cation-exchange was found to achieve better ligand density and adsorption behaviour over complex multi-step linker chemistry, which was used for anion-exchange. The dynamic binding capacity of the microcapillary was lower than the commercially available columns it was compared against. This could be due to multiple variables such as lower overall pore surface area per unit volume, surface ligand chemistry density and fluid flow behaviour due to the presence of microcapillaries. Microcapillary membranes may well be a suitable alternative to purification steps in downstream processing involving high product concentrations, large biomolecules, polishing and fast modular scale-up potential that can be used in continuous processing. Additionally, the novel inorganic support created, using activated carbon embedded into the synthetic copolymer EVOH in a HFM format, can also be used to remove small biomolecule impurities due to its reduced likelihood of non-specific attachment of microorganisms and enzymes and high tolerance to degrading chemicals.

This thesis has opened the area for studying microcapillary membranes for the separation of biological molecules. There are many areas of studying these membranes with various different types of biomolecules, different surface chemistries and further understanding of their flow behaviour and modifying their porosity for improved chromatographic parameters. The materials chemicals cost for the MMCF used in this work is estimated to be only a few pence as the cost of extrusion is low. A major proportion of the scale-up cost is likely to lie in materials and labour expenses for the chemical functionalization and other pilot scale up production requirements. Appropriate environmental treatment would need to be made for the surface chemistry chemicals that would be used in pilot or commercial scale higher volumes, EVOH itself as co-polymer has been used in the food processing industry and is recyclable. The thesis also opens up the use of the novel high-throughput geometry of the microcapillary membranes for removal of organic impurities from bio-degradation, which can be further studied for waste water treatment.

Although this was the first study of its kind using MMCF membranes for biomolecules chromatography, this study had its overall limitations in scope. The porous nature of the microporous microcapillary membranes could be modified further by changing key NIPS parameters to optimise them for higher dynamic binding capacity. Changing the diameter of the microcapillaries will also make a difference to how early the frontal breakthrough appears, albeit at the expense of increasing pressure across the module. Testing pilot fermenter samples would have tested these membranes on complicated cell extracts, especially for adsorbing impurities such as host cell protein, endotoxins and viruses. With the high demand in monoclonal antibodies, developing affinity chemistry on these membranes would be the next most interesting application. Extending the scope of the module geometry to a cross-flow membrane module and

compare it with the straight and helical modules would test the scale-up potential and the most effective module geometry. Even though the MMCF modules were tested in replicates, long term stability studies would be useful to observe membrane fouling and the timescales for decrease in binding capacity under different storage conditions. Some of this limitations of this current study has been critically discussed in the next section.

6.2 Future Work

In this section I have highlighted three key areas that this thesis has justified future investigation into.

6.2.1 Modifying the NIPS process for optimised microstructure and permeability of microcapillary membranes

Further in-depth studies can be carried out on the NIPS process to optimise their microstructure for not only current adsorption based chromatographic techniques but also for other applications in size-exclusion chromatography (Lazar, Mandal, & Slater, 2015). Improved porosity and permeability would have a direct effect on the mass transfer mechanisms across the microcapillary membranes and dynamic binding capacity.

In general, the microstructure of microcapillary membranes depends on how the polymer solution phase separates. Phase separation of polymers is a complex physical phenomenon which is not fully understood. In general, the main parameters that establish the microstructure of a membrane are the polymer solution starting composition and the nature of internal (core fluid) and external coagulants (Baker, 2004). A higher polymer concentration in the starting polymer solution normally leads to a membrane microstructure with a denser skin or addition of salts such as zinc

chloride and lithium chloride as well as polymeric additives such as PVP generally results in the formation of more porous membranes.

The nature of the internal and external coagulants is another important processing parameter which influences the microstructure of the hollow fibres. Normally increasing the solvent amount in the coagulant reduces the coagulation power and leads to the formation of a more open and porous structure within the hollow fibre membranes (Deshmukh & Li, 1998; Rahbari-sisakht, Ismail, & Matsuura, 2012). Both the PVP concentration (Lafreniere & Talbot, 1987) and PVP molecular weight (Jung, Yoon, Kim, & Rhee, 2004) have been shown to affect final membrane morphology and pore size.

In addition to these main parameters, processing parameters such as draw ratio, air-gap distance, polymer solution shear rate and polymer solution and the external coagulant temperature have been found to affect the microstructure of microcapillary membranes.

As the porosity of the microcapillary membranes is optimised, the change of permeability of the membrane and its effect on binding capacity must also be studied. The modification of certain variables in the NIPS process has been shown in literature to alter the permeability. Increasing the polymer concentration in a solution leads to the formation of less porous membranes with smaller pore size. Hence, increasing the polymer concentration normally reduces the membrane permeability while increasing the molecule rejection (Baker, 2004). An increase in air-gap distance could result in a hollow fibre with a lower number of finger-like voids and a significantly lower permeability (Chung & Hu, 1997). High spinning temperature could lead to the formation of hollow fibre membranes consisting of a thin skin-layer and loose sponge-like sublayer with both more permeability and also high solute rejection (Zhu, Yu, Xu,

& Zhu, 2009). It is a common practice in membrane literature to post-treat membranes with a NaOCl solution to remove the residual PVP in the membrane matrix. It has been observed that the NaOCl treatment reduced the thickness of the PVP layer near the outer surface of the MCF by ~ 50%, which could possibly lead to higher permeability of the post-treated membranes.

A quantitative approach to study fluid flow through the porous medium using Darcy's law could also be studied. Darcy's law is a simple proportional relationship between the instantaneous discharge rate through a porous medium, the viscosity of the fluid and the pressure drop over a given distance as shown in the Equation below:

$$Q = \frac{-kA}{\mu}\frac{(P_b - P_a)}{L}$$

(Equation 1)

The total discharge, *Q* (volume per time) is equal to the product of the permeability of the medium, *k*, the cross-sectional area to flow, *A*, and the pressure drop (P_b - P_a), all divided by the viscosity, *μ,* and the column length *L* over which the pressure drop is taking place. This equation can be used to calculate the permeability within the microcapillary membrane.

6.2.2 Microcapillary membranes modified for affinity chromatography

Having validated microcapillary membranes for ion-exchange chromatography, a future surface chemistry application would be in the development of linking Protein A and studying the advantages and limitations of this novel matrix format. In downstream bioprocessing, affinity chromatography is very widely used (Hagel et al., 2008). It is the primary capture step for monoclonal antibodies, reducing volume and concentrating the relatively dilute cell culture supernatant (Shukla, Hubbard, Tressel,

Guhan, & Low, 2007). The purity of the target product from a Protein A solution typically exceeds 95%, and the subsequent purification and polishing steps are necessary to remove residual host cell proteins, leached Protein A, DNA or adventitious agents such as viruses (Hagel et al., 2008). Current Protein A columns have a high cost of resin costing up to 45% of bio-production costs (Subramanian, 2007) and have resin fouling costs overtime. In general, even if Protein A chromatography is used, adequate purity and viral clearance are not achieved unless one or more polishing steps are included afterwards.

Cation-exchange membranes have also been studied as an alternative to the Protein A affinity capture step for direct capture of monoclonal antibodies (Dong et al., 2008; Miesegaes et al., 2012; Tao et al., 2014). Life Technologies have compared their POROS XS beads in relation to Protein A affinity chromatography columns and found two to three times protein binding capacity in some cases with a 4.5 times reduced resin cost, effective host cell protein removal and no generation of leached Protein A.

Comparison of Protein A affinity chemistry on microcapillary membranes against cation-exchange for their relative merits on efficient capture would be an interesting study. The size of the Protein A itself could become a limitation for the pore sizes in the microcapillary membrane. Additionally, the effect of the change of previously discussed porosity and permeability on the capacity of affinity chromatography would be worth exploring.

6.2.3 Microporous microcapillary mixed-matrix membranes for adsorption of larger biomolecules

This thesis has opened up an exciting new research avenue of exploring the highly porous and multi-capillary geometry in incorporating inorganic particles of multiple functionalities for adsorption separations or catalytic properties.

The study on the current AC-HF-MMMs from Chapter 5 can be extended for purification from smaller biomolecules to larger biomolecules such as viruses or even antibodies. Viruses are often found as contaminants in upstream fermentation processing. They have been known to be adsorb onto activated carbon, from studied as early as 1967 *Escherichia coli* bacteriophage T4 was found to adsorb onto activated carbon (Cookson & North, 1967). A recent patent has been granted for activated carbon also adsorbing proteins of sizes 30 kDa or more, glycoproteins or antibodies (Ishihara, 2014).

The use of bio-based or metal-based catalysts in the novel microcapillary membrane geometries may also have a substantial impact on both throughput, capacity and purification of end product.

REFERENCES

Aggarwal, P., Tolley, H. D., & Lee, M. L. (2012). Characterizing Organic Monolithic Columns Using Capillary Flow Porometry and Scanning Electron Microscopy. *Analytical Chemistry*, *84*(1), 247–254. doi:10.1021/ac203010r

Albanese, J., Blehaut, J., Chochois, H., Colin, H., & Guillerm, J. (2011). Industrial-Scale Biochromatography Columns Address Challenging Purification Needs. *BioProcess International*, *9*(2), 60–63.

Al-Rubeai, M. (2011). *Antibody Expression and Production*. Springer Science & Business Media. Retrieved from https://books.google.com/books?id=pRzrKqVa7YsC&pgis=1

Anson, M., Marchese, J., Garis, E., Ochoa, N., & Pagliero, C. (2004a). ABS copolymer-activated carbon mixed matrix membranes for CO2/CH4 separation. *Journal of Membrane Science*, *243*(1-2), 19–28. Retrieved from http://www.scopus.com/inward/record.url?eid=2-s2.0-4544260021&partnerID=tZOtx3y1

Anson, M., Marchese, J., Garis, E., Ochoa, N., & Pagliero, C. (2004b). ABS copolymer-activated carbon mixed matrix membranes for CO2/CH4 separation. *Journal of Membrane Science*, *243*(1-2), 19–28. doi:10.1016/j.memsci.2004.05.008

Avom, J., Mbadcam, J. K., Noubactep, C., & Germain, P. (1997). Adsorption of methylene blue from an aqueous solution on to activated carbons from palm-tree cobs. *Carbon*, *35*(3), 365–369. Retrieved from http://www.scopus.com/inward/record.url?eid=2-s2.0-0030679962&partnerID=40&md5=1ad41472eb3af577846ca0036188c3ce

Avramescu, M.-E., Borneman, Z., & Wessling, M. (2003a). Dynamic behavior of adsorber membranes for protein recovery. *Biotechnology and Bioengineering*, *84*(5), 564–72. doi:10.1002/bit.10807

Avramescu, M.-E., Borneman, Z., & Wessling, M. (2003b). Mixed-matrix membrane adsorbers for protein separation. *Journal of Chromatography A*, *1006*(1-2), 171–183. doi:10.1016/S0021-9673(03)00562-4

Avramescu, M.-E., Borneman, Z., & Wessling, M. (2008). Particle-loaded hollow-fiber membrane adsorbers for lysozyme separation. *Journal of Membrane Science*, *322*(2), 306–313. doi:http://dx.doi.org/10.1016/j.memsci.2008.06.013

Avramescu, M.-E., Gironès, M., Borneman, Z., & Wessling, M. (2003). Preparation of mixed matrix adsorber membranes for protein recovery. *Journal of Membrane Science*, *218*(1-2), 219–233. doi:10.1016/S0376-7388(03)00178-9

Bailey, J. E. (1986). *Biochemical Engineering Fundamentals*. McGraw-Hill. Retrieved from http://books.google.com.ng/books/about/Biochemical_Engineering_Fundamentals.html?id=3s9TAAAAMAAJ&pgis=1

Baker, R. W. (2004). *Membrane Technology and Applications*. Chichester, UK: John Wiley & Sons, Ltd. doi:10.1002/9781118359686

Ballinas, L., Torras, C., Fierro, V., & Garcia-Valls, R. (2004a). Factors influencing activated carbon-polymeric composite membrane structure and performance.

Journal of Physics and Chemistry of Solids, *65*(2-3), 633–637. doi:10.1016/j.jpcs.2003.10.043

Ballinas, L., Torras, C., Fierro, V., & Garcia-Valls, R. (2004b). Factors influencing activated carbon-polymeric composite membrane structure and performance. *Journal of Physics and Chemistry of Solids*, *65*(2-3), 633–637. Retrieved from http://www.scopus.com/inward/record.url?eid=2-s2.0-0942289562&partnerID=40&md5=b338e79d0b5ca3bce3d05b00925199bc

Bhut, B. V, Christensen, K. A., & Husson, S. M. (2010). Membrane chromatography: Protein purification from E. coli lysate using newly designed and commercial anion-exchange stationary phases. *Journal of Chromatography A*, *1217*(30), 4946–4957. Retrieved from http://www.scopus.com/inward/record.url?eid=2-s2.0-77954177820&partnerID=40&md5=1f86c532395769fc6b0f586d6642d5da

Bonyadi, S. (2012). *The Development of Micro Capillary Film Membranes for Separation Processes* (Doctoral dissertation).

Bonyadi, S., & Mackley, M. (2012). The development of novel micro-capillary film membranes. *Journal of Membrane Science*, *389*(0), 137–147. doi:10.1016/j.memsci.2011.10.023

Borneman, Z., & Wessling, M. (2006). Enzyme capturing and concentration with mixed matrix membrane adsorbers. *Journal of Membrane Science*, *280*(1-2), 406–417. doi:10.1016/j.memsci.2006.01.045

Brems, Y., Lapkin, A., & Baeyens, J. (2013). Pollution prevention in the pharmaceutical industry. *International Journal of Sustainable Engineering*, *6*(4), 344–351. doi:10.1080/19397038.2012.730070

Camperi, S. A., del Cañizo, A. A. N., Wolman, F. J., Smolko, E. E., Cascone, O., & Grasselli, M. (1999). Protein Adsorption onto Tentacle Cation-Exchange Hollow-Fiber Membranes. *Biotechnology Progress*, *15*(3), 500–505. doi:10.1021/bp990054g

Capto ™ S, Capto Q, and Capto DEAE. (2006). https://www.gelifesciences.com/gehcls_images/GELS/Related%20Content/Files/1335359522418/litdoc11002576_20120514181545.PDF

Carta, G., & Jungbauer, A. (2010). *Protein chromatography : process development and scale-up*. Weinheim: Wiley-VCH.

Carta, G., & Jungbauer, A. (2010). *Protein Chromatography: Process Development and Scale-Up*. John Wiley & Sons. Retrieved from http://books.google.com/books?hl=en&lr=&id=bILgrKmItv8C&pgis=1

Charcosset, C., Cherfi, A., & Bernengo, J.-C. (2000). Characterization of microporous membrane morphology using confocal scanning laser microscopy. *Chemical Engineering Science*, *55*(22), 5351–5358. doi:10.1016/S0009-2509(00)00151-2

Chase, H. A. (1994). Purification of proteins by adsorption chromatography in expanded beds. *Trends in Biotechnology*, *12*(8), 296–303. Retrieved from http://www.scopus.com/inward/record.url?eid=2-s2.0-0028484263&partnerID=40&md5=85189a77fa74aa0dc9afc50f1d987b95

Chen, Z., Xu, L., Liang, Y., Wang, J., Zhao, M., & Li, Y. (2008). Polyethylene glycol diacrylate-based supermacroporous monolithic cryogel as high-performance liquid chromatography stationary phase for protein and polymeric nanoparticle separation. *Journal of Chromatography. A*, *1182*(1), 128–31. doi:10.1016/j.chroma.2007.12.084

Chung, T.-S., & Hu, X. (1997). Effect of air-gap distance on the morphology and thermal properties of polyethersulfone hollow fibers. *Journal of Applied Polymer Science*, *66*(6), 1067–1077. doi:10.1002/(SICI)1097-4628(19971107)66:6<1067::AID-APP7>3.0.CO;2-G

Cookson, J. T., & North, W. J. (1967). Adsorption of viruses on activated carbon. Equilibriums and kinetics of the attachment of Escherichia coli bacteriophage T4 on activated carbon. *Environmental Science & Technology*, *1*(1), 46–52. doi:10.1021/es60001a002

Cramer, S. M., & Holstein, M. A. (2011). Downstream bioprocessing: recent advances and future promise. *Current Opinion in Chemical Engineering*, *1*(1), 27–37. doi:10.1016/j.coche.2011.08.008

D'Souza, R. N., Azevedo, A. M., Aires-Barros, M. R., Krajnc, N. L., Kramberger, P., Carbajal, M. L., … Fernández-Lahore, M. (2013). Emerging technologies for the integration and intensification of downstream bioprocesses. *Pharmaceutical Bioprocessing*, *1*(5), 423–440. Retrieved from http://www.future-science.com/doi/abs/10.4155/pbp.13.55

Daifullah, a. a. ., Girgis, B. ., & Gad, H. M. . (2004). A study of the factors affecting the removal of humic acid by activated carbon prepared from biomass material. *Colloids and Surfaces A: Physicochemical and Engineering Aspects*, *235*(1-3), 1–10. doi:10.1016/j.colsurfa.2003.12.020

Darton, N. J., Darling, D., Townsend, M. J., Mcnally, D. J., Farzaneh, F., & Slater, N. K. H. (2012). Lentivirus capture directly from cell culture with Q-functionalised microcapillary film chromatography. *Journal of Chromatography A*, *1251*, 236–239. doi:10.1016/j.chroma.2012.06.072

Darton, N. J., Reis, N. M., Mackley, M. R., & Slater, N. K. H. (2011). Fast cation-exchange separation of proteins in a plastic microcapillary disc. *Journal of Chromatography A*, *1218*(10), 1409–1415. Retrieved from http://www.scopus.com/inward/record.url?eid=2-s2.0-79951515334&partnerID=40&md5=986788b0b39991b7dfb56fab6cd42e02

Dean, W. R. (1928). Fluid Motion in a Curved Channel. *Proceedings of the Royal Society of London. Series A* , *121* (787), 402–420. doi:10.1098/rspa.1928.0205

Deshmukh, S. P., & Li, K. (1998). Effect of ethanol composition in water coagulation bath on morphology of PVDF hollow fibre membranes. *Journal of Membrane Science*, *150*(1), 75–85. doi:10.1016/S0376-7388(98)00196-3

Dods, S. R., Hardick, O., Stevens, B., & Bracewell, D. G. (2015). Fabricating electrospun cellulose nanofibre adsorbents for ion-exchange chromatography. *Journal of Chromatography. A*, *1376*, 74–83. doi:10.1016/j.chroma.2014.12.010

Dong, D., Liu, H., Xiao, Q., & Li, R. (2008). Affinity purification of egg yolk immunoglobulins (IgY) with a stable synthetic ligand. *Journal of*

Chromatography B: Analytical Technologies in the Biomedical and Life Sciences, *870*(1), 51–54. Retrieved from http://www.scopus.com/inward/record.url?eid=2-s2.0-45849104575&partnerID=40&md5=d5b23d93733536aa22fc3ad72de8f550

Doorly, D., & Sherwin, S. (2009). Geometry and flow. In L. Formaggia, A. Quarteroni, & A. Veneziani (Eds.), *Cardiovascular Mathematics SE - 5* (Vol. 1, pp. 177–209). Springer Milan. doi:10.1007/978-88-470-1152-6_5

Dorfling, C., Hornung, C. H., Hallmark, B., Beaumont, R. J. J., Fovargue, H., & Mackley, M. R. (2010). The experimental response and modelling of a solar heat collector fabricated from plastic microcapillary films. *Solar Energy Materials and Solar Cells*, *94*(7), 1207–1221. doi:10.1016/j.solmat.2010.03.008

Feng, C. Y., Khulbe, K. C., Matsuura, T., & Ismail, A. F. (2013). Recent progresses in polymeric hollow fiber membrane preparation, characterization and applications. *Separation and Purification Technology*, *111*, 43–71. doi:10.1016/j.seppur.2013.03.017

Ferrando, M., Rrzek, A., Zator, M., Lopez, F., & Guell, C. (2005). An approach to membrane fouling characterization by confocal scanning laser microscopy. *Journal of Membrane Science*, *250*(1-2), 283–293. doi:10.1016/j.memsci.2004.10.043

Flodin, P. (1961). Methodological aspects of gel filtration with special reference to desalting operations. *Journal of Chromatography A*, *5*, 103–115. doi:10.1016/S0021-9673(01)92827-4

Fraud, N., Faber, R., Kiss, C., Demmer, W., Hoerl, H.-H., & Fischer-Fruehholz, S. (2009). Hydrophobic-Interaction Membrane Chromatography for Large-Scale Purification of Biopharmaceuticals. *BioProcess International*, *7*(S6), 30–35. Retrieved from http://www.bioprocessintl.com/downstream-processing/chromatography/hydrophobic-interaction-membrane-chromatography-for-large-scale-purification-of-biopharmaceuticals-184195/

Freitag, R. (2014). Chromatographic techniques in the downstream processing of proteins in biotechnology. *Methods in Molecular Biology (Clifton, N.J.)*, *1104*, 419–58. doi:10.1007/978-1-62703-733-4_25

Gagnon, P. (2008). Eliminating the downstream processing bottleneck with monoliths and simulated moving bed chromatography. In *BioProcess International*. www.validated.com/revalbio/pdffiles/LithSMB.pdf

Gallagher, M. J., Huang, H., Schwab, K. J., Fairbrother, D. H., & Teychene, B. (2013). Generating backwashable carbon nanotube mats on the inner surface of polymeric hollow fiber membranes. *Journal of Membrane Science*, *446*, 59–67. doi:10.1016/j.memsci.2013.06.015

Ghosh, R. (2002). Protein separation using membrane chromatography: Opportunities and challenges. *Journal of Chromatography A*, *952*(1-2), 13–27. Retrieved from http://www.scopus.com/inward/record.url?eid=2-s2.0-0037023369&partnerID=40&md5=e9ccb7ed5265d9f29abb196c9a323100

Giddings, J. C. (1964). Reduced plate height equation: a common link between chromatographic methods. *Journal of Chromatography A*, *13*, 301–304.

doi:10.1016/S0021-9673(01)95123-4

Guillen, G. R., Pan, Y., Li, M., & Hoek, E. M. V. (2011). Preparation and Characterization of Membranes Formed by Nonsolvent Induced Phase Separation: A Review. *Industrial & Engineering Chemistry Research*, *50*(7), 3798–3817. doi:10.1021/ie101928r

Guiochon, G., & Beaver, L. A. (2011). Separation science is the key to successful biopharmaceuticals. *Journal of Chromatography A*, *1218*(49), 8836–8858.

Hagel, L., Jagschies, G., & Sofer, G. (2008). *Handbook of Process Chromatography: Development, Manufacturing, Validation and Economics*. Academic Press.

Hallmark, B., Gadala-Maria, F., & Mackley, M. R. (2005). The melt processing of polymer microcapillary film (MCF). *Journal of Non-Newtonian Fluid Mechanics*, *128*(2–3), 83–98. Retrieved from http://www.sciencedirect.com/science/article/pii/S0377025705000601

Hallmark, B., Hornung, C. H., Broady, D., Price-Kuehne, C., & Mackley, M. R. (2008). The application of plastic microcapillary films for fast transient micro-heat exchange. *International Journal of Heat and Mass Transfer*, *51*(21-22), 5344–5358. doi:10.1016/j.ijheatmasstransfer.2008.01.036

Hammond, P. M. (1995). Bioaffinity chromatography. *Journal of Chemical Technology & Biotechnology*, *64*(1), 105. doi:10.1002/jctb.280640117

Hardick, O., Dods, S., Stevens, B., & Bracewell, D. G. (2015). Nanofiber adsorbents for high productivity continuous downstream processing. *Journal of Biotechnology*. doi:10.1016/j.jbiotec.2015.01.031

Healthcare, G. E. (2010). *Column efficiency testing*. https://www.gelifesciences.com/gehcls_images/GELS/Related%20Content/Files/1352880951136/litdoc28937207_20141127221416.pdf

Hjorth, R. (1999). Expanded bed adsorption: Elution in expanded bed mode. *Bioseparation*, *8*(1-5), 1–9. Retrieved from http://www.scopus.com/inward/record.url?eid=2-s2.0-0033388657&partnerID=40&md5=6355ac9cf09e8e95c30da671c464f02d

Ho, R. J. Y. (2013). *Biotechnology and Biopharmaceuticals: Transforming Proteins and Genes into Drugs*. John Wiley & Sons. Retrieved from http://books.google.com/books?id=HaDyAAAAQBAJ&pgis=1

Hornung, C. H., Hallmark, B., Hesketh, R. P., & Mackley, M. R. (2006). The fluid flow and heat transfer performance of thermoplastic microcapillary films. *Journal of Micromechanics and Microengineering*, *16*(2), 434–447. doi:10.1088/0960-1317/16/2/030

Hornung, C. H., Mackley, M. R., Baxendale, I. R., & Ley, S. V. (2007). A Microcapillary Flow Disc Reactor for Organic Synthesis. *Organic Process Research & Development*, *11*(3), 399–405.

Hubbuch, J., & Kula, M. R. (2008). Confocal laser scanning microscopy as an analytical tool in chromatographic research. *Bioprocess and Biosystems Engineering*, *31*(3), 241–59. doi:10.1007/s00449-008-0197-5

Ishihara, T. (2014, February 13). Method of purifying protein. Retrieved from

http://www.google.com/patents/US20140046038

Jung, B., Yoon, J. K., Kim, B., & Rhee, H.-W. (2004). Effect of molecular weight of polymeric additives on formation, permeation properties and hypochlorite treatment of asymmetric polyacrylonitrile membranes. *Journal of Membrane Science*, *243*(1-2), 45–57. doi:10.1016/j.memsci.2004.06.011

Jungbauer, A. (2010). *Protein chromatography :process development and scale-up* . Weinheim: Wiley-VCH.

Kalia, S., Kaith, B. S., & Kaur, I. (2011). *Cellulose Fibers: Bio- and Nano-Polymer Composites* (19th ed.). Berlin Heidelberg: Springer-Verlag.

Kelley, B. (2009). Industrialization of mAb production technology: the bioprocessing industry at a crossroads. *mAbs*, *1*(5), 443–452. Retrieved from http://www.scopus.com/inward/record.url?eid=2-s2.0-77950354715&partnerID=40&md5=caa900f8011c5dcfca82b08e2db28dbe

Klein, E. (2000). Affinity membranes: A 10-year review. *Journal of Membrane Science*, *179*(1-2), 1–27. Retrieved from http://www.scopus.com/inward/record.url?eid=2-s2.0-0034669857&partnerID=40&md5=6a96d22763a60adbf0b62d017d92ac29

Kluge, T., Rezende, C., Wood, D., & Belfort, G. (1999). Protein transmission during dean vortex microfiltration of yeast suspensions. *Biotechnology and Bioengineering*, *65*(6), 649–658. Retrieved from http://www.scopus.com/inward/record.url?eid=2-s2.0-0033590256&partnerID=tZOtx3y1

Kosior, A., Antošová, M., Faber, R., Villain, L., & Polakovič, M. (2013). Single-component adsorption of proteins on a cellulose membrane with the phenyl ligand for hydrophobic interaction chromatography. *Journal of Membrane Science*, *442*, 216–224. Retrieved from http://www.scopus.com/inward/record.url?eid=2-s2.0-84877883606&partnerID=40&md5=821f5ab1a260105b38e6646563baea10

Kuakuvi, D. N., Moulin, P., & Charbit, F. (2000). Dean vortices: a comparison of woven versus helical and straight hollow fiber membrane modules. *Journal of Membrane Science*, *171*(1), 59–65. doi:10.1016/S0376-7388(99)00379-8

Lafreniere, L., & Talbot, F. (1987). Effect of poly (vinylpyrrolidone) additive on the performance of poly (ether sulfone) ultrafiltration membranes. *Industrial & …*, 2385–2389.

Lazar, R. A., Mandal, I., & Slater, N. K. H. (2015). Effect of bore fluid composition on microstructure and performance of a microporous hollow fibre membrane as a cation-exchange substrate. *Journal of Chromatography A*. doi:10.1016/j.chroma.2015.03.037

Leinweber, F. C., & Tallarek, U. (2003). Chromatographic performance of monolithic and particulate stationary phases. *Journal of Chromatography A*, *1006*(1-2), 207–228. doi:10.1016/S0021-9673(03)00391-1

Lenhoff, A. M. (2011). Protein adsorption and transport in polymer-functionalized ion-exchangers. *Journal of Chromatography. A*, *1218*(49), 8748–59. doi:10.1016/j.chroma.2011.06.061

Li, J., & Chase, H. A. (2009). Characterization and evaluation of a macroporous adsorbent for possible use in the expanded bed adsorption of flavonoids from Ginkgo biloba L. *Journal of Chromatography. A*, *1216*(50), 8730–40. doi:10.1016/j.chroma.2009.02.092

Libecki, B., & Dziejowski, J. (2008). Optimization of humic acids coagulation with aluminum and Iron(III) salts. *Polish Journal of Environmental Studies*, *17*(3), 397–403. Retrieved from http://www.scopus.com/inward/record.url?eid=2-s2.0-45249105977&partnerID=40&md5=7ef121e4419806d2d225f02944db6adf

Loeb, S., & Sourirajan, S. (1964). High flow porous membranes for separating water from saline solutions. http://www.google.co.uk/patents/US3133132

Lopez-Rubio, A., Hernsndez-Munoz, P., Gimenez, E., Yamamoto, T., Gavara, R., & Lagaron, J. M. (2005). Gas barrier changes and morphological alterations induced by retorting in ethylene vinyl alcohol-based food packaging structures. *Journal of Applied Polymer Science*, *96*(6), 2192–2202. doi:10.1002/app.21690

Lottes, F., Arlt, W., Minceva, M., & Stenby, E. H. (2009). Hydrodynamic impact of particle shape in slurry packed liquid chromatography columns. *Journal of Chromatography. A*, *1216*(30), 5687–95. doi:10.1016/j.chroma.2009.05.090

Lowe, C. R. (Charles R. (1979). An introduction to affinity chromatography. *Laboratory Techniques in Biochemistry and Molecular Biology ; vol.7, Part 2*. Amsterdam [etc.]: North-Holland,. Retrieved from http://search.lib.cam.ac.uk/?itemid=|cambrdgedb|1544720

Lundblad, R. L., & Macdonald, F. (2010). *Handbook of Biochemistry and Molecular Biology, Fourth Edition* -. CRC Press. Retrieved from http://www.crcpress.com/product/isbn/9780849391682

Lv, Y., Lin, Z., & Svec, F. (2012). Hypercrosslinked large surface area porous polymer monoliths for hydrophilic interaction liquid chromatography of small molecules featuring zwitterionic functionalities attached to gold nanoparticles held in layered structure. *Analytical Chemistry*, *84*(20), 8457–60. doi:10.1021/ac302438m

Mandal, I., Townsend, M. J., Darton, N. J., Bonyadi, S., & Slater, N. K. H. (2014). A microporous walled micro-capillary film module for cation-exchange protein chromatography. *Journal of Membrane Science*, *466*, 123–129. doi:10.1016/j.memsci.2014.04.049

Marsh, K., & Bugusu, B. (2007). Food Packaging—Roles, Materials, and Environmental Issues. *Journal of Food Science*, *72*(3), R39–R55. doi:10.1111/j.1750-3841.2007.00301.x

Mayani, M., Filipe, C. D. M., & Ghosh, R. (2010). Cascade ultrafiltration systems—Integrated processes for purification and concentration of lysozyme. *Journal of Membrane Science*, *347*(1–2), 150–158. doi:http://dx.doi.org/10.1016/j.memsci.2009.10.016

Mayer, J. M., Kaplan, D. L., Stote, R. E., Dixon, K. L., Shupe, A. E., Allen, A. L., & McCassie, J. E. (1996). Biodegradation of Polymer Films in Marine and Soil Environments. In *Hydrogels and Biodegradable Polymers for Bioapplications* (Vol. 627, pp. 13–159). American Chemical Society. doi:doi:10.1021/bk-1996-

0627.ch013

McCreath, G. E., Owen, R. O., Nash, D. C., & Chase, H. A. (1997). Preparation and use of ion-exchange chromatographic supports based on perfluoropolymers. *Journal of Chromatography A*, *773*(1-2), 73–83. doi:10.1016/s0021-9673(97)00191-x

Miesegaes, G. R., Lute, S., Strauss, D. M., Read, E. K., Venkiteshwaran, A., Kreuzman, A., … Brorson, K. (2012). Monoclonal antibody capture and viral clearance by cation exchange chromatography. *Biotechnology and Bioengineering*, *109*(8), 2048–58. doi:10.1002/bit.24480

Moulin, P., Manno, P., Rouch, J. ., Serra, C., Clifton, M. ., & Aptel, P. (1999). Flux improvement by Dean vortices: ultrafiltration of colloidal suspensions and macromolecular solutions. *Journal of Membrane Science*, *156*(1), 109–130. doi:10.1016/S0376-7388(98)00333-0

Müller, W. (1990). New ion exchangers for the chromatography of biopolymers. *Journal of Chromatography A*, *510*(0), 133–140. doi:http://dx.doi.org/10.1016/S0021-9673(01)93746-X

Ng, J. B. S., Kamali-Zare, P., Brismar, H., & Bergström, L. (2008). Release and molecular transport of cationic and anionic fluorescent molecules in mesoporous silica spheres. *Langmuir : The ACS Journal of Surfaces and Colloids*, *24*(19), 11096–102. doi:10.1021/la801179v

Orr, V., Zhong, L., Moo-Young, M., & Chou, C. P. (2013). Recent advances in bioprocessing application of membrane chromatography. *Biotechnology Advances*, *31*(4), 450–65. doi:10.1016/j.biotechadv.2013.01.007

Peng, N., Widjojo, N., Sukitpaneenit, P., Teoh, M. M., Lipscomb, G. G., Chung, T.-S., & Lai, J.-Y. (2012). Evolution of polymeric hollow fibers as sustainable technologies: Past, present, and future. *Progress in Polymer Science*, *37*(10), 1401–1424. doi:10.1016/j.progpolymsci.2012.01.001

Peterson, E. A., & Sober, H. A. (1956). Chromatography of Proteins. I. Cellulose Ion-exchange Adsorbents. *Journal of the American Chemical Society*, *78*(4), 751–755. doi:10.1021/ja01585a016

Potgieter, J. H. (1991). Adsorption of methylene blue on activated carbon: An experiment illustrating both the langmuir and freundlich isotherms. *Journal of Chemical Education*, *68*(4), 349–350. Retrieved from http://www.scopus.com/inward/record.url?eid=2-s2.0-20044389918&partnerID=40&md5=703f48ee45471af95932184a29315747

Rahbari-sisakht, M., Ismail, A. F., & Matsuura, T. (2012). Effect of bore fluid composition on structure and performance of asymmetric polysulfone hollow fiber membrane contactor for CO2 absorption. *Separation and Purification Technology*, *88*, 99–106. doi:10.1016/j.seppur.2011.12.012

Reichert, U., Linden, T., Belfort, G., Kula, M.-R., & Thömmes, J. (2002). Visualising protein adsorption to ion-exchange membranes by confocal microscopy. *Journal of Membrane Science*, *199*(1-2), 161–166. doi:10.1016/S0376-7388(01)00693-7

Sandle, T., & Saghee, M. R. (2011). Some considerations for the implementation of disposable technology and single-use systems in biopharmaceuticals.(Original

Article). *Journal of Commercial Biotechnology*, *17*(4), 319(11). Retrieved from http://find.galegroup.com/gtx/infomark.do?&contentSet=IAC-Documents&type=retrieve&tabID=T002&prodId=AONE&docId=A272168368&source=gale&srcprod=AONE&userGroupName=learn&version=1.0

Saufi, S. M., & Fee, C. J. (2011). Recovery of lactoferrin from whey using cross-flow cation exchange mixed matrix membrane chromatography. *Separation and Purification Technology*, *77*(1), 68–75. doi:10.1016/j.seppur.2010.11.021

Shukla, A. A., Hubbard, B., Tressel, T., Guhan, S., & Low, D. (2007). Downstream processing of monoclonal antibodies-Application of platform approaches. *Journal of Chromatography B: Analytical Technologies in the Biomedical and Life Sciences*, *848*(1), 28–39. Retrieved from http://www.scopus.com/inward/record.url?eid=2-s2.0-33847611596&partnerID=40&md5=bce2a84ceed52378ae84c70ffc13cf8a

Strang, R. (1984). Purification of egg-white lysozyme by ion-exchange chromatography. *Biochemical Education*, *12*(2), 57–59. doi:10.1016/0307-4412(84)90003-7

Subramanian, G. (2007). *Bioseparation and Bioprocessing*. Kent: WILEY-VCH Verlag GmbH & Co. KGaA.

Summers, R. S., & Roberts, P. V. (1988). Activated Carbon Adsorption of Humic Substances I. Heterodisperse Mixtures and Desorption R. SCOTT SUMMERS 1 AND PAUL V. ROBERTS 2, *122*(2).

Svec, F., Tennikova, T. B., & Deyl, Z. (2003). *Monolithic Materials: Preparation, Properties and Applications*. Elsevier. Retrieved from https://books.google.com/books?id=XjLHaF4r-zYC&pgis=1

Tan, S. C., & Yiap, B. C. (2009). DNA, RNA, and Protein Extraction: The Past and The Present. *Journal of Biomedicine and Biotechnology*, *2009*, 10. doi:http://dx.doi.org/10.1155/2009/574398

Tao, Y., Ibraheem, A., Conley, L., Cecchini, D., & Ghose, S. (2014). Evaluation of high-capacity cation exchange chromatography for direct capture of monoclonal antibodies from high-titer cell culture processes. *Biotechnology and Bioengineering*, *111*(7), 1354–1364. doi:10.1002/bit.25192

Thermo Scientific. (2008a). Calculate dye:protein (F/P) molar ratios. https://tools.thermofisher.com/content/sfs/brochures/TR0031-Calc-FP-ratios.pdf

Thermo Scientific. (2008b). Instructions NHS-Rhodamine.

Thermo Scientific. (2012). Instructions Zeba Spin Desalting Columns.

Tijink, M. S. L., Wester, M., Glorieux, G., Gerritsen, K. G. F., Sun, J., Swart, P. C., … Stamatialis, D. (2013). Mixed matrix hollow fiber membranes for removal of protein-bound toxins from human plasma. *Biomaterials*. Retrieved from http://www.scopus.com/inward/record.url?eid=2-s2.0-84880184513&partnerID=40&md5=3ad816a461c971ee307b15b5b0f8845b

Trilisky, E. I., Koku, H., Czymmek, K. J., & Lenhoff, A. M. (2009). Relation of structure to performance characteristics of monolithic and perfusive stationary phases. *Journal of Chromatography. A*, *1216*(36), 6365–76.

doi:10.1016/j.chroma.2009.07.005

Wang, L., & Ghosh, R. (2008). Fractionation of monoclonal antibody aggregates using membrane chromatography. *Journal of Membrane Science*, *318*(1-2), 311–316. doi:10.1016/j.memsci.2008.02.056

Webb, P. A. (2001, January 1). An Introduction To The Physical Characterization of Materials by Mercury Intrusion Porosimetry with Emphasis On Reduction And Presentation of Experimental Data. doi:10.1177/004057368303900411

Weetall, H. H., & Lee, M. J. (1989). Antibodies immobilized on inorganic supports. *Applied Biochemistry and Biotechnology*, *22*(3), 311–330. doi:10.1007/BF02921764

Wickramsinghe, S., Carlson, J., Teske, C., Hubbuch, J., & Ulbright, M. (2006). Characterizing solute binding to macroporous ion exchange membrane adsorbers using confocal laser scanning microscopy. *Journal of Membrane Science*, *281*(1-2), 609–618. doi:10.1016/j.memsci.2006.04.032

Wienk, I. M., Boom, R. M., Beerlage, M. A. M., Bulte, A. M. W., Smolders, C. A., & Strathmann, H. (1996). Recent advances in the formation of phase inversion membranes made from amorphous or semi-crystalline polymers. *Journal of Membrane Science*, *113*(2), 361–371. doi:10.1016/0376-7388(95)00256-1

Woodgate, J. M. (2001). *Purification of plasmid DNA for use in human gene therapy*. University of Aston.

Wurm, F. M. (2004). Production of recombinant protein therapeutics in cultivated mammalian cells. *Nature Biotechnology*, *22*(11), 1393–8. doi:10.1038/nbt1026

Yamashita, S., Tanaka, T., Tanii, H., Kubotsu, A., & Kawai, S. (1982). Method of producing ethylene-vinyl alcohol copolymer hollow fiber membranes. Japan.

Yu, D., McLean, M. D., Hall, J. C., & Ghosh, R. (2008). Purification of a human immunoglobulin G1 monoclonal antibody from transgenic tobacco using membrane chromatographic processes. *Journal of Chromatography. A*, *1187*(1-2), 128–37. doi:10.1016/j.chroma.2008.02.016

Zhang, F., Zhang, Y., Li, G., & Li, H. (2009). Preparation and characterization of EVAL hollow fiber membrane adsorbents filled with cation exchange resins. *Frontiers of Chemical Engineering in China*, *3*(4), 462–467. doi:10.1007/s11705-009-0011-1

Zhu, L.-P., Yu, J.-Z., Xu, Y.-Y., & Zhu, B.-K. (2009). The effects of spinning temperature on morphologies and properties of polyethersulfone hollow fiber membranes. *Journal of Applied Polymer Science*, *113*(3), 1701–1709. doi:10.1002/app.30163

Appendix 1: Standard Operating Procedure for Cambridge Solution Processing Platform (CSPP)

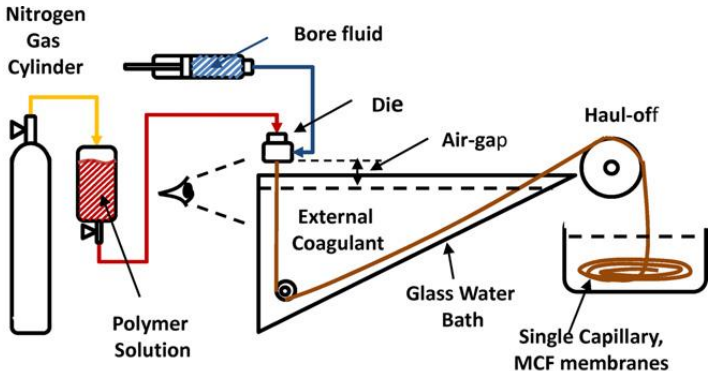

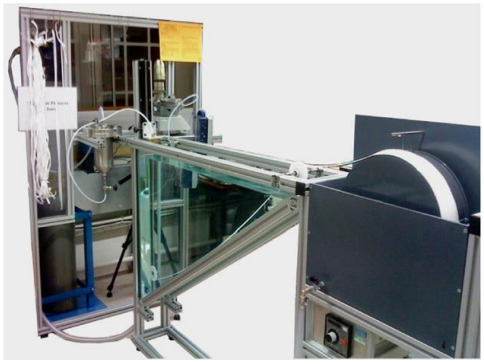

Setup

1. Fill the stainless steel polymer solution container with the prepared polymer solution, taking care not to introduce air bubbles while transferring.
2. Fill the glass coagulation tank with water using the plastic tube attached to the tap on the left side of the rig. Do not leave the tube unattended while the tank is being filled to prevent possible flooding.
3. Using a suitable water container fill the grey washing tank with water. Be careful when pouring the water inside not to splash water outside the tank.
4. Carefully mount the assembled clean die into the vertical traverse and connect the polymer solution and the core fluid tubing to the die.
5. Connect the compressed air gas line to the stainless steel polymer solution container. Before pressurizing the cylinder make sure that the relief valve is closed and the container is fully sealed and the bottom discharge valve is closed.

Operation

6. Gently open the polymer solution valve and then set the compressed air pressure gauge to start off between 5-10 bar. Wait for the polymer solution to be transferred to and discharge from the die.
7. Turn on the peristaltic pump and the drum motor by switching on the plug connected to the extension. At this point, the peristaltic pump will start working and the water will be splashed on the drum from the metallic sparger. Turn the motor on by switching on the red button on the motor control panel below the washing container.
8. After adjusting the volumetric flow rate of the polymer solution, start the syringe pump containing the bore fluid to a fixed flow speed.
9. After the two-phase flow discharges from the die and enters to the coagulation bath, guide it with a metal rod around the roller at the bottom of the tank and then pass it above the second roller at the right hand side and attach the nascent fibre to the rotating drum.

Shutdown

10. For shutting down the apparatus, switch off the electricity at the plug connected to the extension next to the roll tank.
11. Switch off the core fluid pump.
12. Close the polymer solution needle valve.
13. Close the gas regulatory valve and slightly open the pressure relief valve at the top of the cylinder.
14. Take off the die from the traverse and clean it with a suitable solvent.
15. Drain the water in the coagulation bath into the suitable waste drums.